UNIVERSITY OF STRATHCLYDE

NEUROPHYSIOLOGY LAB

DERTERMINING THE OPTIMAL PARADIGM FOR INVESTIGATING IF M1 ACTIVATIONS ASSOCIATED WITH STEP TRACKING WRIST MOVEMENTS ARE DIRECTION OR MUSCLE RELATED USING EEG

Ross Alexander Wilson

MSc Bioengineering

2013

Copyright

Signed: Date:

Project supervisors:

Dr. Campbell Reid

Prof. Bernard Conway

Abstract

This study investigated whether activations detected within the primary motor cortex (M1) during a wrist step tracking task encoded movement direction or specific muscle groups used to achieve the movement. This will provide information on the processes which occur within M1 of the human brain.

Experiments were designed to examine in more detail the results of a functional Magnetic Resonance Imaging (fMRI) study (Toxopeus, et al., 2011a) *which detected spatially disjoint areas within the wrist area of M1 that appeared to process movement within horizontal and vertical directions. The experiments combined electroencephalography (EEG) and source localisation to observe M1 activations and confirm whether they resulted from the processing of discrete movements or specific muscle groups.*

The results of a pilot EMG test indicated that a 90° change in forearm orientation did not sufficiently disassociate direction and muscle use. Changing forearm orientation from fully pronated to supine sufficiently dissociated the movement direction from the muscles used to produce the movement. The new paradigm recorded 64-channel EEG. Observation of task related epochs during artefact rejection indicated the presence of a time locked artefact caused by eye movements (saccades). The effects of artefact detection and reduction methods applied to the raw EEG data to remove this artefact were compared. Independent component analysis was applied to the averaged epochs and components resulting from artefacts were removed. Source localisation methods were applied to the processed averages and their results assessed for physiological and anatomical feasibility.

Artefact reduction methods were found to be ineffective at removing saccades when applied to raw EEG data, indicating the need for more advanced artefact reduction techniques such as Independent Component Analysis (ICA) to be applied to the data. The paradigm required the correct choice of a linear distribution source localisation model with 40µm spatial resolution to produce feasible results.

Acknowledgements

I would like to extend my thanks to everyone who has helped me throughout this project especially to my supervisor, Dr. Campbell Reid who was involved in its initial creation. It was thanks to him proposing this MSc project that presented me with the opportunity to explore into an interesting field, gaining invaluable skills and experience, as well as increasing my thirst for knowledge. I greatly appreciate the time he has put into this project and without his knowledge, expertise and guidance, this dissertation would not be possible.

Thanks also must be given to Prof. Bernard Conway, the head of department for allowing me the opportunity to conduct this work. His contributions within the department are indispensable and it was thanks to advice he gave that I gained a better understanding of the experimental techniques I have used.

My gratitude goes to those working within the neurophysiology lab that provided me with invaluable assistance in learning experimental techniques used as well as acting as willing subjects when needed.

Table of Contents

Copyright 2

Abstract 3

Acknowledgements 4

List of figures 8

List of Tables 10

1. Introduction 11

1.1 Models of motor control 12

1.1.1 Feedback control 12

1.1.2 Feedforward control 13

1.1.3 Theories of motor control 14

1.1.4 Forward motor command model 15

1.1.5 Equilibrium point movement model 16

1.1.6 Significance of goal based task solving during movement 16

1.1.7 Internal modelling of the environment 17

1.2 Physiology of motor processing 18

1.2.1 Skeletal muscle physiology, actuation of movement 18

1.2.2 Locating the muscles involved with wrist movement 21

1.2.3 Neurophysiology of motor processing 24

1.3 Electrophysiological theory 31

1.3.1 Neural origins of EEG 31

1.3.2 Source localisation 32

1.3.3 Event related potentials 34

1.3.4 Muscle origins of EMG 34

1.3.5 STFFT 35

1.1 Current aims 36

2. Literature review 37

2.1 Role of the motor cortex in motor control and the processing of motor commands 37

2.2 The importance of goal based movement in directional processing 41

2.3 Methods used in source localisation 44

2.4 Summary of literature review and statement of aims 50
3. Methods 52
3.1 Experimental paradigm 52
3.2 Participants 53
3.3 Experimental design and setup 54
3.3.1 Final design of task 54
3.3.2 Final experimental protocol 56
3.4 Data processing 59
3.4.1 Spike2 60
3.4.2 Neuroscan 61
3.4.3 Source localisation 65
4. Results 67
4.1 Subject selection 67
4.2 Electrode interpolation 68
4.3 Saccades observed during task 69
4.4 Spike 2 muscle EMG results 71
4.5 Averages for each direction 75
4.5.1 Minimally processed data averages 75
4.5.2 ICA of averages 81
4.6 Source localisation dipole analysis 86
5. Discussion 94
5.1 Implications due to EMG pilot 94
5.2 Implications of results of primate studies 95
5.3 Ideal experimental conditions 95
5.3.1 Experimental setup and design 95
5.3.2 Removal of saccades 96
5.3.3 Observation of artefact rejection and reduction methods 97
5.3.4 Observation of source localisations 102
5.4 Further study 103
6. Conclusion 105

Bibliography 107
Appendix A – Participant information sheet 111
Appendix B – Participant consent form 116
Appendix C – EMG pilot test 118
Appendix C.1.1 – EMG pilot experimental design 118
Appendix C.1.2 – EMG pilot experimental setup 120
Appendix C.2 - EMG pilot results 121
Appendix C.2.1 First pilot test results 122
Appendix C.2.2 Second pilot test results 127
Appendix D – Changes made to experimental setup and design 132
Appendix D.1 - Changes to experimental setup 132
Appendix D.2 - Changes to experimental Design 132

List of figures

Figure 1 Feedback control diagram 13
Figure 2 Feed forward control 14
Figure 3 Muscle connective tissue 19
Figure 4 Contraction cycle 20
Figure 5 Extensors of the wrist 22
Figure 6 Flexors of the wrist 23
Figure 7 Flexor digitorum profundus 24
Figure 8 Corticospinal pathway 25
Figure 9 Nerve cell 26
Figure 10 Several aspects of membrane function 27
Figure 11 Action potential propagation 27
Figure 12 Diagram indicating location of the reticular formation 28
Figure 13 Areas of the cortex involved motor in processing, medial and lateral views 29
Figure 14 Basal ganglia and cerebellum and frontal lobe 30
Figure 15 The optic pathway 30
Figure 16 Example of a STFFT spectrogram 36
Figure 17 Final experimental setup 55
Figure 18 Target display used in task 55
Figure 19 Final Position of EMG electrodes 57
Figure 20 Location of electrode placement according to international 10-20 System 58
Figure 21 SynAmps2 Quick-Cap 64 channel Montage, used in study 58
Figure 22 Subject 03 undertaking experimental task 59
Figure 23 Spike 2 example display of raw data 61
Figure 24 Example of the Curry 7 interface displaying averaged epoch of all channels used 64
Figure 25 FEMi model use in source localisations 65
Figure 26 Example of a source localisation with Curry 5 software 66
Figure 27 Curry 7 interface displaying electrode impedances 68
Figure 28 Filtered average of activity in one movement direction 69
Figure 29 Example of a saccade artefact (Shwartzman & Kranczioch, 2011) 71
Figure 30 EMG results in the direction of target 12 (upwards) 72
Figure 31 EMG results in the direction of target 6 (downwards) 73
Figure 32 Averaged epoch for target 6 with the forearm pronated 77
Figure 33 Averaged epoch for target 6 forearm supinated 78
Figure 34 Averaged epoch for target 12 forearm pronated 79
Figure 35 Averaged epoch for target 12 forearm supinated 80
Figure 36 Example of an ICA analysis of averaged response to target 6 when the forearm is pronated 82

Figure 37 Example of an ICA analysis of averaged response to target 6 when the forearm is supinated 83
Figure 38 Example of an ICA analysis of averaged response to target 12 when the forearm is pronated 84
Figure 39 Example of an ICA analysis of averaged response to target 12 when the forearm is supinated 85
Figure 40 Example of a moving dipole source localisation of response to trigger 6 when forearm is pronated 87
Figure 41 Example of a single moving dipole source localisation of response to trigger 6 when forearm is supinated 88
Figure 42 Example of a 6 rotating dipole source localisation of response to trigger 6 when forearm is pronated 89
Figure 43 Example of a six rotating dipole source localisation of response to trigger 6 when forearm is supinated 90
Figure 44 Example of a six fixed ICA dipole source localisation of response to trigger 6 when forearm is pronated 91
Figure 45 Example of a six fixed ICA dipole source localisation of response to trigger 6 when forearm is supinated 92
Figure 46 Example of an epoch rejected due to blink artefact 98
Figure 47 Effect of artefact reduction on HEO 100
Figure 48 Example of components rejected using ICA 101
Figure 49 Example of rejected epochs 102

Figure A - 1 Example manipulandum design 119
Figure A - 2 Manipulandum used in study with patients forearm supinated 120
Figure A - 3 Initial position of EMG electrodes 121
Figure A - 4 Average EMG results for movements in response to target 3 123
Figure A - 5 Average EMG results in response to target 6 124
Figure A - 6 Average EMG results in response to target 9 125
Figure A - 7 Average EMG results in response to target 12 126
Figure A - 8 Average EMG results in response to target 3 second method 128
Figure A - 9 Average EMG results in response to target 6 second method 129
Figure A - 10 Average EMG results in response to target 9 second method 130
Figure A - 11 Average EMG results in response to target 12 second method 131

List of Tables

Table 1 EEG Bands 32
Table 2 The number of accepted epochs for each subject 67
Table 5 EMG result Key 71
Table 4 Summary of EMG results 74

Table A - 1 Table of EMG electrodes for first pilot test 122
Table A - 2 EMG electrodes for second pilot test 127

1. Introduction

It is well established that movement, both voluntary and involuntary, is an action that all animals are capable of. In humans, movement is a part of everyday life, present in many aspects from the beating of your heart to the contraction of your blood vessels or the movement of your eyes as you read this page. It is already well established that movement is a result of cardiac, smooth or skeletal muscles which are facilitated by motor neurons from the central nervous system, which in turn is facilitated by the motor cortex of the brain. While the use of these areas is well known, the role of each component and the areas that facilitate the motor cortex are still under debate.

Studies of motor control have been taking place since earlier than 1899 (Woodworth, 1899). Motor control was originally studied from a psychology or neurophysiology perspective using different methods. More modern studies have progressed to a combination of the two perspectives and methods. This has resulted in a number of definitions originating from these studies.

Movement can be classified as reflexive, where the movements have been 'hardwired' into the body (Kalaska & Crammond, 1992), or learned as part of the development of skills (Guthrie, 1952). These movements themselves are either feedback, where they are controlled by a feedback loop using information gained by the senses, or non-feedback where the movement is predefined before onset. How reflexes and learned movements are used together to produce voluntary movements, if at all, is under debate and there is yet to be a definite theory that is accepted as an adequate explanation for the control of movement.

It has long been known that the primary motor cortex (M1) plays an active role in the processing of motor commands (Martini, et al., 2012), which are physiological signals passed through the nervous system to the muscles that stimulate movement onset.

However, the extent to which the commands are processed within the primary motor cortex is unclear. A previous fMRI study (Toxopeus, et al., 2011c) detected spatially segregated activations for the processing of wrist movements in specific directions within the motor cortex. This indicates that direction of movement is encoded within the human primary motor cortex.

This pilot study intends to assess the feasibility of reproducing these results using EEG source localisation methods, a method which uses physiological knowledge and recorded scalp potentials to predict the location of sources of activation within the brain.

This first chapter will describe the theorised 'software' used by the brain to achieve voluntary movement while providing background information relevant to the motor control field.

1.1 Models of motor control

1.1.1 Feedback control

Feedback, or closed loop, control takes place during slow movements where a subject is focusing on precision of movement. Displayed in Figure 1, closed loop control represents movement which is influenced by sensory input. Using a basic motor program with only initial movement instructions, information gathered by the senses (such as, force position or velocity) is used to alter the motor output resulting in continuously controlled actions.

The speed of closed loop movements is determined by the speed of sensory processing; as a result, if a movement is too fast (e.g., a ballistic movement) the accuracy of movement cannot be determined by sensory information and must instead rely on feed-forward control.

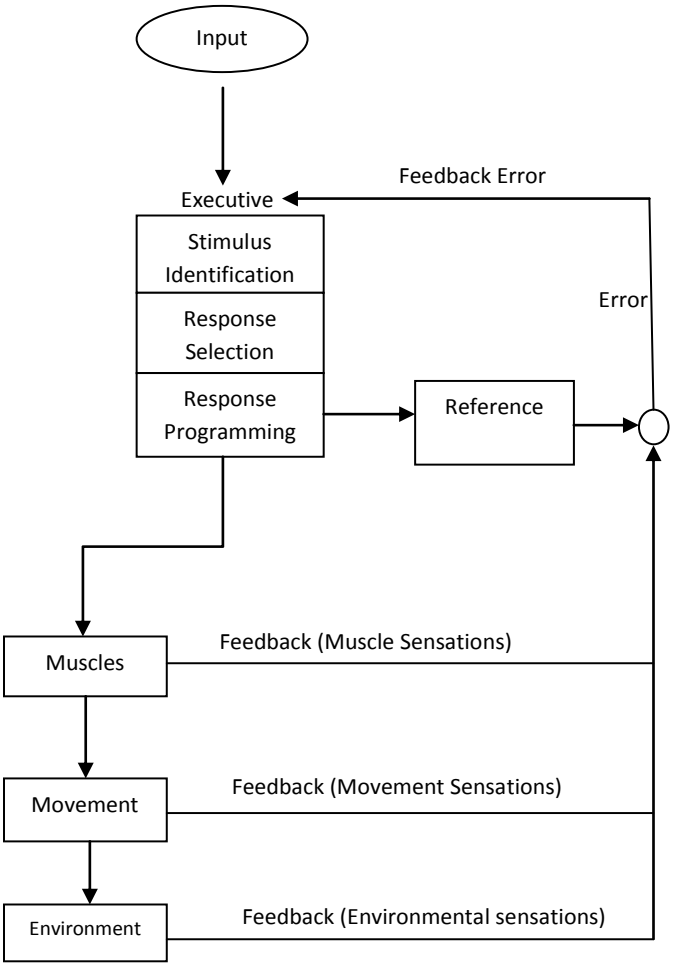

Figure 1 Feedback control diagram

Figure Adapted from Figure 01, chapter 4 page 7: (Millslagle, 2013)

1.1.2 Feedforward control

Feedforward control occurs in fast movements where movement occurs at a speed too fast for feedback control. In such situations, the accuracy of the movement will depend upon the initial motor command used to initiate the movement. This means for accurate movement, a prediction of the events that make up the course of the movement is necessary, allowing the entire movement to be predefined before onset. Figure 2 displays feedforward control where a desired trajectory input is processed by a predetermined model to result in a motor command which can achieve the intended movement.

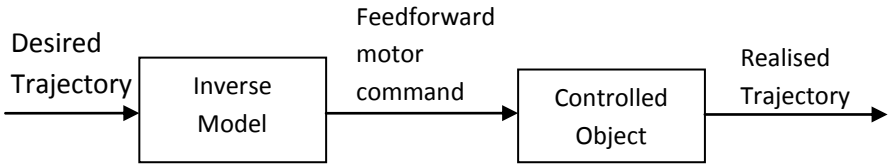

Figure 2 Feed forward control

Based upon figure 1: (Kawato, 1999)

1.1.3 Theories of motor control

Motor control theories describe and explain how, in varying environments, the nervous system produces coordinated movements or motor skills: learned sequences of movements that combine to execute smooth movement, to accomplish specific tasks.

Motor control theories have been developed to explain the processes that lead from sensory input to a motor output. The role of learning during this process is of great importance as adaptation to an unfamiliar situation increases the accuracy of the movement end point compared to the intended end point, and results in a straighter trajectory of movement (Kawato, 1999). Prediction of the method which will lead to the intended outcome is essential to goal based movement as it determines the movement that will occur. This leads to most theories questioning the process by which sensory information is processed along with learnt predictive models to result in a command signal that leads to movement.

The two dominating theories of how motor control is achieved are: the hierarchical model, where the command is processed by distinct areas of the brain in a specific order; and the equilibrium point model where physiological conditions of the muscles moving themselves allow complex movement.

These two oppose each other as the former states that most of the processing for movement takes place inside the brain resulting in complex motor signals passing through the Central Nervous System (CNS) to achieve movement, while the latter

states that the motor signals sent will be relatively simple and that the majority of the processing takes place in the CNS itself.

1.1.4 Forward motor command model

One of the commonly accepted theories of how motor control is achieved is that the motor cortex makes use of forward and inverse models to control musculoskeletal movement. Inverse models predict the motor command necessary to achieve a desired movement, e.g., reaching to grasp an object. Forward models predict the changes that will occur in sensory information as a result of actions taken: proprioceptive information for tracking body position, and information from the other senses for tracking surroundings. Forward models permit rapid error detection allowing the brain to quickly deal with changes in surroundings during movement, while inverse models make use of information about the surroundings within the brain to create the motor commands needed to achieve smooth movement with minimal motor commands and energy loss.

This theory originates from the field of robotics and control systems where both models are used to determine motion of a frame to achieve its objective (Kawato, 1999). This applies to systems where a significant time delay, e.g. the 25ms transmission time of motor commands between the forearm muscles and the brain, exists between a control system and an effector, a condition which also applies to the human body.

Alternate names for the forward and inverse model are the forward dynamic model and forward sensory model, respectively. These models contribute the most to movement during feed forward control that takes place during rapid movements where an accurate response to surroundings needs to take place without proprioceptive feedback during the ongoing command.

1.1.5 Equilibrium point movement model

Like the forward motor control model before it, the equilibrium point model has origins in the field of robotics. An analogy to how the theory works makes use of a robot arm with each motor replaced with opposing rubber bands, simulating muscles controlling a joint. The equilibrium point of a system is the point where the robotic joint would settle into when released. This joint position is determined by the length tension properties of the bands that hold the arm, for example resting length or stiffness. The equilibrium point model as described in The Equilibrium Point Hypothesis for Control of Movements (Shadmehr, 1998) likens the muscles to these rubber bands and suggests that the contraction of motor units within the muscle, indicating the final position of a joint, can determine the equilibrium point by determining the level of contraction in the muscle. The theory further indicates that smooth movements are the product of transition between equilibrium points allowing a more simple control of motion by the brain.

While this theory can be combined with the forward motor command theory, the two are currently held to be separate as smooth control of movements achieved by the equilibrium point theory are inferred to negate the need for a forward dynamic model to achieve smooth movements. Further models proposed have either been based on forward motor control, equilibrium point, or both. However, no one theory is currently established as fact.

1.1.6 Significance of goal based task solving during movement

Most voluntary movements result from the moving organism attempting to complete a goal based task, this task can range from less complicated activities such as consuming food to performing complex tasks such as tying a knot. The process the brain goes through to achieve such tasks involves translation of sensory information, most often visually acquired, into an appropriate motor output achieved by specific muscle patterns. In the case of visually guided movements this can be viewed analytically as

the process of transforming movement related signals from an extrinsic frame to a muscle based frame (Kalaska & Crammond, 1992).

To successfully translate between these two frames and thus achieve a goal based movement the brain must first solve the degrees of freedom problem.

The degrees of freedom problem was proposed by Nikolai Bernstein who noted that purely feedforward commands in neural control are insufficient for dealing with changing contingencies in the environment because of the unpredictable nature of environmental loads (Chiel, et al., 2009). The degrees of freedom problem notes that due to the large number of degrees of freedom during goal based movement, kinematic chains due to organism structure and inertial forces complicate the ability of the CNS to generate motor commands due to producing an infinite number of different solutions to achieve the intended movement. In addition the presence of muscles across a joint further complicates matters due to their numbers often exceeding the number of degrees of freedom of said joint resulting in an infinite number of solutions of muscle patterns used to achieve movement solutions. Bernstein proposed that the CNS solves this inverse problem by freezing degrees of freedom resulting in a reduced number of possible solutions.

1.1.7 Internal modelling of the environment

A defining concept on the decision to undertake movement is the sensory information gained concerning a subject's surroundings. The information gained by the senses is used by the brain to update an internal model of the environment around the perceiver. This model makes use of a reference frame constructed from horizontal, vertical and depth axes that is usually a binocular centre-viewed frame, but can change depending on ongoing conditions (Battaglia-Mayer, et al., 2003). The reference frame is used to locate targets for goal based movement relative to the body, information on which is further used to produce target vectors which will be used in the processing of motor commands.

1.2 Physiology of motor processing

As previously mentioned, it is well established that movement is a result of muscles (cardiac, smooth or skeletal) which are facilitated by motor neurons from the central nervous system, which in turn is facilitated by the motor cortex of the brain. This section will add further physiological detail to each of these processes as well as the processes preceding them. The following section will back track through the processes that finalise with movement, providing physiological information on the organs and tissues the motor command has passed through, beginning with the muscles that achieve onset of movement.

1.2.1 Skeletal muscle physiology, actuation of movement

Movement is achieved via the controlled contraction of skeletal muscles which lie across a joint. By applying forces to the bones they are attached to, muscles achieve a movement either in extension (increasing an angle), flexion (decreasing an angle) across a joint, or rotation of the joint. This movement is kept in check via antagonist muscles which resist the forces applied by the protagonist muscle. Muscles can also act as synergists to aids the antagonist or agonist muscles by preventing joint movement around undesired axes. The contractions of muscles occur in controlled burst patterns of agonist-antagonist activity which allow a movement to reach its goal (Martini, Nath, & Batholomew, 2012; Gordon & Ghez, 1984).

Skeletal muscles consist of three layers of tissue: epimysium, a dense layer of collagen fibres which separate the muscle from nearby tissues; perimysium, which divides the muscle into a set of compartments containing fascicle muscle fibre bundles supported by blood vessels and nerves; and endomysium, a connective tissue which surrounds individual muscle fibres in a fascicle containing supporting capillaries, nerve cells and myosatellite cells. These layers are woven together to form tendons and aponeuroses which firmly connect to bone through the use of collagen fibres that attach to a bones matrix. Figure 3 displays an example muscle labelling all tissues.

http://missazua.com/Site_2/Q2_Notes_Anat_files/droppedImage.jpg

Figure 3 Muscle connective tissue
Figure Sourced from Figure 10-1, Unit 2, Chapter 10 (Muscle tissue), Page 281 (Martini, et al., 2012)

A muscle fibre contains a series of myofibrils that extend through the sarcoplasm that can actively shorten to allow contraction of the muscle fibre. Each myofibril contains thin filaments of actin and thick filaments of myosin, organised into repeating units called sarcomeres.

A muscle contraction begins when a muscle fibre is activated by stimulation from a motor neuron conducting an action potential. The action potential causes the release of acetylcholine (ACh) which leads to the production of a second action potential within the sarcolemma of the muscle fibre. The action potential is carried by transfer tubules within the terminal cisternae chambers where it triggers the release of calcium ions (Ca^{2+}).

Contraction of the sarcomeres takes place within a contraction cycle (Figure 4) which causes the myosin heads of the thick filaments to pull on nebulin active sites of thin filaments, facilitated by the presence of Ca^{2+}. The contraction of multiple sarcomeres results in the contraction of the muscle fibre and the contraction of multiple fibres

results in the overall contraction of the muscle. The strength of a contraction is controlled by the number of fibres activated, allowing control of muscle activity.

http://www.baileybio.com/plogger/images/anatomy___physiology/05._powerpoint_-_muscular_system/muscle_contraction_-_physiology.jpg

Figure 4 Contraction cycle
Figure sourced from: BaileyBio.com 2008

As mentioned previously, each muscle fibre is facilitated by a motor neuron which controls a number of other muscle fibres. A motor unit is the grouping of these fibres and the motor neuron controlling them. The number of fibres controlled within a motor unit determines the degree of control possible over muscle contraction: larger motor units, which contain large numbers of muscle fibres facilitated by a single neuron, are less controlled resulting in less precise movements. Motor neurons connect to the peripheral nervous system which in turn connects to the central nervous

system which carries motor commands from the brain, allowing control of skeletal muscles.

1.2.2 Locating the muscles involved with wrist movement

Wrist movements occur as the product of multiple antagonist and agonist muscles. The bellies of these muscles lie on the on the upper forearm while the wrist movements are actuated through tendons that connect to the carpal bones. Many of the muscles involved have multiple functions facilitating radial and ulnar deviations that change the wrist orientation as well as flexing and extending the joint. The muscles associated with wrist movements are identified below together with methods of identification (J.C.Andrews, 1986).

1.2.2.1 Extensor Carpi Radialis Longus

Function: Extensor Carpi Radialis Longus (ECRL, Figure 5) is involved in wrist extension and radial deviation of the hand.

Identification: ECRL is the first muscle lateral to the most lateral edge of the Brachioradialis. The edges can be defined by making a fist and extending the wrist.

1.2.2.2 Extensor Carpi Radialis Brevis

Function: Extensor Carpi Radialis Brevis (ECRB, Figure 5) is involved in wrist extension.

Identification: ECRB is lateral to the lateral edge of the mid-portion of the Brachioradialis. The muscle belly extends more distally than the belly of the ECRL.

1.2.2.3 Extensor Carpi Ulnaris

Function: Extensor Carpi Ulnaris (ECU, Figure 5) is involved in wrist extension, ulnar deviation of the hand and fixation of the wrist for a strong grip.

Identification: If the arm is supine and the forearm pronated, ECU is the first muscle dorsal to the dorsal border of the Ulna.

http://droualb.faculty.mjc.edu/Lecture%20Notes/Unit%203/Muscles_of_forearm_posterior_view.jpg

Figure 5 Extensors of the wrist

Sourced from: Lecture slides by Dr. Robert, Droual Modesto Junior College

1.2.2.4 Flexor Carpi Radialis

Function: Flexor Carpi Radialis (FCR, Figure 6) is involved in wrist flexion and radial deviation of the wrist joint.

Identification: FCR is located between the upper and middle thirds of the forearm along the line of the tendon. The tendon of the muscle is the most lateral of the 3 prominent tendons on the ventral surface of the lower forearm when held in midpronation.

1.2.2.5 Flexor Carpis Ulnaris

Function: Flexor Carpi Ulnaris (FCU, Figure 6) is involved in wrist flexion and ulnar deviation of the wrist joint.

Identification: FCU is located between the upper and middle thirds of the forearm along the line of its tendon. The tendon of the muscle is the most proximal of the 3 prominent tendons on the ventral surface of the lower forearm when held supine.

Figure a

http://droualb.faculty.mjc.edu/Lecture%20Notes/Unit%203/Muscles_of_forearm.jpg

Figure 6 Flexors of the wrist

Sourced from: Lecture slides by Dr. Robert, Droual Modesto Junior College

1.2.2.6 Flexor Digitorum Profundus

Function: Flexor Digitorum Profundus (FDP, Figure 7) is involved in flexion of the distal interphalangial joints of the four medial digits. It helps flex every joint its tendons pass through, including the wrist.

Identification: FDP is located ventrally from the medial surface of the Ulna when the arm is supine and the forearm pronated.

Figure (c)

http://droualb.faculty.mjc.edu/Lecture%20Notes/Unit%203/Muscles_of_forearm.jpg

Figure 7 Flexor digitorum profundus

Sourced from: Lecture slides by Dr. Robert, Droual Modesto Junior College

1.2.3 Neurophysiology of motor processing

The commands that activate motor neurons are sent from the brain through the central nervous system to the muscles involved. A motor command originates in the motor cortex where it passes through the corticospinal pathway(Figure 8) to the motor nuclei. The motor command leaves the motor cortex through the corticobulbar tracts which synapse to the lower motor neurons. The corticospinal tracts synapse on the

lower motor neurons on the anterior grey horns of the spinal cord, after passing through the midbrain, crossing over in the decussating pyramids of the medulla oblongata and passing through the lateral corticospinal tract. The motor commands finally leave the CNS via the ventral root. In the case of skeletal muscles, they pass through axons carried by the dorsal or ventral ramus which innervate the back and limbs respectively. It is known that some processing of motor commands takes place within the lower areas of the CNS which allows for fast unconscious reactions to stimuli (Martini, Nath, & Batholomew, 2012).

http://brainmind.com/images/Pyramidaltract.jpg

Figure 8 Corticospinal pathway

Sourced from Figure 15-8, Unit 3, Chapter 15, Page 509 (Martini, et al., 2012)

1.2.3.1 Nerve physiology

Nerves, which are used to transfer information throughout the body, consist of a cell body which contains the nucleus, and axons, dendrites and terminals which are used for carrying signals shown in Figure 9. Signals picked up by the dendrites are transferred through the nerve axon to the axon terminals which synapse to the dendrites of other neurons via potentials on the membrane of the cell.

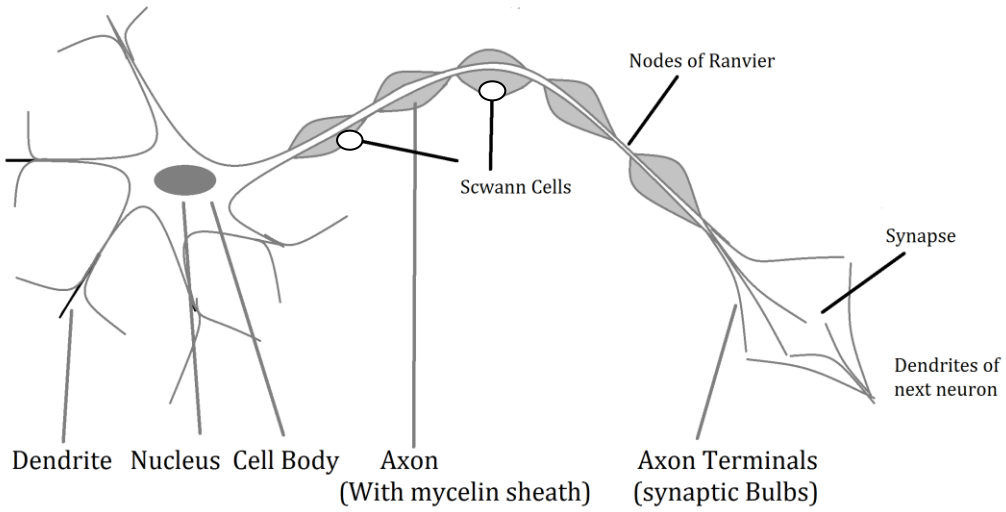

Figure 9 Nerve cell

Drawing of nerve cell depicting Key anatomical points: Dendrite, Nucleus, Cell body, Axon, Schwann cells, Nodes of Ranvier, Axon terminals and point where cell synapses.

Nerves transmit signals via action potentials: if the sum of all signals gathered by a nerve's dendrites has a potential above the threshold value, an action potential is triggered on the nerve's cell membrane. Voltage-activated gates (Figure 10) within the membrane are opened, causing the release of positively charged potassium ions along the concentration gradient into the extracellular matrix. This results in the cell membrane becoming negatively charged on one side and positively charged on the other resulting in a potential difference (voltage) across the membrane. This voltage

activates successive gates, or synapses, passing the signal along the nerve (Figure 11). The myelin sheathes of nerve axons insulate the nerve preventing the conduction of electrical current across the cell membrane. This allows the action potential to 'jump' between the non insulated nodes of ranvier, allowing faster and more efficient transmission of signals across the nerve axon.

http://www.bio.miami.edu/tom/courses/protected/MCB6/ch23/23-06.jpg

Figure 10 Several aspects of membrane function

Figure Sourced from: Figure 23-6 (Lodish, et al., 2008)

http://www.arts.uwaterloo.ca/~bfleming/psych261/image25.gif

Figure 11 Action potential propagation

Figure sourced from: Diagrams by B. Fleming, University of Waterloo

1.2.3.2 Brain Physiology

One of the later areas of the brain to involve processing of motor commands before the commands are sent to the CNS is the reticular formation of the midbrain (Figure 12). The descending reticular formation is involved in posture and equilibrium, incorporating sensory information to maintain control of balance and posture through skeletal muscles.

http://classconnection.s3.amazonaws.com/661/flashcards/1011661/png/image531332864378177.png

Figure 12 Diagram indicating location of the reticular formation

Sourced from: Reticular Formation; how the brain stem relays the info, A View of Life, Pasadena City College

The primary motor cortex (M1) controls all voluntary movement. The motor cortex lies on the surface of the precentral gyrus which forms the anterior border of the central sulcus, which separates it from the primary sensory cortex. Pyramidal cells, neurons within the primary motor cortex, control somatic motor neurons within the brain stem and spinal cord, conveying voluntary motor impulses to achieve direct voluntary movement.

It is currently theorised that the motor cortex is not capable of processing information and instead is stimulated by other areas of the motor cortex. A specific example is the premotor cortex (PMC), which is involved in the coordination and processing of more complex movements and has direct input to the primary motor cortex (Martini, Nath, & Batholomew, 2012). A depiction of the brain including areas known to be involved in motor processing is displayed in Figure 13.

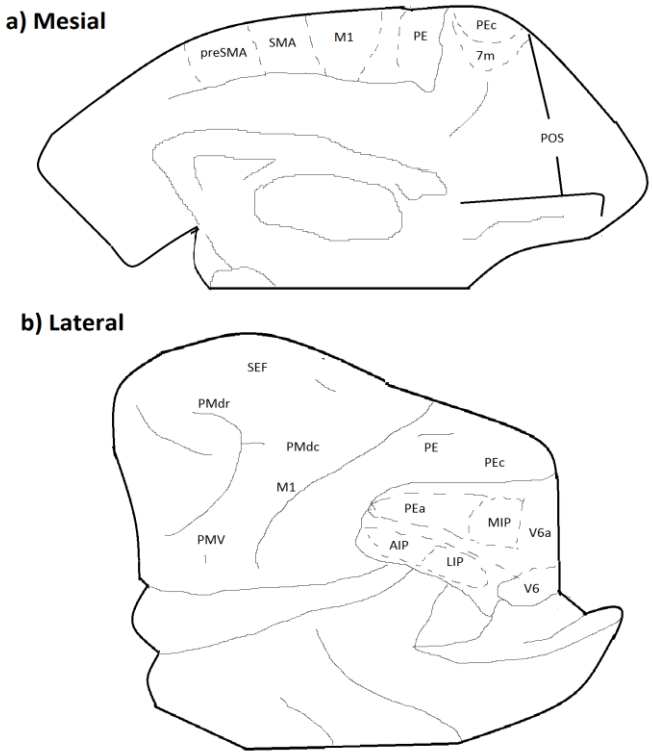

Figure 13 Areas of the cortex involved motor in processing, medial and lateral views

Based upon figure sourced from (Caminiti, et al., 1998)

Supplementary Motor Area(SMA), Primary Motor Cortex (M1), Parietal Area (PE_), Parieto-occipital sulcus (POS), Supplementary Eye Fields (SEF), Premotor Cortex Area (PM_), Intraparietal Area (_IP), Visual area (V_)

The motor cortex is part of the frontal lobe. This is where decision making is suspected to occur. Integrative centres, for example the prefrontal cortex, integrate information from sensory association areas and perform intellectual functions.

The Basal Ganglia and Cerebellum (Figure 14) are also integrated into the motor control process. The Basal Ganglia integrate semi-voluntary movements like walking, swimming and laughing while the cerebellum modifies and adjusts the output of the motor cortex to improve accuracy and adaptability, most likely playing an important part in feedforward and feedback control.

http://www.decodedscience.com/wp-content/uploads/2011/11/basal-ganglia-structures.png

Figure 14 Basal ganglia and cerebellum and frontal lobe

Image sourced from: US Food and Drug Administration

This experiment will use a visual stimulus. When seen by the eyes, this stimulus will be processed by the visual cortex in the occipital lobe on the opposite side to the eye which gathered the information. Light captured by the eye stimulates the photoreceptors of the retina and transferred via the Optic Pathway (Figure 15). The potential generated is transferred to the lateral geniculate nucleus on the opposite side on the body by the optic nerve travelling through the optic chiasm and optic tract. The visual information is then sent from the lateral geniculate nucleus to the visual cortex, superior colliculus, diencephalon and brain stem. Information from the visual cortex will be used to determine the motor commands used to achieve the desired response action to the stimulus.

http://wine4soul.files.wordpress.com/2012/10/visual_pathway.jpg

Figure 15 The optic pathway

Sourced from: (WINE FOR SOUL, 2012)

1.3 Electrophysiological theory

1.3.1 Neural origins of EEG

Electroencephalography (EEG) records electrical activity across the scalp, recording the potential difference between 2 electrodes, an active electrode and a reference, over time. First used in 1924 by Hans Berger, who proposed the technique as a "window to the mind", EEG allows observation of internal activity taking place in the brain due to the effect of the post synaptic potentials of cortical pyramidal neurons being visible on the scalp.

Postsynaptic potentials, caused by the 'signals' that pass into a neuron can be classified as either excitatory postsynaptic potentials (EPSP) or inhibitory postsynaptic potentials (IPSP). EPSPs occur if positive ions such as potassium (K+) and sodium (Na+) flow into the cell through open ligand-gated ion channels while negative ions flow out of the cell. Alternatively, IPSPs occur in the reversed situation: if negative ions flow into a cell and positive ions flow out of the cell into the extracellular fluid. The electrical potential detected at the scalp by EEG is the result of the potential differences generated by the flow of ions towards the dendrites triggered by EPSP and IPSPs. Ordinarily these voltages would be too small to detect, however PSPs can be detected on the scalp due to the organisation of the cortical pyramid neurons within the brain. Due to coherent orientation of dendrite trunks, the sum of tens of thousands of synchronously activated cortical pyramid neurons produces a potential difference large enough to propagate to the scalp surface, allowing detection by electrodes used in EEG.

The voltage detected by EEG electrodes at the scalp is the sum of multiple synchronous activations of pyramidal neurons throughout the entire brain; these activations can be negative in the case of superficial EPSPs and deep IPSPs, or positive in the case of superficial IPSPs and deep EPSPs. As the potential difference detected is the sum of multiple types of activity including muscle and eye artefacts, EEG activity is normally described by a number of identified frequency bands to observe activity; lower

frequencies can be associated with the activation of large areas of synchronised neurons while higher frequencies can be associated with the activation of smaller neuron assemblies. Table 1 lists these frequency bands, their identified frequency range, associated activity and identified sources.

Table 1 EEG Bands

Band name	subcategories	Frequency (HZ)	activity	source
delta		1-4	Prominently sleep	Subgenual prefrontal cortex
theta		4-8	Prominently sleep	Septo-hippocampus
	"Widespread scalp distribution"		Decreased alertness	
	"frontal midline"		Focused attention, mental effort	Anterior cingulate cortex
alpha		8-13	Relaxed wakefulness	Posterior occipito-temporal, parietal regions
	Upper alpha	10-12 desynchronization	Task specific Sensory somatic processing Long term memory	
beta		13-30	Increased attention, vigilance Replaces alpha cognitive activity	
gamma		36-44	Attention, arousal, object recognition, top down modulation of sensory processes, perceptual binding, brain activation direct association	Large scale integration and synchronization of widely distributed neurons, Intracardial circuitries Synaptic interactions of the cortex and thalamus, brainstem

1.3.2 Source localisation

As EEG records data from a large number of locations across the scalp, the activations from various neuron assemblies can be seen in multiple electrodes. Source localisation

uses electrophysiological theory to solve the inverse problem, finding the generating sources from activity recorded on the scalp. The main aspects that source localisation has to overcome, aside from the infinite solutions to the inverse problem, are the distorting effects of the head volume, signal-to-noise ratio and limited spatial sampling while providing results within a millisecond temporal and millimetre scan resolution.

These difficulties are solved by postulating solutions of EEG sources that are physiologically and anatomically logical using the laws of electrodynamics. The two important aspects in making this postulation are the head model used and the inverse solution used to find these sources.

The head model is used to take account of spatial properties when finding EEG sources. There are currently 3 types of head model that are commonly used. The simplest model, the 3 sphere model, models the head as 3 spheres: the scalp, the skull and the brain. Sources are located based on the electrophysiological properties within each sphere. This is the least accurate of the 3 models, as it least corresponds to the natural physiology of the human head. The boundary element model (BEM) and finite element model (FEM) approximate the volume conductor properties of the head as realistic shaped compartments with homogenous isotropic conductivities. The BEM model ignores the anisotropic and fine structure of the surrounding tissues while the FEM model takes these properties in to account, requiring more computation (Fuchs, Wagner, & Kastner, 2001).

The inverse solution determines the method used to select the best number out of the infinite possible sources of the inverse model. There are 2 common methods: the equivalent dipole and the linear distribution approach. The equivalent dipole method models the sources of EEG as a number of specific areas of activation, identified as dipoles with specific orientation and depth. The number of dipoles must be defined prior to localisation, which can lead to inaccuracies in the results generated if the wrong a priori assumptions are used to define the number of dipoles. The linear

distribution approach progresses from the dipole model by assuming activity within all source locations. This improves the accuracy but also increases the computation time.

1.3.3 Event related potentials

The brain is constantly processing a large amount of information from many sources, including memory, sensory and movement. As such it can be difficult to identify activity within the brain that is related to specific stimuli. Event related potentials are a way of assessing stimulus-locked activity that averages out activity not related to their stimulus allowing a clearer observation of related activity. Event Related Potentials (ERPs) are electrical potentials generated by the brain related to specific internal or external events that originate from PSPs involved in neurotransmission. ERPs can be used to provide information on a broad range of cognitive processes making them a common tool in physiological research (Luck, 2012). ERP results can be detected in the absence of behavioural responses and possess precise temporal resolution but poor spatial resolution, making them ideal for observing activations in the time domain but poor for locating them spatially.

There are a number of ERP component types: exogenous, which are triggered by the presence of a stimulus; endogenous, which are triggered by task dependant neural processes; and motor components, which are due to preparation and execution of a given motor response.

1.3.4 Muscle origins of EMG

Electromyography (EMG) is the recording of the potential difference that results from the depolarisation of the sarcolemma of a muscle when motor units are recruited to achieve a skeletal muscle contraction. This voltage can be recorded by surface electrodes or wire electrodes implanted inside the muscle itself which record the potential difference between the EMG electrode and a reference electrode usually placed on the process of a bone near the joint the muscle is facilitating (Merletti & Parker, 2004). When a motor unit is activated, the action potentials of its individual

fibres causes an electrical dipole to travel along the surface of the muscle fibres which causes a potential difference to be generated between the two recording electrodes. As the electrodes record the extent of the fibres innervated by a motor unit, these signals sum up into a triphasic motor action potential (Konrad, 2005). The EMG electrodes detect the supposition of all motor unit action potentials (MUAPs) of a fibre.

The two important factors of an EMG signal are the recruitment of MUAPs within the muscle and the firing frequency of the MUAPs which reflect the main control strategies used to manage the force the muscle is applying and adjust its contraction process.

When a muscle is inactive the EMG signal being detected will be a relatively noiseless baseline allowing clear observation of when motor unit recruitment begins. The EMG signal can be affected by a number of issues, namely: underlying tissue characteristics between the muscle and the electrode; physiological cross-talk with neighbouring muscles; geometry changes of the muscle they are detecting; the presence of noise such as external 50 Hz mains noise or internal noise such as artefacts caused by cardiac activity, and electrode and amplifier quality.

1.3.5 STFFT

Short Time Fast Fourier Transform (STFFT) is a faster method of processing a Fast Fourier transform (FFT) which converts time domain signals into the frequency domain, and is typically plotted on a spectrogram (Figure 16). This allows viewing of the frequency components that are present within in a non-stationary signal across the time range of the signal. Fourier Transforms allows the amplitude or power of a number of frequencies present within a signal to be discerned, and if they are associated with events within the time frame being observed. By extracting several frames from a signal which moves with time, the STFFT allows comparison of the amplitude of frequency components across a signal with time and is an effective way of observing increases within EEG activity bands.

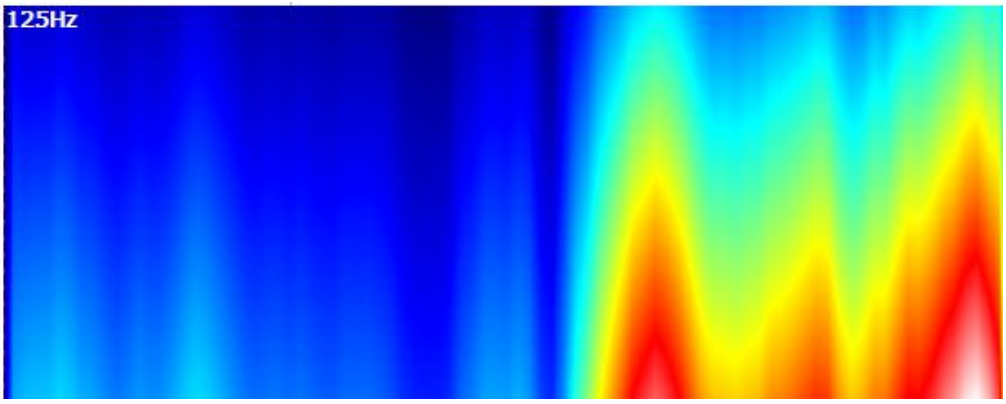

Figure 16 Example of a STFFT spectrogram

The example spectrogram above shows an increase in the amplitude of signal frequency components in the latter half of the time frame. The horizontal axis represents time and the vertical axis represents frequency the signal is observed over. The power of each frequency component is represented by the colour of the pixel that represents the frequency at the specific time observed. In the example above there are patches of red and orange colouration extending from the lower half of the latter half of the spectrogram. As red and white indicate higher amplitudes this gives an indication that there is greater activity within the observed frequency bands at this point, especially grouped towards the lower frequencies, which can indicate the presence of a neurological process.

1.1 Current aims

This study will investigate a proposed experimental design to observe spatially segregated activations for the processing of wrist movements in specific directions within the motor cortex using scalp-based EEG.

Potential distributions of the scalp will be recorded using 64 channel EEG while the participants perform a motor step tracking task using a manipulandum controlled by wrist movements. Epochs will be gathered for wrist movements to a number of directions and averaged. These averaged epochs will be used with source localisation techniques to detect the spatial location of the sources of motor-related cortical potentials that are generated during the movements. These will be compared with the results of the same task repeated with a different forearm orientation, with the intention of observing spatially distinct processing of each directional movement and observation of the effect of using different muscles to achieve the same directional movement on the location of the sources.

2. Literature review

2.1 Role of the motor cortex in motor control and the processing of motor commands

One current theory states that the role of the motor cortex is like the keys of a piano while the premotor area acts as the pianist: in other words, no processing takes place within the primary motor cortex and the majority of processing is done inside the premotor cortex which stimulates the motor cortex to make it 'play' motor commands (Martini, Nath, & Batholomew, 2012). However, Principles of Anatomy and Physiology (Tortora & Anagnostakos, 1984) only states that stimulation of specific points on the motor cortex result in muscular contractions and the premotor area is associated with learned muscular activities, indicating that the theory has been developed between the publishing of the two textbooks.

A recent functional Magnetic Resonance Imaging (fMRI) study (Toxopeus, et al., 2011c) indicated that the motor cortex may provide a more active contribution to motor processing within the brain. The study aimed to observe how the intended direction of hand movement was incorporated into the somatic representation of the M1 manual effector system. In doing so the intention was to reproduce recent primate study findings in humans and identify a neural substrate encoding direction. When undertaking a visual step tracking task involving extension, flexion and radial-ulnar deviation of the right wrist using a manipulandum similar to the one used in a previous primate study (Hoffman, Strick & Kakei, 1999), fMRI scans of the participants exhibited clear differences in the foci of activation between the 4 main directions 0^{o} (extension), 90^{o} (radial deviation), 180^{o} (flexion), and 270^{o} (ulnar deviation), with the directions involving flexion and extension having stronger activations. The authors speculated that this indicated that there was distinct processing taking place within the M1 area of the motor cortex for each movement direction.

This is concurrent with the results of primate studies where it was observed that directional tuning was present in M1, with areas of activation for each direction spatially mapped along the cortical surface indicating the presence of a neural substrate that links goal direction to the processing of final motor commands.

There is a large body of information on the behaviour of neurons in tM1 area of the primate brain, these studies have been undertaken due to the similar physiology of many primates to humans, allowing single neuron studies of voluntary movement to take place and be observed using methods not permissible in humans (Georgopoulos, et al., 1993). The most notable outcomes of studies into the role of the motor cortex are the population vector and identification of the parameters used by the cells of the motor cortex (Scott, 2003).

The population vector (Georgopoulos, et al., 1983) for a specific representative area, e.g. the wrist, sums all the preferred direction (PD) vectors (the vector of body part movement at which a cell's activity maximises in a sharp peak). The resulting population vector was found to provide an indication of the direction of movement processed by that specific area. This indicates that either the neurons in M1 specify global performance related to the direction they are processing (Caminiti, et al., 1990) or that the results were due to symmetrically tuned cells with uniformly distributed direction across the samples used. Such cells would hold no coupling between their preferred directions and how much a cell modulates activity during movement (Scott, 2003). However, since non-uniform distribution of PDs has been observed, the specification of global performance seems more likely. The population vector was noted to be an inexact prediction of final direction, with the vector direction being skewed away to the left when the subject is reaching away from its body or the right when the subject is reaching towards their body. Reasons for this have been suggested as: non-uniform distribution PD of neurons and a bias in distribution due to preferred direction of limb (Scott, 2003).

It has been identified that the cells of M1 do not code for any single parameter (Scott, 2003). Cells have been identified that code for parameters such as: limb position; posture; global goal; spatial direction; muscle force; sensory signals; and contrilateral, ipsilateral and bilateral movements. A single neuron may reflect several of the above parameters, each with a different temporal contribution to the cell discharge. While many parameters are processed they are not randomly distributed across a cell population, links have been found between global tuning across M1 and parameters such as: sensitivity to load, visuo-motor transformations of motor commands.

A number of notable reports concerning the role of direction in the motor cortex involving single cell recordings of primates have been published (Kakei et al., 2003; Ben-Shaul et al.,2003; Georgopoulos et al., 2006).

The first report (Kakei, Hoffman & Strick, 2003) indicated the presence of cells directionally tuned to an extrinsic axis (a coordinate frame fixed to external space, i.e. target location in space), an intrinsic axis (a coordinate frame based on limb position), and extrinsic axes with gain determined by limb orientation (used to translate between the two axes). The study observed how coordinate frames were used within the primary motor and premotor cortex to provide an insight into sensory motor transformation within these areas. Of particular interest was the transformation between the information related to extrinsic spatial locations of a movement target to the intrinsic information required for controlled muscle activations. The task used by Hoffman et al (Hoffman, Strick & Kakei, 1999) was undertaken by trained primates with arms in supination, pronation and midway between the two to disassociate the effect of joint angle. Single cell recordings of neural activity were taken during the tasks and used to predict the preferred direction (PD) of the cells by determining the direction of wrist movement in which the cell discharge peaked. As the change in forearm posture resulted in a shift in the preferred direction of a muscle, cells were determined to be muscle related and thus intrinsic if their preferred direction shifted with forearm

posture. Extrinsic cells with gain modulation were identified from the remaining extrinsic cells by observing if the cells experienced gain across the different forearm postures. Within the M1, 28 of the 72 recorded cells were determined to be muscle-like, 27 of the 72 cells were determined to be extrinsic with gain modulation, and 17 of the 72 cells were determined to be extrinsic, uninfluenced by posture or muscle activity. This indicated that a significant number of the cells recorded within M1 played a role in processing direction.

The second mentioned report (Ben-Shaul, et al., 2003) observed the representation of PD of cells across the cortical surface by studying pair-wise PD differences and variance in the M1 area of primates during a centre out reaching task. The variance test identified that the PDs were not randomly allocated across the areas sampled, indicating that the cells responding to specific directions were grouped. This was further proven by the comparison of the PD differences of electrodes where the differences were observed to be larger for separated electrodes than electrodes adjacent to each other and smaller at the same site. This indicates that for each directional movement distinct activation groups should be visible.

The results of a study by Naselaris et al (Naselaris et al, 2006) further supports the evidence that directional processing takes place within the M1 area. The study observed how direction was represented within the spatial organisation of the arm area of the motor cortex using single cell recordings from monkeys during a 3 dimensional (3D) centre-out reaching task. The study found that while cells with a PD in any given direction were located in multiple sites across the full extent of M1, 3 mm^2 localised contiguous cortical regions were determined to contain an enrichment of representation for the same forward and backward primary directions together with a representation of all 3D reaching directions. This was compared to previous studies where cells within 80 µm diameter vertical columns and those displaced less than 150 µm were determined to represent similar reaching directions cells. Cells that were

displaced longer distances (approximately 400 µm) were also noted to represent divergent reaching directions. The study noted a dispersion of activation areas between subjects; this was suggested to be due to neuroplasticity, the expansion of areas associated with repeated movement directions possibly resulting from differences in movements learnt by the monkey. Finally, the study identified the concept of a neural substrate for translating directional signals generated by local regions based on the concept that each cell within a region makes a contribution to arm reaches in its PD by making a differentially related contribution to the activation of the group of muscles represented within and accessible by its local area.

As the previously mentioned studies were primate studies, the question to ask is do factors such as PD occur within humans? A relevant human study, (Cowper-Smith, et al., 2010) questioned this by using fMRI to observe the blood oxygen level dependant (BOLD) signal of human participants as they undertook a step tracking task controlled by wrist movements moving a joystick. The results of this study showed that the M1, premotor cortex and sensorimotor areas encoded direction in a manner functionally homogenous to non-human primates. The study also made note that the directional tuning of cells followed a cosine like pattern with cell output being halved at 45 degrees from PD. Interestingly, this study also noted how the direction of movement and the muscle groups achieving this were confounded, meaning that the brain may be encoding specific muscle groups rather than direction. Thanks to a 2003 study By Kakei et al (Kakei, et al., 2003), which identified that the majority of cells maintained their PD encoding across various wrist postures, the activations were assumed to be direction based.

2.2 The importance of goal based movement in directional processing

The indication that direction is important in motor control processing lies in the processing required to translate sensory information into an appropriate muscle output, a process essential for goal based movement. To achieve dynamic interaction

with the world around them, a human must translate the many types of sensory information they gain into the appropriate muscle output (Kalaska & Crammond, 1992). One of the main ways this is theorised to take place is through the mapping of the surroundings via the eyes into a visuo-spatial framework from which target vectors are calculated.

This process of deriving extrinsic parameters which are used to define final motor commands is described as beginning with locating where the objective of interaction is relative to the body and surrounding objects during mapping of personal space (Toxopeus, et al., 2011c). Such mapping is undertaken constantly to provide an updated mental map locating surrounding objects in the depth, horizontal and vertical axes. This constantly updated map is then used to calculate the direction vectors; it is these vectors which are used as extrinsic parameters mentioned above.

A review (Battaglia-Mayer, et al., 2003) concerning the role of eye and hand movements in neural activity provided further information concerning the reference mapping between the extrinsic coordinates of a target and the reference vector needed to move the hand. As mentioned above, the eyes are used to gain information about the distance and direction of the goal that the body is required to move towards to achieve the intended goal. In the context of a hand based reaching movement, the eyes gather information on direction via mapping that is assisted by the structure of the retina, and distance which is achieved through monocular methods such as relative size observation and binocular cues such as ocular convergence. The brain uses the information concerning direction and distance to calculate the vector the hand is required to move along to reach the target using a mentally derived frame of reference. The simplest frame used to define this vector would be a hand-centred frame only taking account of hand position, the vector starting point would not be required. To achieve this hand-centred frame, a series of remapping transformations would have to take place, in this case from the initial target coordinates to a binocular

centre-viewed frame, and finally to body and hand frames. This remapping of target coordinates would make use of retinal, extra-retinal and somatosensory information to take account of the initial coordinates of the body parts used in said frames. Error observation has revealed that the reference frame used in goal based body movements is not fixed. The reference frame used to determine the vector that is used for motor commands is determined by available sensory information, task constraints, visual background and cognitive context, with the brain making use of the least amount of remapping possible. An interesting observation in a study (Battaglia-Mayer, et al., 2003), is that direction and distance are processed in parallel to each other, as observed by the difference in memory degradation when moving to a remembered point meaning distinct direction processing areas should be present in the CNS.

Two methods have been proposed for the translation of direction from a visual space to independent movements (Baraduc, et al., 2001). The first proposed method that could lead to a correct transformation involved a linear supposition of directional solutions for each possible arm position. This method suggested that neurons were tuned to specific arm orientations, achieved via a Hebbian model which would allow transformations to occur to the visual representation or target vector for each arm position to control movement. This method was determined unlikely due to the excessive number of neurons required to achieve the transformation, which experiences an exponential increase due to the number of degrees of freedom involved in each position, and the lack of experimental evidence. The second method proposed suggested the presence of an approximating network which approximates an output from input parameters using learned information. This network would use retinal, extra-retinal and somatosensory information to approximate an output movement based on the learning experience a human has gained. The difference between this approximation and actual target location would be accounted for by error correction which is processed in parallel to the movement. This method was considered the more likely of the two, however it was lacking proprioceptive components prompting the

paper to propose a revised method that involved the use of arm position in the approximation of appropriate output.

2.3 Methods used in source localisation

By itself, EEG presents an effective temporal method for viewing activities that take place within the brain and there are many established methods, such as ERPs, for observing the progress of activations within the brain. However, to view the activations from a spatial perspective, more processing is required. Most studies observing the location of spatial activations within the brain make use of fMRI to detect the changes in blood flow caused by the activation of the neurons during a task. The result of which is an indication of areas of the brain active during a task with good spatial but poor temporal resolution. As fMRI uses expensive equipment that is large and involves long scanning times, fMRI can prove impractical for some investigative activities into the processes of the brain. Source localisation presents a method by which the spatial location of activations within the brain can be predicted by solving the 'inverse problem' using recordings from EEG electrodes placed on the scalp. Such results provide greater temporal resolution at the cost of spatial resolution, and a greater number of feasible tasks that a subject can undertake while being recorded.

A large body of information concerning the source localisation of EEG is provided in a recent review (Pizzagalli, 2007), which described recent advances in the EEG Field. The main limitation noted regarding source localisation of EEG is the distortion of spatial locations. This can be attributed to: limited spatial sampling due to the number of electrodes, poor signal to noise ratio, the distorting effects of the different tissue types the signal from the electrical generator passes through before reaching the recording electrode, and the neuromagnetic 'inverse problem' where there are an infinite number of possible solutions for the location of generating sources of signals. These distorting effects are solved through the application of physiologically sound assumptions to the processing of results. The forthcoming paragraphs will discuss

solutions and recommended methods of implementing the solutions (Pizzagalli, 2007), followed by some examples of how source localisation was achieved in recent studies.

The minimum number of electrodes recommended for adequate spatial sampling is 60, with greater numbers recommended due to the increased spatial resolution granted by high density recordings. Electrode number is limited by subject discomfort and application time, resulting in a trade-off between electrode number and the comfort of subjects. Regardless of these concerns, a uniform homogenous covering of the scalp is of great importance. Accuracy can be improved further with the measurement of electrode position, for example with a digitiser. Presence of corrupted channels either due to excess artefacts or technical malfunction must be taken in to account as source localisation is heavily reliant on full electrode coverage. Two suggested methods of dealing with corrupted channels are: linear interpolation, which uses a weighted average of nearby neighbours; and spline interpolation, which uses the calculated potential distribution across the entire scalp from all the sensors to predict the values of the missing channels. Spline interpolation is recommended as the most effective method as linear interpolation has less accuracy due to fewer electrodes being used and ignores the maxima and minima of the data. Choice of reference electrode is noted to bear little influence on spatial analysis.

The majority of noise detected in EEG is due to artefacts caused by electrical activity of non-cerebral origin, thus reducing the effects of artefacts improves the signal-to-noise ratio of EEG. Artefacts result from artificial sources such as 60/50 Hz power line noise, or physiological sources which are recorded by electrocardiography (ECG), electrooculography (EOG), and EMG. Artificial noise including power line noise can be removed simply with the application of a notch filter, grounding and pre-digitisation filtering, but physiological noise is more difficult to deal with. As physiological artefacts occur randomly they are most often detected and rejected via visual identification, this is due to the artefacts being intermixed with EEG data resulting in loss of information if

filtered out. A suggested method of dealing with such artefacts is via Independent Component Analysis (ICA) which can be used to remove components resulting from artefacts present within the data.

The final two sources of spatial distortion, the attenuating effects of the brain, cerebrospinal fluid, skull and scalp and the neuromagnetic inverse problem can be solved via the choice of head model and source localisation method used during source localisation.

The choice of head model determines the assumed conditions between a detected source and the signal recorded at the scalp, thus the closer these conditions are to reality the fewer distortions are unaccounted for and the more constraints placed upon the inverse model when determining conditions. This results in the choice of head model being a balance between accuracy and processing speed. There are 3 types of head model, listed in order of simplicity: the sphere head model which models the scalp brain and skull and sometimes cerebral spinal fluid (CSF) as 3 or 4 homogenous spheres; BEM which models the head as a collection of homogenous compartments taking into account realistic head geometry; and the FEM which uses a map of the head made from inhomogeneous compartments to model the effect of real tissue with anisotropic properties. More complex models are recommended as they provide conditions closer to the physiological conditions of the head, however they involve more processing as their complexity increases.

The source localisation method determines how the inverse problem is solved. There are two general methods: dipole analysis techniques and linear distributed source techniques. Dipole techniques are a basic method that assumes a specific number of sources which represent patches of grey matter containing approximately 10,000 simultaneously activated, parallel pyramid cells. Dipole analysis can involve different methods which can be determined by the amount of parameters they allow to vary, such as moving dipoles which allows all parameters to vary, or rotating dipoles which

constrains the location to a single point but allows orientations and strength to vary. A persistent flaw with dipole driven methods is the hypothesis driven manner in which sources are determined. The number of sources is arbitrarily chosen and determined by the anatomic feasibility of the solution resulting in the sources selected possibly not being the intended source. The number of sources could possibly be determined via Multiple Signal Classification (MUSIC), which breaks down signals into their underlying components to determine the number of components involved.

Linear distributed source localisation techniques assume that all areas of the brain are active at once, a more physiologically likely statement and so instead of determining the location of sources involved; the contribution of each area to the detected potentials is calculated instead. As this leaves the inverse problem unsolved further calculation methods are needed to achieve source localisation. Methods that have been determined to be spatially accurate are Low Resolution Electromagnetic Tomography (LORETA), standardized LORETA (sLORETA), Variable Resolution Electromagnetic Tomography (VARETA), Local Auto-Regressive Average (LAURA) and Bayesian solutions. LORETA is currently the most commonly used method in labs, and has been identified to provide spatial resolution with little blurring. However, it has been found to be unable to distinguish sources of activity that are in close proximity to each other, blurring focal sources. VARETA is able to estimate discrete and distributed sources with equal accuracy, however substantial blurring has been observed to be present. LAURA has been shown to detect multiple simultaneously active sources in simulation. Bayesian solutions incorporate prior information into various models to provide an accurate method of localisation even in the presence of noise providing promising results. There are a number of examples of recent studies involving source localisation (Knyazev, 2013; McMenamin, et al., 2010; Plummer, et al., 2010).

The first report (Knyazev, 2013), compared the discrepancies between EEG and fMRI data. Two approaches to ICA were compared: standard temporal analysis via EEGlab (a

Matlab compatible neurophysiological analysis toolbox), and fMRI-based spatial analysis applied to sLORETA results. Source localisation was achieved via equivalent dipole methods. The EEG data was processed using a temporal ICA to remove artefact components by only retaining components which were less than 15% of the residual EEG value. The processed data was used for equivalent dipole analysis, the correct number of dipoles was determined via cluster tightness, a calculation of the mean distance from each dipole to the dipole cluster centroid, solutions with higher tightness values were selected. The results were compared with the results of spatial ICA performed on sLORETA of the raw EEG data. The report concluded that both methods were similarly effective for observing widely distributed sources but the temporal method was better for analysing two closely spaced sources oscillating at different frequencies.

The second report (McMenamin, et al., 2010) investigated the validity of ICA in removing EMG artefacts for source localisation by simulating the injection of real or artificial EMG activity into an otherwise artefact-free EEG. The resulting signal was observed in the alpha band and PCA was used to reduce the number of components before input into ICA. Multiple rejection criteria for ICA filtering were tested depending upon the level of EMG activity and filtering of non-myogenic signals. Source localisation was achieved using LORETA, making use of a 3 sphere head model normalised to a standard anatomical template from the Montreal Neurological Institute (MNI). The report found that while source localisations containing uncorrected EMG activity were sourced near the muscular origin of the EMG artefact, ICA was inadequate for removal of EMG components when concerning a source space. Reasons for this observation were suggested to be due to an invalid specification of the number of components used in analysis or a violation of key assumptions of the ICA algorithm during processing.

The final report (Plummer, et al., 2010), assesses the clinical utility of non-invasive EEG source modelling in focal epilepsy, to address concerns over a lack of clinical literature comparing the performance of multiple source localisation types across the same patient cohorts. The study observed the effect of model choice on: orientation; location; and Current Source Density (CDR) of sources of commonly known epileptic spikes. Before source localisation was applied, EEG data was epoched 200 milliseconds prior and 500 milliseconds post spike peak and the resulting signals were filtered using a 50 Hz notch filter and 0.5-70 Hz band pass filter. Electrode positions were label-matched and co-registered using predefined electrode locations for realistic models (MNI sourced). Components within the signals were identified using principle component analysis (PCA) which then underwent Independent component analysis (ICA). The 5 resulting components for each subject were electrographically averaged and used for source localisation. The study compared 3 head models: BEM, leadfield-interpolated BEM (BEMi) and leadfield-interpolated FEM (FEMi); 4 inverse models: LORETA, sLORETA, Minimum Norm Least Squares (MNLS) and minimum L1 norm; and 4 subspace constraints: whole volume (3D), cortex with rotating sources (CxR), cortex with fixed sources normal to cortex (CxN), and cortex with fixed extended sources with 30 mm patch (patch). The results of the study indicated that the head model had the least impact on the best fit CDR result used to assess the models, with FEMi and BEMi producing similar results. Choice of inverse model had greater impact: sLORETA was the most consistent, L1 was found prone to scattering detected locations, LORETA performed poorly under more anatomically informed subspace constraints, and MNLS solutions were determined to be weak and difficult to resolve qualitatively. The subspace constraints chosen where determined to have great impact on CDR maps, with patch providing a dominant effect making it recommended out of the constraints used, notably CxN solutions were fragmented and difficult to interpret and CxR provided implausible solutions.

2.4 Summary of literature review and statement of aims

The purpose of this study was to pilot the processes that can be used to determine, using non-invasive electrophysiological evidence, whether the activations detected in the M1 area of the motor cortex are organised depending upon the direction of the movement it is processing. It has been discovered through fMRI studies (Toxopeus et al, 2011a) that during the processing of wrist movements the areas that activate within the motor cortex for each direction of movement are spatially distinct. This is concurrent with the internal model theory where a 3D visuo-spatial framework (Battaglia-Mayer, et al., 2003) is used to develop target vectors for goal based movement (Kalaska & Crammond, 1992). However as the experimental method used in the Toxopeus study only observed movements with the forearm in one orientation (midway between pronation and supination), the activated muscles and direction of movement were not disassociated from one another. Therefore the reason for the spatial distribution observed may be due to the specific muscle groups that are used during the movement.

Information gathered from primate studies, which have been determined to encode direction in a manner functionally homogenous to humans (Cowper-Smith, et al., 2010), indicated that cells which were involved in the processing of direction were found in the premotor cortex. These cells were not randomly allocated (Ben-Shaul, et al., 2003) and were observed to be in vertical columns which represented similar reaching directions (Naselaris, et al., 2006). This was the organisation that was suspected to have been observed in the study (Toxopeus, et al., 2011c) which indicates that in humans there is more processing involving direction in the primary motor cortex than described in textbook definitions (Martini, et al., 2012).

This pilot study evaluated a proposed method to confirm whether the spatially distinct distribution of activations that is detected within the M1 wrist area during wrist movement can be attributed to either the processing of specific directions or the

processing of the specific muscle groups used to achieve the movements. To confirm this, either the activated muscle pattern or the direction of goal based movement will have to be altered while keeping the other the same to allow disassociation of the muscle group from direction. Spatial location of M1 activity associated with activated muscles will be detected via source localisation using recorded scalp EEG data. Methods used will be based upon a review (Pizzagalli, 2007) which provided a large body of information concerning the source localisation procedure.

3. Methods

3.1 Experimental paradigm

For this study a modified version of a predefined motor step tracking task similar to the method used by Kakei et al was used (Kakei, Hoffman & Strick, 2003). This task was used extensively to gather data in a number of other studies (Toxopeus et al, 2012; Conway, Reid & Halliday, 2004; Toxopeus et al, 2011a; Toxopeus et al, 2011b). The aim of the modified protocol was to provide a motor related cortical potential which can be observed using EEG that dissociates the muscles used to perform a movement from the external reference frame used to define the direction of the movement. The protocol was further modified after pilot experiments revealed that the original method of disassociating muscles from movements, by altering the subjects forearm posture between fully pronated and midway between pronated and supine, caused minimal changes to the muscle pattern used to achieve directional wrist movements thus insufficiently disassociating muscle pattern used from direction. The final protocol involved changing the orientation of the forearm from fully supine to fully prone which was required to adequately dissociate the muscle activations from the movement direction. Appendix C provides details of the pilot experiments that investigated various orientations of the forearm. Appendix D details the changes made to the experimental paradigm due to the results of the EMG pilot.

The final task involved the participant executing a rapid wrist movement from a neutral position to one of 2 targets that appeared at either the 6 or 12 o'clock positions. Movement of the wrist within the manipulandum was transduced and displayed as a cursor on the screen, providing the participant with feedback on the movement. Each target was positioned 30° of angular wrist displacement from the central, neutral position. The participant was required to execute ballistic movements to the new targets when they appeared, ensuring a feed forward movement which made use of an internal model necessary for accurate movement. This task was repeated twice by the

participant using different forearm orientations: fully pronated and fully supinated, to disassociate movement direction with muscle pulling direction during the task. To allow observation of EEG activity with reference to the muscle movements themselves, EMG was used to record movement onset times which were used to derive epochs from the recorded data.

3.2 Participants

For this kind of study, participants should be healthy young volunteers of similar age. Should this pilot study successfully identify a viable protocol, a full study with 20 participants should be carried out to mimic the number used by the study (Toxopeus et al, 2011b). Participants should be screened beforehand to remove those with underlying neurological conditions, e.g., neurological damage or epilepsy. Additionally, participants who have experienced injury resulting in motor neuron damage should be removed as neuroplasticity will result in a change of the somatic repression of the motor cortex (Sanes, et al., 2007). Subjects with learning difficulties such as Dyslexia or Dyspraxia should also not be included as differences in neural processing may affect results. All subjects should have normal or corrected vision. EEG data containing excessive noise such as movement and blink artefacts should be ignored.

Prior to experimentation, the process should be explained to the participant and written consent should be obtained.

The data gathered during the development of this experiment was recorded from 3 healthy volunteers. Two of the volunteers participated in the EMG pilot experiments described in Appendix C. All subjects reported no history of neurological problems and only minor, if any; visual impairments which were not in need of correcting. Subject 02 was reported to possess a motor learning disability called Dyspraxia, which can be described as an “impairment or immaturity of the organisation of movement” (Dyspraxia Foundation, 2013) which may cause anomalies within the results. Informed written consent was obtained from each participant.

3.3 Experimental design and setup

3.3.1 Final design of task

Participants were asked to respond to the appearance of targets on a screen in front of them, a cursor controlled by a manipulandum of similar design to the one used in (Toxopeus, et al., 2011a), was visible onscreen. After positioning the cursor in the centre target, a second target was displayed at one of the 2 positions: 0° and 180°; corresponding to the 12 o'clock and 6 o'clock hours on a clock face. Figure 18 displays how these targets are presented on the computer monitor. After the appearance of the target, the subject was instructed to execute a rapid wrist movement in the direction of the new target. The target remained visible for 2 to 3 s before disappearing again. The participant was instructed to keep the cursor in the target while it was visible, and once it had disappeared to slowly move the cursor back to the central position, after which the next trial started. The participant completed 200 movements per block throughout which EMG and EEG data were recorded. The orders in which the targets appeared and the delay before the target appeared was randomised to prevent the participant from becoming habituated to the task.

The cursor was controlled by a manipulandum which transduced angular displacement of the wrist around 2 axes, displayed in Figure 17 a),b). Displacement of the manipulandum was registered by two potentiometers. The output of the potentiometers was calibrated such that the position show in Figure 17 was defined as zero degrees and the cursor could be moved to the targets with clearly defined movements.

After completing the required number of trials in the first orientation, the manipulandum handle was rotated by 90^{o}, resulting in a change of orientation of the forearm from fully supinated to fully pronated, as shown in Figure 17, and the task repeated a second time.

a) 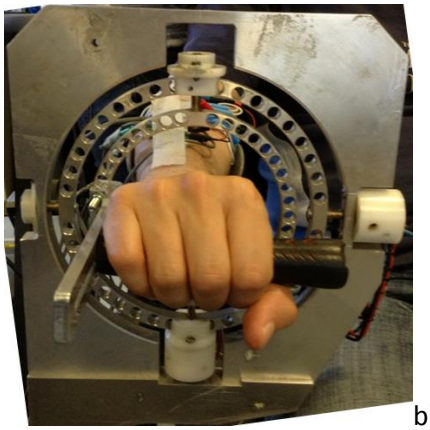 b) 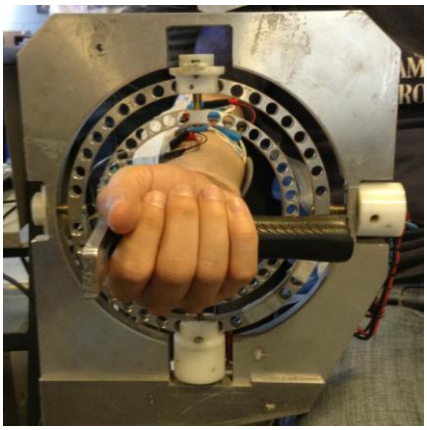

Figure 17 Final experimental setup

a) Image of manipulandum with forearm fully pronated, grasping the handle; b) Image of manipulandum with forearm fully supinated, grasping the handle.

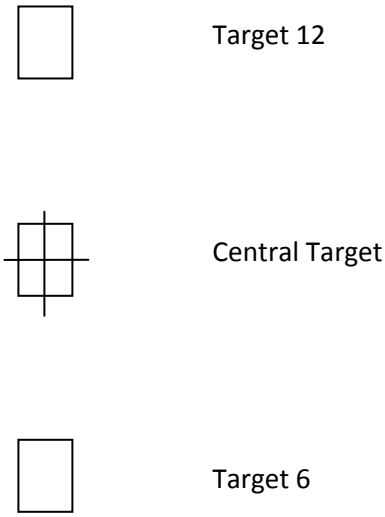

Figure 18 Target display used in task

3.3.2 Final experimental protocol

Before the start of each experiment, participants had 14 EMG electrodes attached to their right forearm: Extensor Carpi Radialis Longus, Extensor Carpi Radialis Brevis, Extensor Carpi Ulnaris, Flexor Carpi Radialis, Flexor Carpi Ulnaris, Flexor Digitorum Profundus and two electrodes to act as ground. The wires connecting the electrodes were taped to the arm to prevent artefacts generated by movement of the wires. Figure 19 displays these positions.

Participants were asked to sit in a comfortable chair and rest their arm on a support and grasp the manipulandum, with the thumb taped to the fingers to prevent movement of the fingers and improve the comfort of the participant; Figure 22 displays the setup for the experiment. Participants performed the step tracking task grasping the manipulandum in a pronated orientation as shown in Figure 17a, after the second position and the task was repeated a second time with the manipulandum grasped in a supine position as shown in Figure 17b. Two computers were used in this experiment; one computer ran the experimental control and EMG data acquisition while the other computer was used for the acquisition of the EEG data. The EMG analogue-to-digital (ADC) converter generating timing pulses related to the appearance of the targets that were also used to synchronise the EEG data and time locked it with the EMG data.

EEG recordings were made using a NeuroScan Synamps^2 system and Curry 7 software (Compumedics Limited, Abbotsford, Victoria Australia). An EEG cap using Ag/AgCl electrodes was used to record the data. While a cap using 256 channels was available, a 64 channel cap was used due to time constraints. Electrodes were positioned on the elastic cap in the positions shown on Figure 21. The electrode positions were in accordance with the extended international 10-20 electrode placement system (Figure 20), where electrodes are placed at either 10% or 20% intervals in the transverse and medial plains of the skull. The electrode Cz was positioned at the vertex of the scalp at the central intersection of the sagittal and coronal planes. This is found by locating the

position midway between the naison and inion, and midway between the two pre-auricular points.

EMG was recorded using Ambu Blue Sensor N single patient use electrodes (Ambu, Ballerup, Netherlands). The electrodes were connected to preamplifiers which were attached to a Neurolog rack (both from Digitimer Ltd, Hertfordshire, England). The Neurolog rack was connected to a Micro 1401 ADC (Cambridge Electronic Designs (CED) Ltd, Cambridge, England) which connected to the computer system recording the EMG results. The EMG results were recorded by the Spike2 software, the same program that ran the step tracking task, also produced by CED.

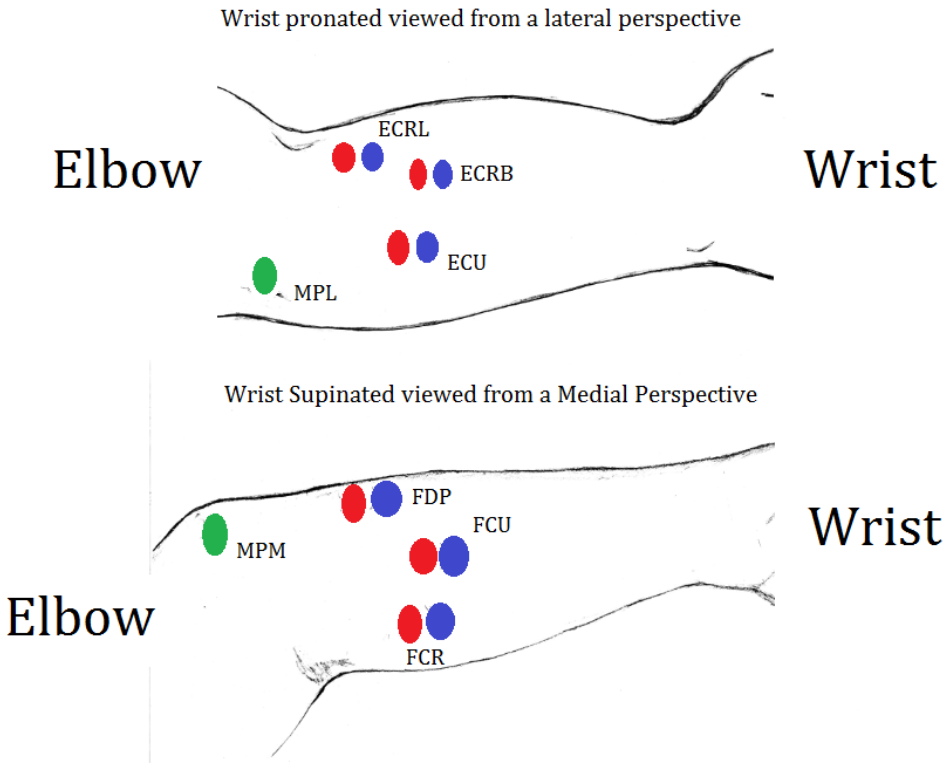

Figure 19 Final Position of EMG electrodes

Green electrodes represent reference electrodes that were attached to the processes of the humerus (MPM, MPL); Red electrodes represent positive lines while blue electrodes represent negative lines. Electrodes were used in pairs and placed over: Extensor Carpi Radialis Longus (ECRL), Extensor Carpi Radialis Brevis (ECRB), Extensor Carpi Ulnar (ECU), Flexor Carpi Ulnar (FCU), Flexor Carpi Radialis (FCR) and Flexor Digitorum Profundus (FDP).

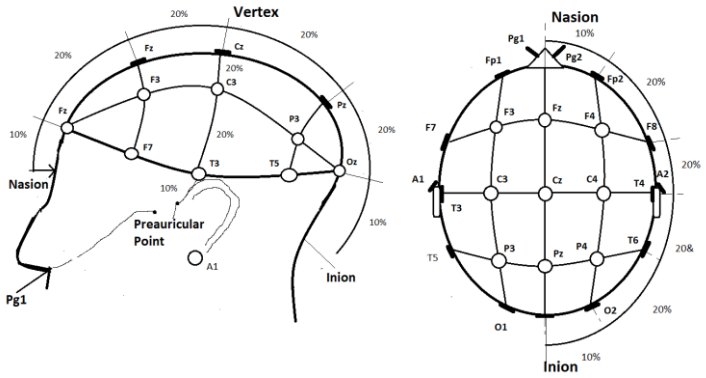

Figure 20 Location of electrode placement according to international 10-20 System

Based upon figure from: (Saeid Sanei, 2008)

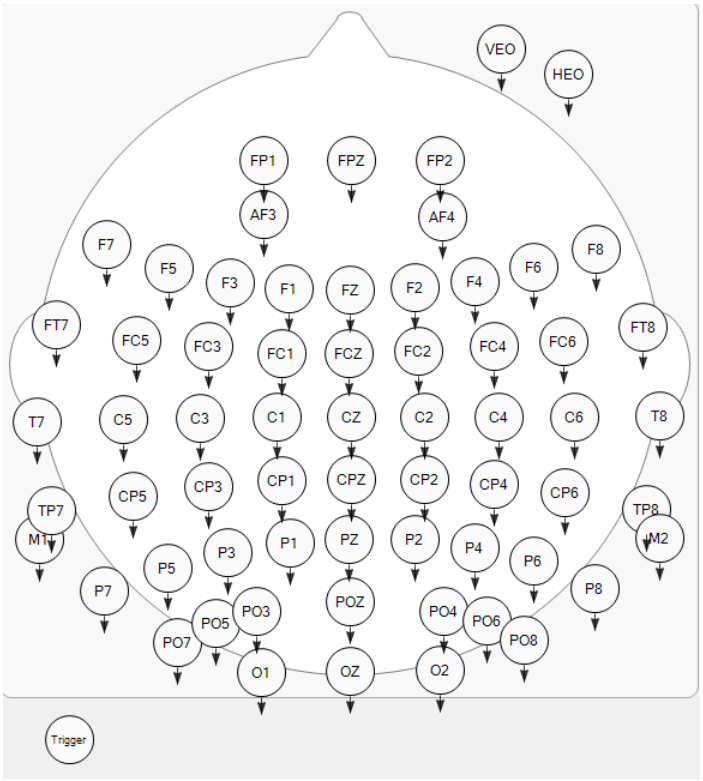

Figure 21 SynAmps2 Quick-Cap 64 channel Montage, used in study

Figure shows a plan view of electrode positions taken from the Curry 7 Interface. The nose is at the top of the figure and the ears are to the sides allowing electrode position to be viewed in comparison to the location of these features. Electrodes are represented as circles containing electrode name the arrows indicate which electrode the electrode is being referenced against. In this montage electrodes are being referenced against the common average of all electrodes as indicated by downwards pointing arrows which are not connected to any other electrodes.

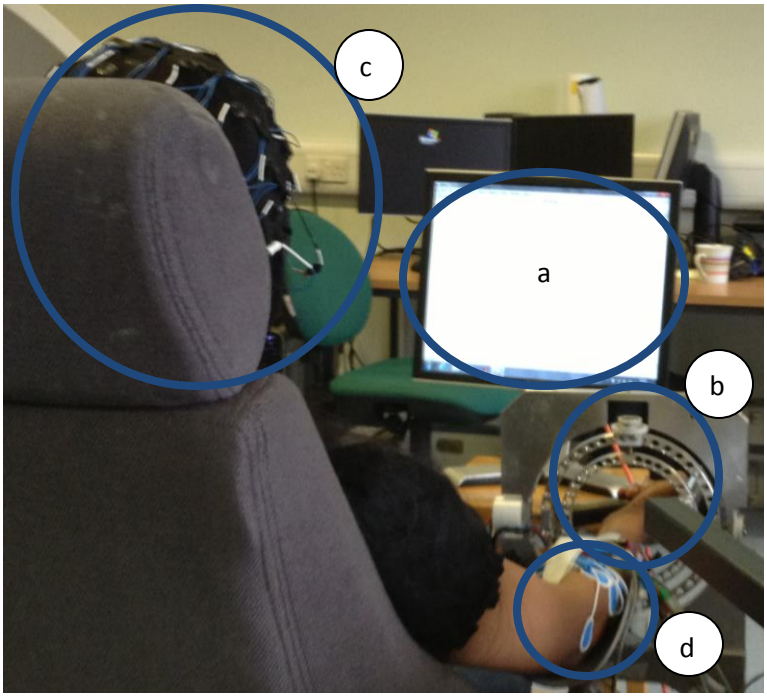

Figure 22 Subject 03 undertaking experimental task

Figure 22 displays a photograph of one of the subjects undertaking the final experimental task. The photograph is taken from behind and displays: a) the screen used to display the task, b) manipulandum in use, c) cap used to take EEG results, d) electrodes used to record EMG during task.

A cursor controlled by the use of the manipulandum (b) is visible on screen (a) to the subject. As the subject moves the cursor to respond to targets on screen potentials caused by muscle use are recorded through the EMG electrodes (d). During the experimental procedure the EEG cap (C) records neural activity which is used to observe neural phenomena of the subject during the experimental task.

3.4 Data processing

Prior to analysis, data was pre-processed to time-lock EEG data to the intended direction and to remove artefacts within the data to allow effective source localisation. During the task the impedance of a number of electrodes was too high to use, resulting in large amounts of environmental noise in said channels. Additionally, large artefacts were caused by eye blinks, muscle movements and saccades (small eye tracking movements) which had to be identified and removed. One of the aims of this study was

to determine the optimal pre-processing procedure to produce high quality data for further analysis.

3.4.1 Spike2

EMG data was recorded from the Extensor Carpi Radialis Brevis, Extensor Carpi Radialis Longus, Extensor Carpi Ulnaris, Flexor Carpi Ulnaris, Flexor Carpi Radialis and Flexor Digitorum Profundus. Electrodes on the bony processes of the elbow were used as a reference.

Spike 2 recorded the EMG data and output from the potentiometers of the manipulandum, the results of which were used to calculate the manipulandum angular displacement which was used to control the on-screen cursor during the event related task.

During the task, the appearance of the targets was recorded as an event and the same event was sent to the Neuroscan system as a transistor-transistor logic (TTL) pulse, to synchronise the EEG data with the EMG and events.

To allow observation based on onset of movement, EMG can be used to track the beginning of the movements from which an event list can be generated for the EEG data.

Processing of data took place within the Spike 2 program. Figure 23 displays an example of how EMG results are displayed in Spike 2. The EMG results were rectified and averaged using in functions of the software. Averages were taken using a mean of all results for each specific direction 0.2 seconds pre-stimulus and 0.5 seconds post stimulus. 4 graphs were produced for each trial; 2 graphs representing the average EMG for each direction of movement while fully supine and 2 graphs representing average EMG for each direction of movement when fully supinated.

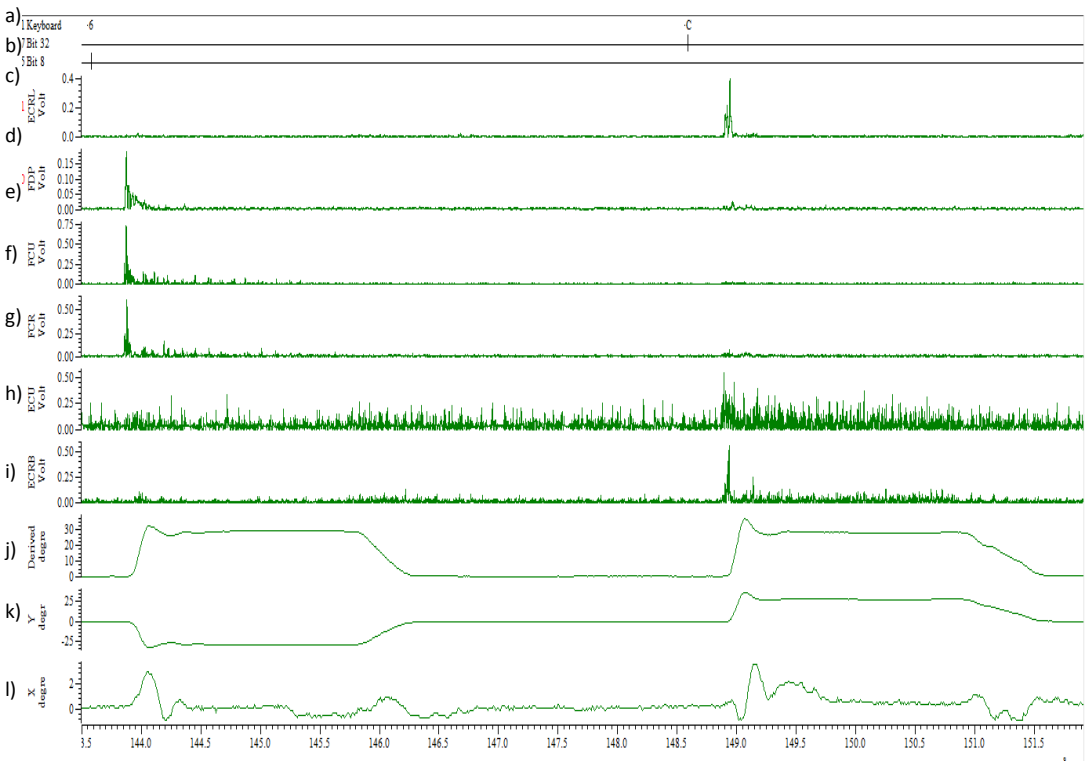

Figure 23 Spike 2 example display of raw data

Results display of spike 2 data displaying: a) target code; b) digital marker for target 12; c) Digital marker for target 06 d) EMG recordings of Extensor Carpi Radialis Longus (ECRL) activity during experiment; e) Flexor Digiorum Profundus (FDP) activity during experiment; f) Flexor Carpi Ulnar (FCU) activity during experiment; g) Flexor Carpi Radialis (FCR) activity during experiment; h) Extensor Carpi Ulnar (ECU) activity during experiment; i) Extensor Carpi Radialis Brevis (ECRB) activity during experiment; j) Derived angular displacement from centre activity during experiment; k) X axis angular displacement from centre, l) Y axis angular displacement from centre.

3.4.2 Neuroscan

EEG data was processed using Curry 7 from Neuroscan. Figure 24 illustrates the Curry 7 interface, showing an example of the results display of all channels.

The EEG electrodes were physically referenced to a linked ear reference, but then re-referenced to the common average of all the EEG electrodes.

EEG electrodes with overly high impedance (arbitrarily set to above 100kΩ) were interpolated from the surrounding functioning electrodes using a difference weighted average to allow more effective source localisation.

Common baseline correction was applied to the EEG channels to remove any direct current (DC) offset or signal drift before processing.

Template matching was used to identify artefacts such as muscle or eye movements by visually selecting archetypal artefacts within the data. The properties of the selected archetypal artefacts were then used to identify similarly shaped artefacts throughout the continuous raw data. The most obvious source of artefacts was the EOG channels, often caused by eye blinks or eye movements, so template matching and other artefact detection methods such as threshold analysis available in the Curry 7 software were applied to the horizontal electro-oculogram (HEO) and vertical electro-oculogram (VEO) eye channels to detect artefacts for rejection. The majority of these EOG artefacts could be detected using a $\pm 150 \mu V$ threshold, a method which was applied to identify many of the artefacts identified in this study. A particular type of eye movement artefact was present during the task, and time-locked to the movement to the new target. These were identified as saccades, fast involuntary eye movements time locked to the stimulus appearance. The effect of saccades and how to deal with them will be discussed later in this thesis (section 4.3).

Once identified, the influence of artefacts that were determined to be an unavoidable part of experimental procedure was reduced by artefact reduction methods present within the software. Methods used were: covariance, which subtracts a coefficient of the artefact signal from the other electrodes depending on the distance from the artefact channel; subtraction, which removes a rolling average of the defined artefact from each channel; and independent component analysis (ICA). The effect of these on the EEG data will be discussed later in section 5.3.2 and section 5.3.3.

Once artefacts in the raw data were reduced, the altered data was epoched using the trigger events sent from the Spike2 system. Epochs were taken 200 ms prior to and 500 ms post event; epochs were saved separately for each trigger type to allow observation of EEG activity associated with each movement direction.

The epochs for each movement direction were analysed separately: epochs containing artefacts were visually identified and removed by observing the time domain signals and spatial distribution maps.

Averages were taken for each movement direction from the processed data; these averages were then used in source localisation and ERP analysis.

An alternate artefact reduction method present within the software was to apply ICA or PCA to the epoched data instead of the raw data. This presented a method of removing components of the original channel based on the spatial distribution across the scalp, allowing identification of artefacts originating from concentrated frontal EOG as well as peripheral EMG sources.

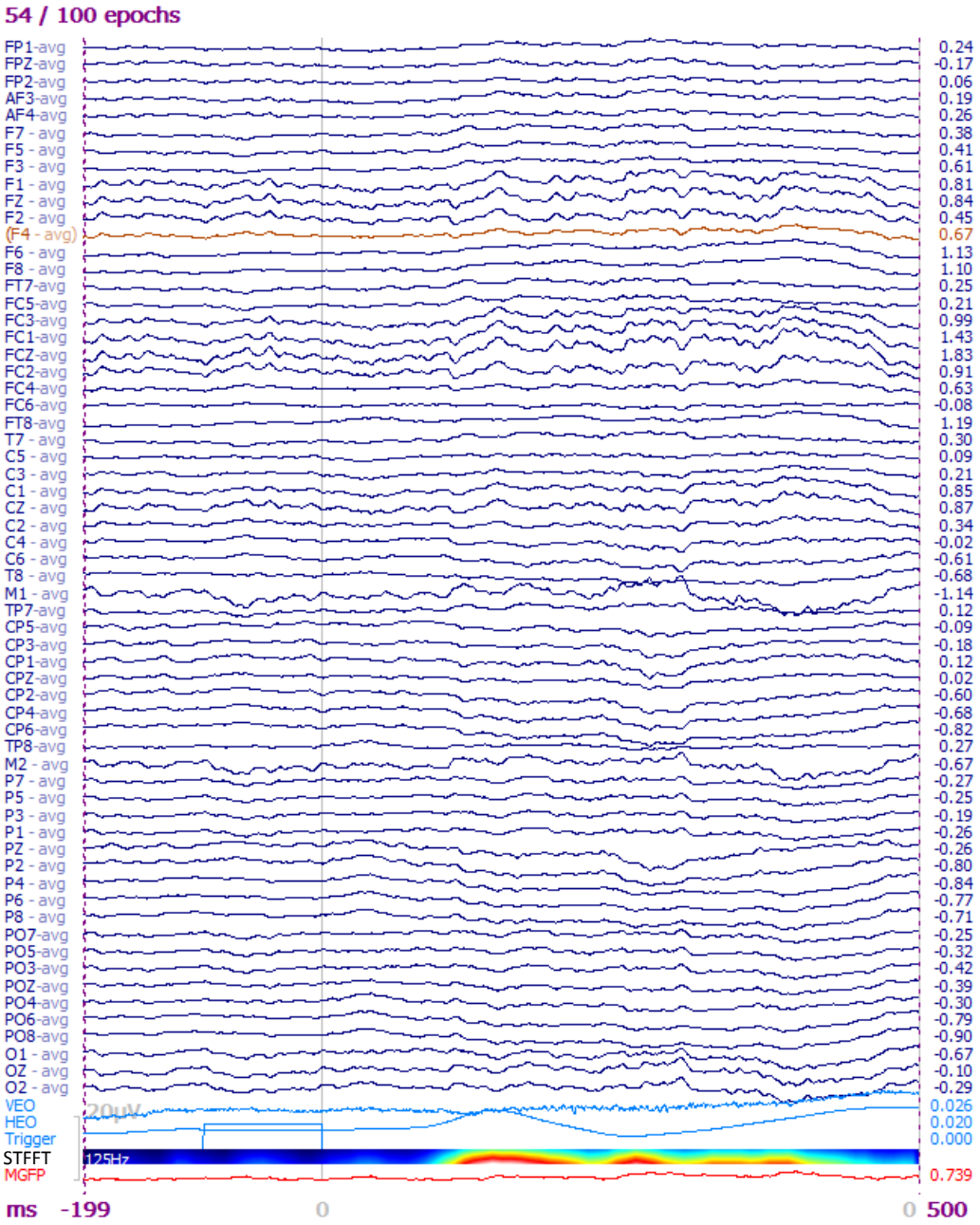

Figure 24 Example of the Curry 7 interface displaying averaged epoch of all channels used

Figure displays an example of the Curry 7 interface showing an epoch of EEG data All EEG channels are listed in order including, HEO, VEO and trigger channels. Channels are displayed as potential difference (V) vs. time (s) graphs. The final two graphs show the STFFT of the data (displayed as a frequency spectrogram) and global field power of channels (displayed as potential difference (V) vs. time (s) graph).

3.4.3 Source localisation

Curry 7 was also used for source localisation. Predesigned FEMi models, such as the model displayed in Figure 25, from within the software were used during this experiment to apply dipole and linear source localisations to the experimental data.

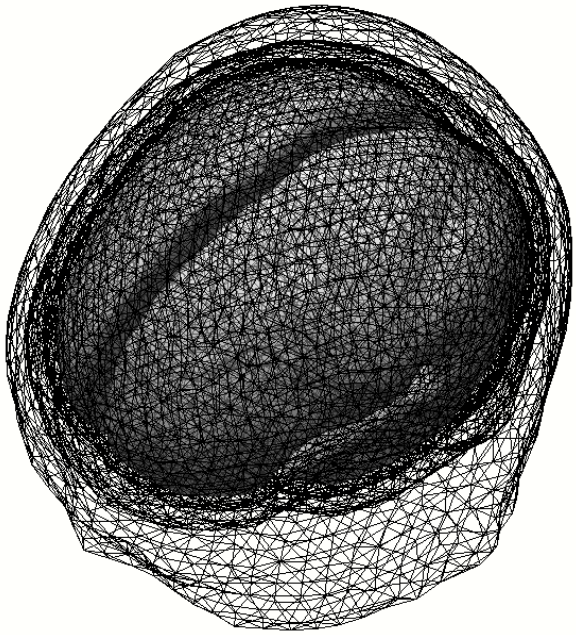

Figure 25 FEMi model use in source localisations

Originally this study intended to use both linear equivelent dipole and current source density analysis (examples of which are displayed in Figure 26) to observe the distributions and determine the validity of both methods towards the experimental paradigm. However, due to software error and time constraints only equivilent dipole analysis has been performed. A comparison between moving, rotating and fixed ICA dipoles can be found within section 4.6.

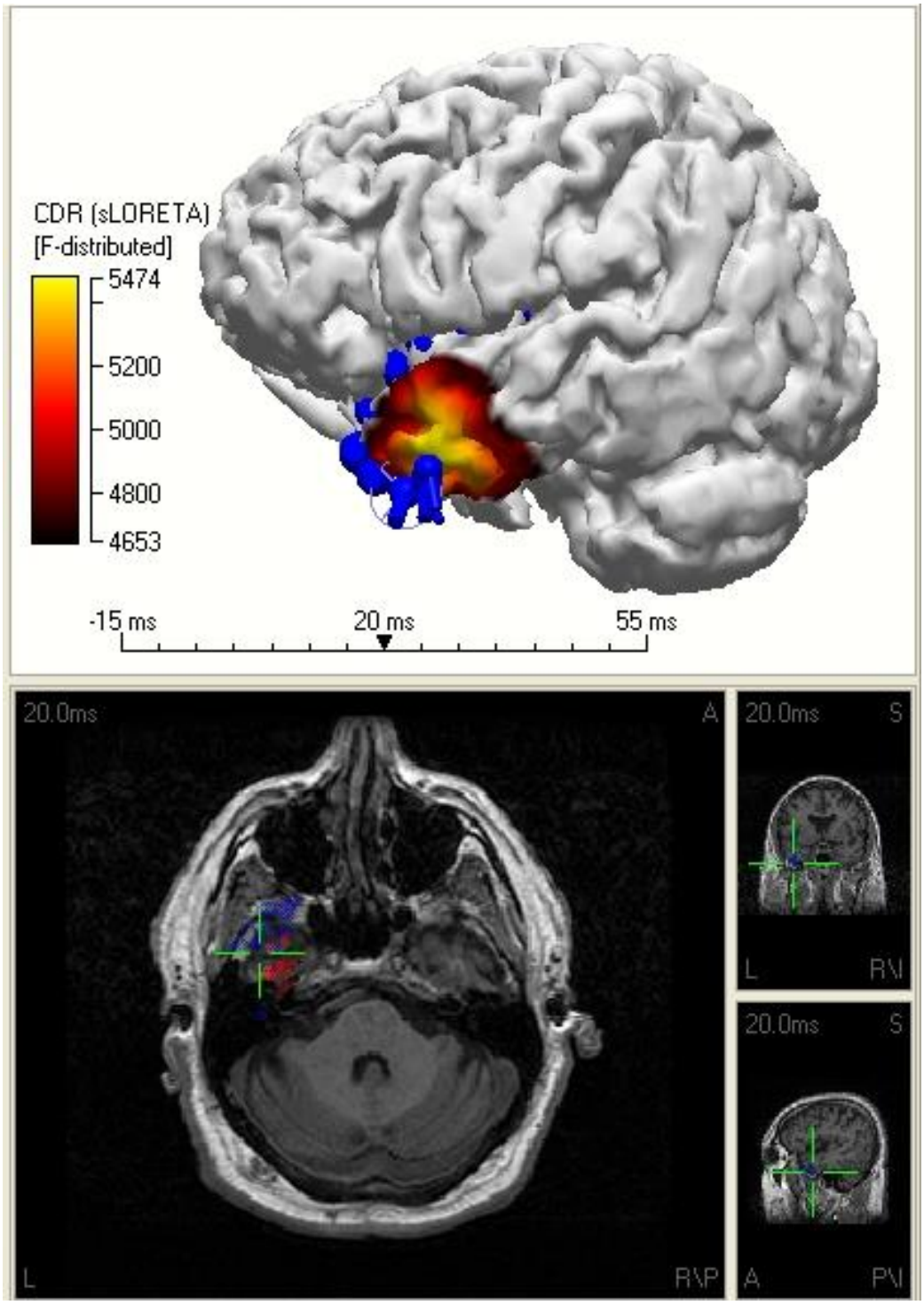

Figure 26 Example of a source localisation with Curry 5 software

Example source localisations linear and dipole for curry 5 software. Source localisations are displayed on 3D model and MRI images. Linear localisations can be observed as patches of colour while dipole localisations can be observed as speres present throughout the structure.

4. Results

This chapter will provide details on the results of the experiments used in this study.

4.1 Subject selection

As stated in section 3.4.2, Curry 7 software was used to epoch continuous EEG recordings between 200 milliseconds prestimulus and 500 milliseconds post stimulus. The epochs were then baseline corrected and epochs containing artefacts were removed. Table 2 displays the number of accepted epochs for each movement direction stimulus. The data observed for the remainder of this study was based wholly on subject 01 due to this being the only recorded data to possess more than 50 acceptable epochs for each direction. The recording from subject 02 had a large number of blink artefacts reducing the amount of EEG epochs available, and the detachment of a number of the dorsal electrodes during the scanning of subject 03 resulted in the data being unreliable. Interpolation methods could not recover the data from the electrodes in subject 03, as there were physical breaks in the wires connecting the electrodes to the amplifier.

Table 2 The number of accepted epochs for each subject

Subject and forearm orientation	**Number of accepted epochs for response to specific target**	
Subject 01	**Target 06**	**Target 012**
Pronated	52	50
Supinated	54	51
Subject 02		
Pronated	28	33
Supinated	18	32
Subject 03		
Pronated	62	50
Supinated	55	46

4.2 Electrode interpolation

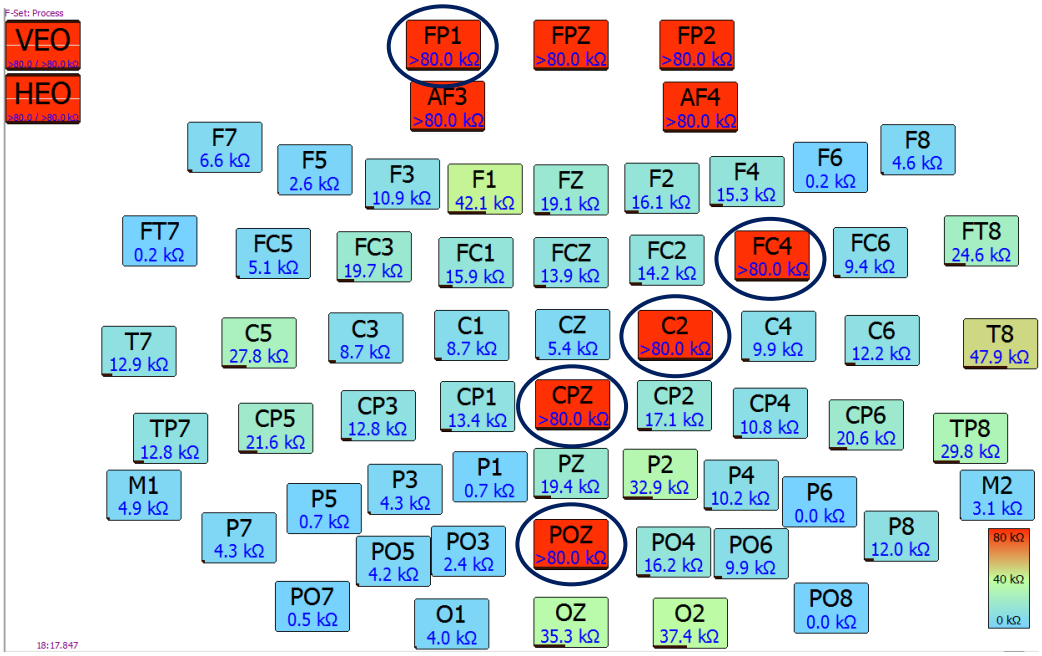

Figure 27 Curry 7 interface displaying electrode impedances

The impedance value of each electrode is displayed in a topographical layout with the nasion to the top. Impedance is displayed as a colour scale (bottom right) from 0 kΩ in blue to 80 kΩ in red. Electrodes with impedances greater than 80 kΩ are circled, these channels required interpolation for further analysis.

During scanning, electrodes F1, FC4, C2, CPZ and POZ (displayed in Figure 27) consistently displayed very high impedances across all participants, and potentially indicated damage to the electrodes. Due to these impedances, the electrodes were interpolated using a linear interpolation function that was present within the Curry 7 software. The 8 surrounding channels, excluding any of the other high impedance channels, were used to generate a distance weighted average which was used to generate 'replacement channels'. This action was taken rather than deselecting the electrodes as discarded electrodes can have a large effect on source localisation (Pizzagalli, 2007).

4.3 Saccades observed during task

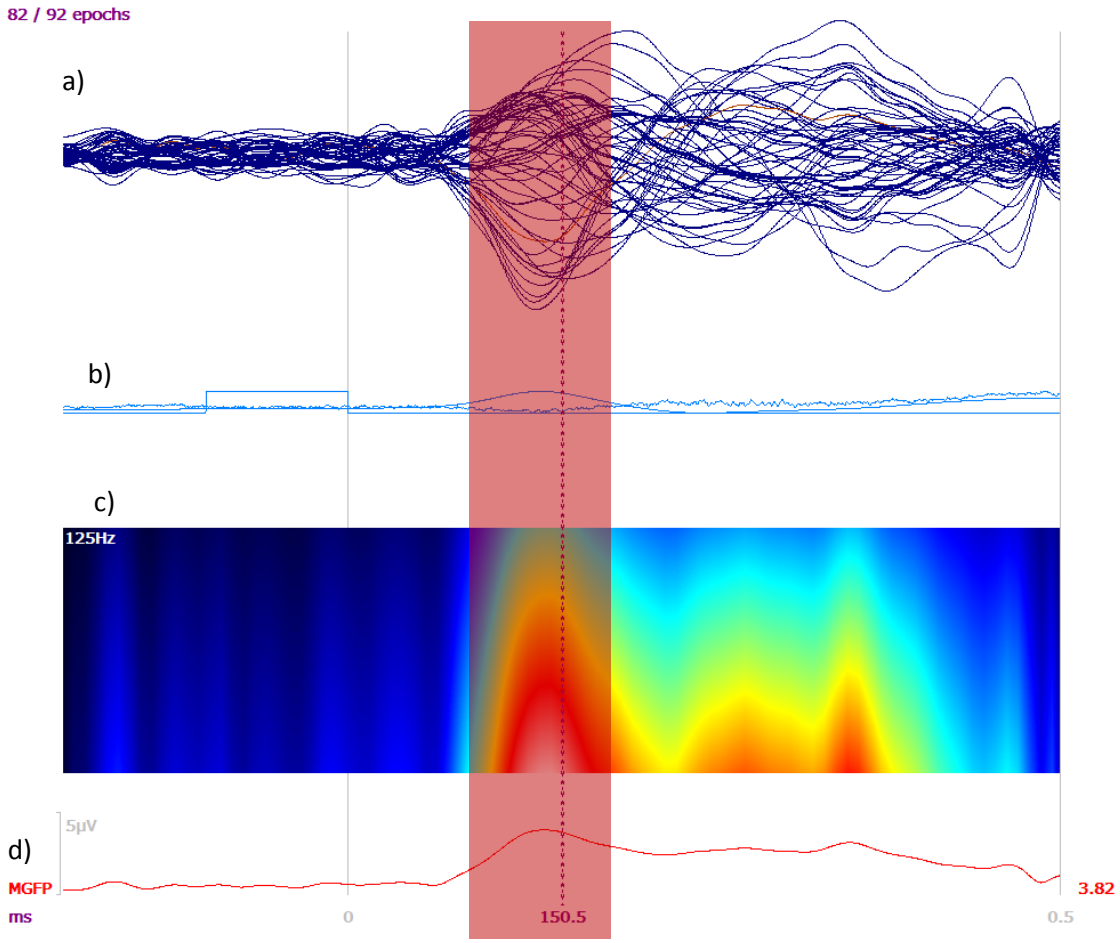

Figure 28 Filtered average of activity in one movement direction

Four graphs are displayed: a) butterfly pot of EEG channels across example average; b); Trigger HEO and VEO channels across example average, displayed as separate graph; c) STFFT Spectrogram of frequencies present in channel across example average; d)mean global field potential (MGFP), global voltage against time (s).

As can be seen from the Figure 28, a component within the HEO channel was present, time-locked to the task activity (highlighted in red). As this activity had an opposite polarity for the two different task directions it could be attributed to eyes moving in opposite directions to locate the targets. This indicates that the component is a saccade, performed by the subject during the experimental procedure when mapping the new target locations.

Saccades are rapid eye movements used to identify features of objects being observed. These movements are involuntary and controlled via internal feedback in most cases, however are not considered ballistic due to the control mechanisms used (Purves, et al., 2001). Saccades can be observed to have a distinct shape as evidenced in Figure 29.

Frequency analysis (STFFT) of the results identified the main activity detected in the EEG to be during the saccades. In addition, large spikes in the frontal channels indicated that these movements were causing significant artefact within the EEG, time-locked to the task. This can have a large effect on source localisation so it was decided to use artefact reduction methods to reduce these artefacts.

The effect of saccadic artefacts on the gamma frequency band have been well documented recently, as many studies observing gamma band activity may have been effected by this artefact (Carl et al, 2012; Keren, Yuval-Greenberg, & Deouell, 2010; Shwartzman & Kranczioch, 2011). Notably these studies have pointed out the relative difficulty of detecting these artefacts as they are too small to be usually picked up by standard methods, i.e., threshold detection. These studies have also identified that due to the frequent occurrence of these artefacts during activity, such as responses to new stimuli, artefact rejection of epochs containing these artefacts is pointless unless small epochs were used (approximately less than 100 ms). Many methods of artefact reduction were also proposed, the most common being independent component analysis (ICA) of the artefact channel.

It was decided to first reject artefacts in the HEO channel that were due to eye blinks by using the automatic bad block identification process to reduce sections containing eye blinks to zero, then use thresholds to detect rises and falls within the data to detect the saccades. After detection, the saccades were processed by artefact reduction methods within the Curry 7 software to identify appropriate methods of reducing their impact on the source localisation.

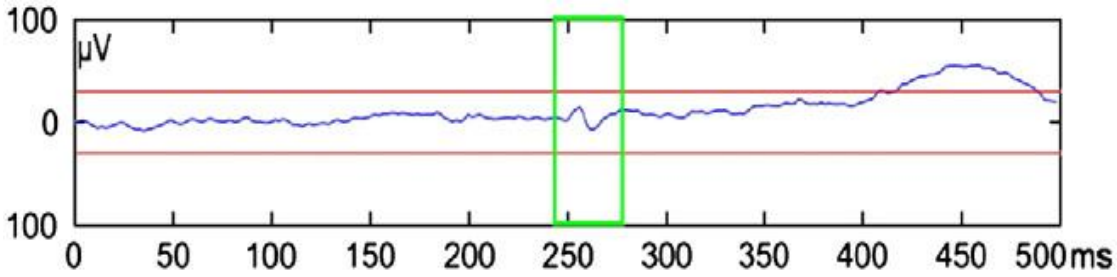

Figure 29 Example of a saccade artefact (Shwartzman & Kranczioch, 2011)

4.4 Spike 2 muscle EMG results

The graphs (Figure 30 and Figure 31) below show the average rectified EMG activity plotted against time. Observation of these graphs allows identification of agonist, antagonist and synergist muscles and identification of the onset of muscle activity.

Table 3 EMG result Key

EMG channel	Muscle Abbreviation	Muscle name	Color on graph
Emg1	ECRL	Extensor Carpi Radialis Longus	Orange
Emg2	FDP	Flexor Digitorum Profundus	Purple
Emg3	FCU	Flexor Carpi Ulnaris	green
Emg4	FCR	Flexor Carpi Radialis	blue
Emg5	ECU	Extensor Carpi Ulnaris	red
Emg6	ECRB	Extensor Carpi Radialis Brevis	black

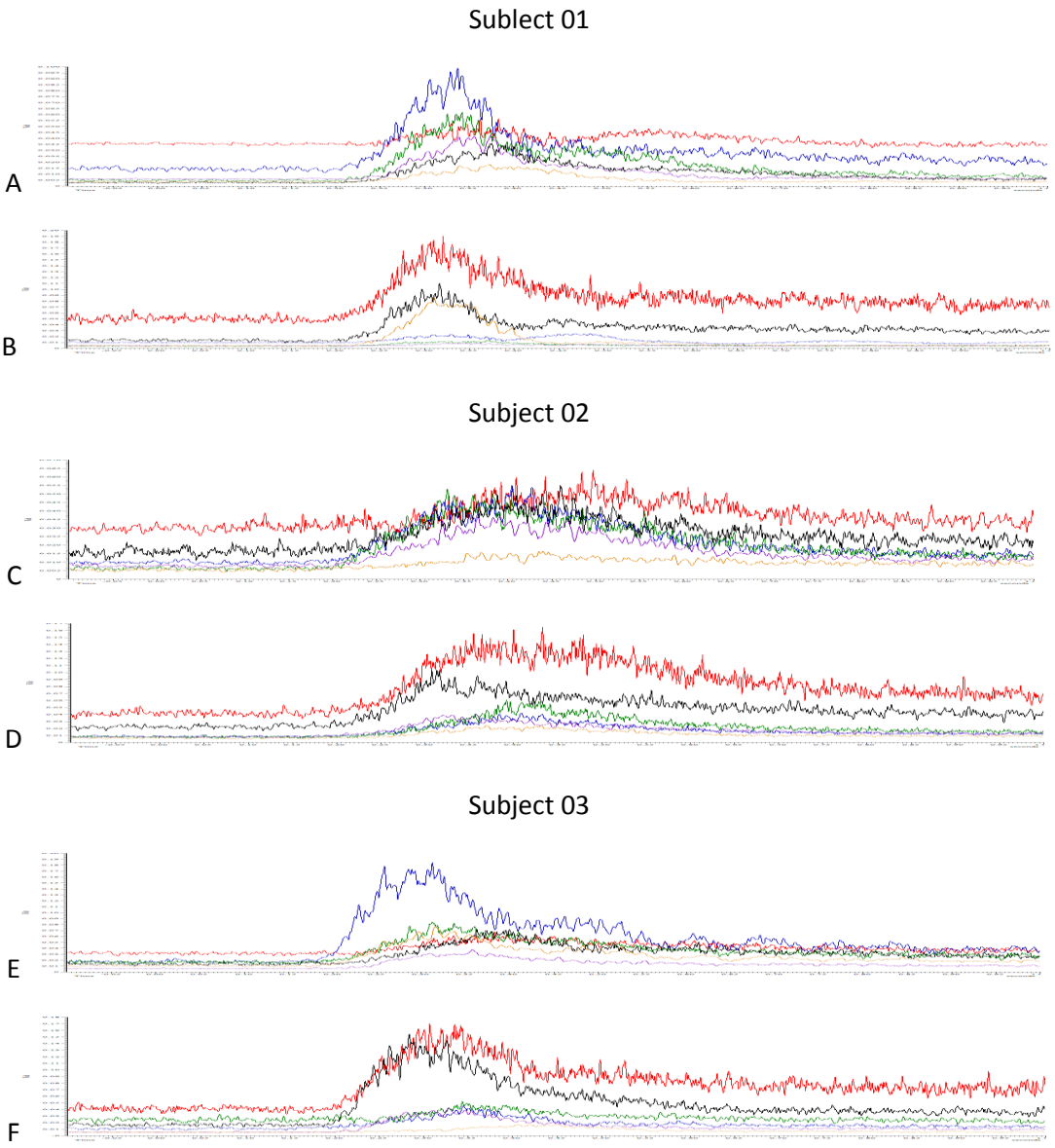

Figure 30 EMG results in the direction of target 12 (upwards)

A) Average EMG activity (V) from movement to target 12 by subject 1 with the forearm supinated. Displayed on graph against time (s). B) Average EMG activity (V) from movement to target 12 by subject 1 with the forearm pronated. Displayed on graph against time (s). C) Average EMG activity (V) from movement to target 12 by subject 2 with the forearm supinated. Displayed on graph against time (s). D) Average EMG activity (V) from movement to target 12 by subject 2 with the forearm pronated. Displayed on graph against time (s). E) Average EMG activity (V) from movement to target 12 by subject 3 with the forearm Supinated. Displayed on graph against time (s). F) Average EMG activity (V) from movement to target 12 by subject 3 with the forearm pronated. Displayed on graph against time (s). The six muscles presented are ECRL (orange line), ECRB (black line), ECU (redline), FCR (blue line), FCU (green line), FDP (purple line). Averages taken from -0.2 s prior to target appearance to 0.5 s post target appearance. Graph scales arbitrarily chosen.

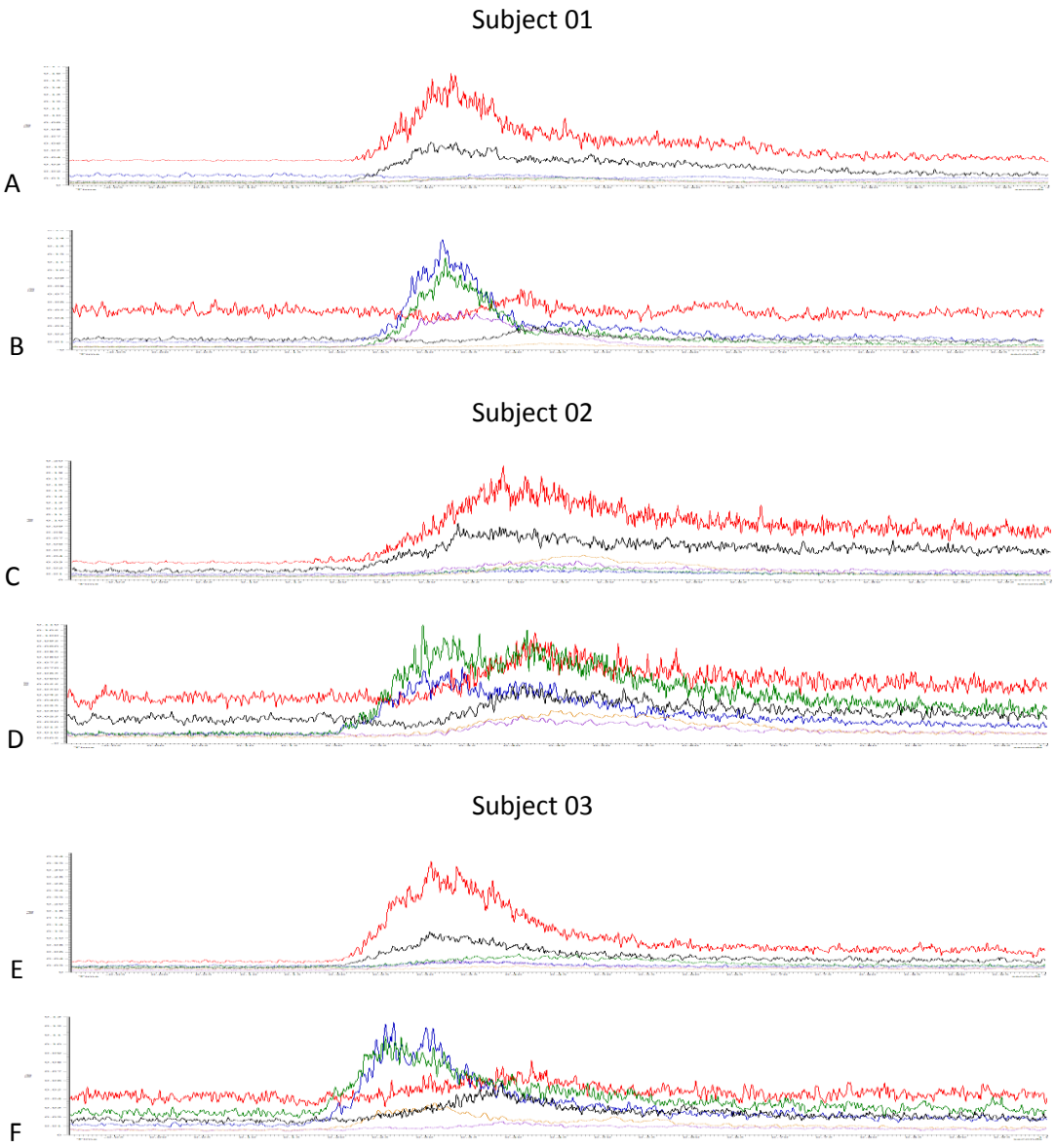

Figure 31 EMG results in the direction of target 6 (downwards)

A) Average EMG activity (V) from movement to target 6 by subject 1 with the forearm supinated. Displayed on graph against time (s). B) Average EMG activity (V) from movement to target 6 by subject 1 with the forearm pronated. Displayed on graph against time (s). C) Average EMG activity (V) from movement to target 6 by subject 2 with the forearm supinated. Displayed on graph against time (s). D) Average EMG activity (V) from movement to target 6 by subject 2 with the forearm pronated. Displayed on graph against time (s). E) Average EMG activity (V) from movement to target 6 by subject 3 with the forearm Supinated. Displayed on graph against time (s). F) Average EMG activity (V) from movement to target 6 by subject 3 with the forearm pronated. Displayed on graph against time (s). The six muscles presented are ECRL (orange line), ECRB (black line), ECU (redline), FCR (blue line), FCU (green line), FDP (purple line). Averages taken from -0.2 s prior to target appearance to 0.5 s post target appearance. Graph scales arbitrarily chosen.

Features of these graphs have been identified and tabulated in table 6.

Table 4 Summary of EMG results

subject	Agonist		Antagonist		Synergist		Onset Time (S)	
Pronated	Target 12	Target 6	Target 12	Target 6	Target 12	Target 6	Target 12	Target 6
01	ECU	FCR	FCR FCU	ECRL ECRB ECU	ECRB	FCU, FDP	0.200	0.250
02	ECRB	FCR	FCR FCU FDP	ECRL ECRB ECU	ECU	FCU FDP	0.219	0.225
03	ECU	FCU	FDP	ECRB ECU	ECRB	FCR FDP	0.194	0.181
Supinated								
01	FCR	ECU	ECRB ECRL ECU	FCU FDP	FCU FDP	ECRB	0.249	0.249
02	FCU	ECU	ECRB ECRL ECU	FCU FDP	FCR	ECRB	0.210	0.280
03	FCR	ECU	ECRB ECRL ECU	FCU FDP	FCU	ECRB	0.200	0.215

There was a clear change in the muscles recruited to achieve movement to target 6 when the forearm was pronated and when it was supinated. When supinated, the movement was achieved using agonist activity from ECU with rapid recruitment which was shortly followed by ECRB acting as a synergist, followed by antagonistic activity from FCU with slower recruitment. When pronated, FCR and FCU both facilitated the movement in this direction with FCR experiencing slightly faster recruitment than FCR, ECRL acted as a synergist, and this was followed by antagonist activity from the ECRB.

The opposite can be seen in movements to target 12. When supinated, the movement was achieved using agonist activity from FCR possessing rapid recruitment which was shortly followed by FCU and FDP acting as synergists, this was then followed by antagonistic activity from ECU with slow recruitment. When pronated, ECRB and ECU both facilitated the movement in this direction with ECRB experiencing slightly faster

recruitment than EFCR. ECRL acted as a synergist; this was followed by antagonist activity from FCR, FCU and FDP.

Subject 02 showed different muscle activity patterns compared to the other two subjects which was most apparent when achieving flexion (Figure 31C, Figure 30D) where a bias to one specific agonist can be seen (FCU for Figure 31D) and activation of antagonist muscles during agonist activation (ECRB, Figure 30C).

Movement responses typically occurred between 180ms – 300 ms after target appearance, indicating that epochs of up to 500 ms after target appearance should be able to view both pre and post processing of motor commands.

The results show a clear difference in the way specific muscle groups are used to achieve the two directional movements between supinated and pronated postures as had been discerned during the EMG pilots (Appendix C). As subject 02 displayed differences in activity patters this could represent variability in the activations to achieve directional movements in humans or be due to error in experimental procedure, i.e. a difference in forearm posture. It would be advisable to maintain awareness of muscle groups used during further study, however when comparing results from the same subject this should present little problem.

4.5 Averages for each direction

4.5.1 Minimally processed data averages

Due to a lack of sucess using artefact reduction methods (described in further detail in section 5.4.3 averages of EEG results were made using raw EEG epochs which had only undergone atefact rejection to discard artefact containing epochs. The graphs in Figure 32, Figure 33, Figure 34 and Figure 35 represent the EEG results for the chosen subject with only artefact rejection procedures applied. Epochs were observed to look for evidence of ongoing EMG or EOG activity. These were detected via two methods. The first involved observation of raw data and removal of epochs containing: high voltage

($\pm 150\mu V$) eye blink spikes, cardiac artefacts such as ECG artefacts which cause QRS complexes within EEG channels, electrode artefacts such as lead movement which causes brief transients limited to single electrodes and those containing high frequency localised bursts of activity (EOG). Scalp maps were used in the second method to detect artefact containing epochs as EOG and EMG artefacts can be detected via scalp potentials being focused on the peripheral electrodes. The criteria for artefact rejection shall be further discussed in section 5.4.2.

Position plots of EEG results show the fore-mentioned visual artefact caused by saccades present in the frontal channels F and AF, the effects of which can be seen reaching as far posterior as Cz contaminating the central EEG channels during all averages. A second waveform can be viewed on the posterior electrodes with similar timing to the saccade spike, the shape of which can be seen on all the dorsal electrodes up to but not including Pz. This waveform may be due to visual processing of the target by the occipital lobe and not due to artefact.

The position plots for Figure 32 also reveal the presence of a high frequency artefact on the anterior right electrodes of the head this artefact may be due to artificial sources such as electrical noise or due to EMG (indicated by its peripheral position).

When comparing the plots with the same target together (Figure 32a with Figure 33a and Figure 34a with Figure 35a) a number of similarities can be seen. The peripheral electrodes on the anterior left side of the head detect a waveform consisting of two peaks, the second of which being smaller and with opposite polarity to the first. Interestingly, the polarity of these peaks reverses between the two configurations and can be seen between response to target 12 while pronated (Figure 34a) and supinated as well as between responses to target 6 when pronated (Figure 32 and supinated Figure 33). This waveform may be due to EMG artefact, however if so it would not show a reversal between the two configurations.

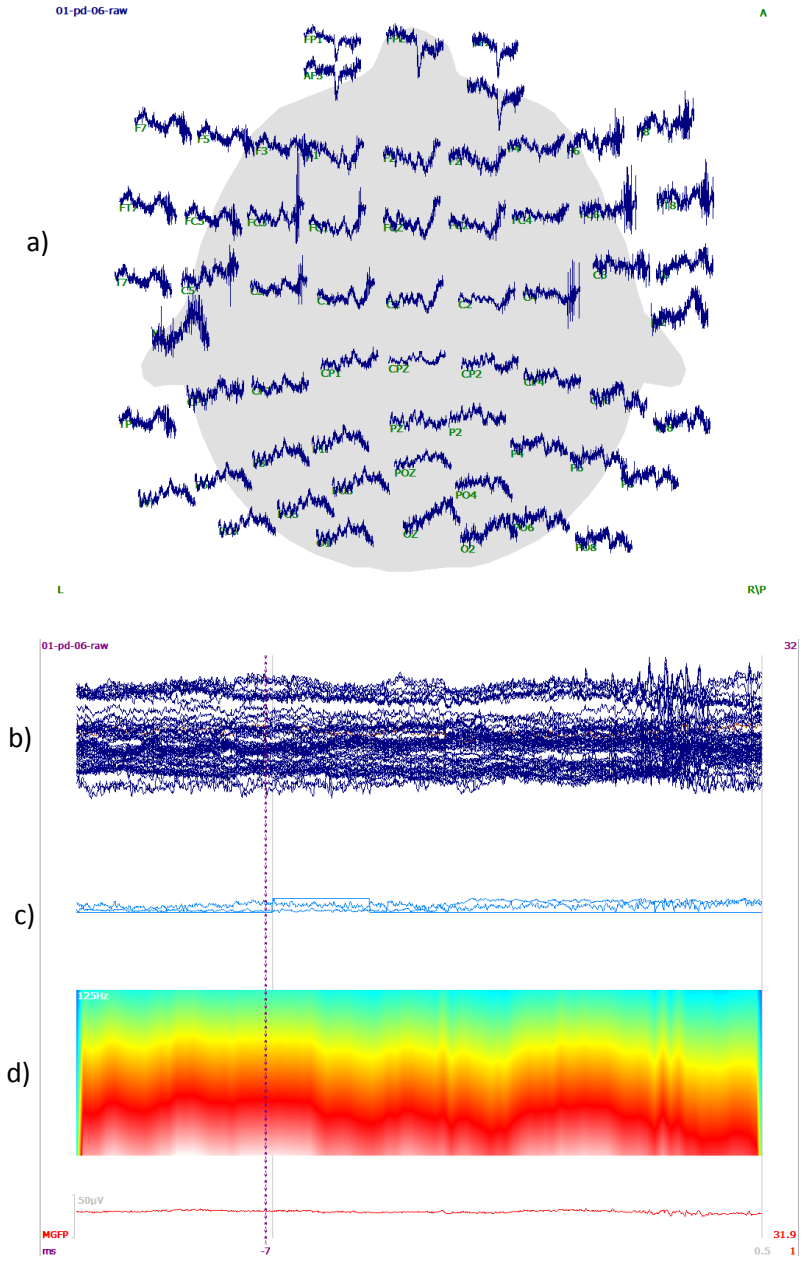

Figure 32 Averaged epoch for target 6 with the forearm pronated

a) Position plot of EEG graphs of each electrode from average of movements to target 6 by subject 1 with the forearm pronated (dark blue lines). EEG graphs are placed depending upon electrode position on scalp. Underlying head image is an indicator for direction with nose pointing anterior. b) Butterfly plot of average EEG results of movements to target 6 by subject 1 with the forearm pronated, c) Trigger and HEO channels of average EEG results of movements to target 6 by subject 1 with the forearm pronated, d) STFFT spectrum of average EEG results of movements to target 6 by subject 1 with the forearm pronated. EEG shown in dark blue lines, HEO, VEO and the trigger shown in light blue. STFFT shown from 0 to 125 Hz. Averages taken from -0.2 s prior to target appearance to 0.5 s post target appearance.

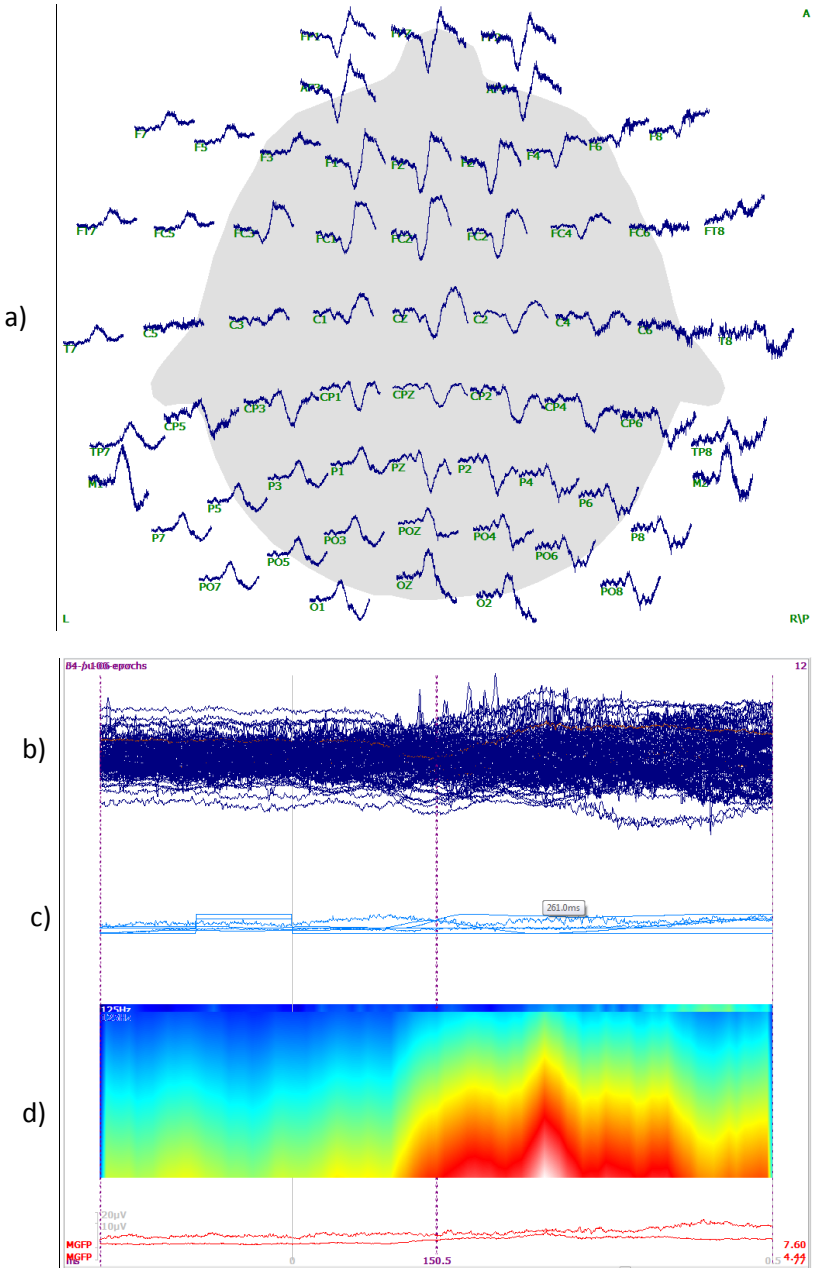

Figure 33 Averaged epoch for target 6 forearm supinated

a) Position plot of EEG values of each electrode from average of movements to target 6 by subject 1 with the forearm supinated (dark blue lines). EEG graphs are placed depending upon electrode position on scalp. Underlying head image is an indicator for direction with nose pointing anterior. b) Butterfly plot of average EEG results of movements to target 6 by subject 1 with the forearm supinated, c) Trigger and HEO channels of average EEG results of movements to target 6 by subject 1 with the forearm supinated, d) STFFT spectrum of average EEG results of movements to target 6 by subject 1 with the forearm supinated. EEG shown in dark blue lines, HEO, VEO and the trigger shown in light blue. STFFT shown from 0 to 125 Hz. Averages taken from -0.2 s prior to target appearance to 0.5 s post target appearance.

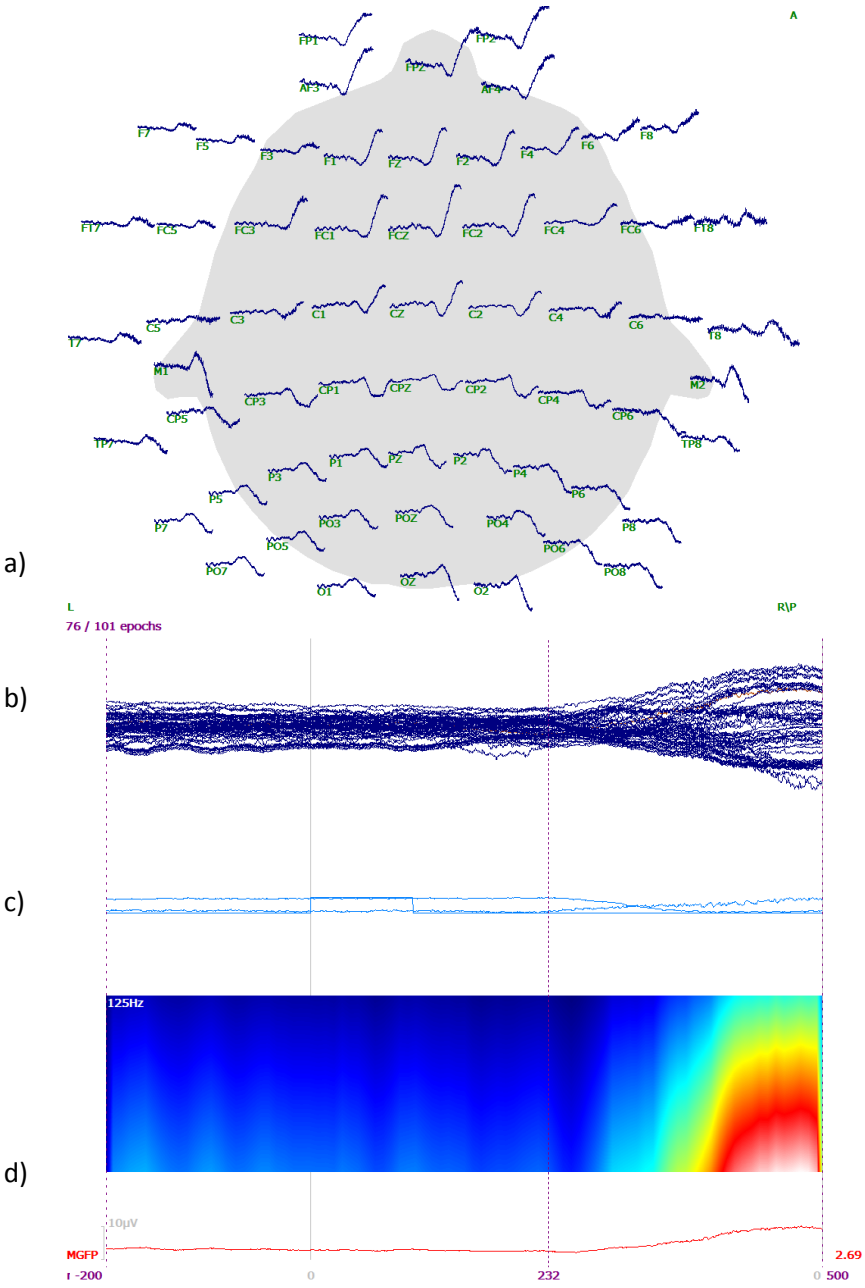

Figure 34 Averaged epoch for target 12 forearm pronated

a) Position plot of EEG values of each electrode from average of movements to target 12 by subject 1 with the forearm pronated (dark blue lines). EEG graphs are placed depending upon electrode position on scalp. Underlying head image is an indicator for direction with nose pointing anterior. b) Butterfly plot of average EEG results of movements to target 12 by subject 1 with the forearm pronated, c) trigger and HEO channels of average EEG results of movements to target 12 by subject 1 with the forearm pronated, d) STFFT spectrum of average EEG results of movements to target 12 by subject 1 with the forearm pronated. EEG shown in dark blue lines, HEO, VEO and the trigger shown in light blue. STFFT shown from 0 to 125 Hz. Averages taken from -0.2 s prior to target appearance to 0.5 s post target appearance.

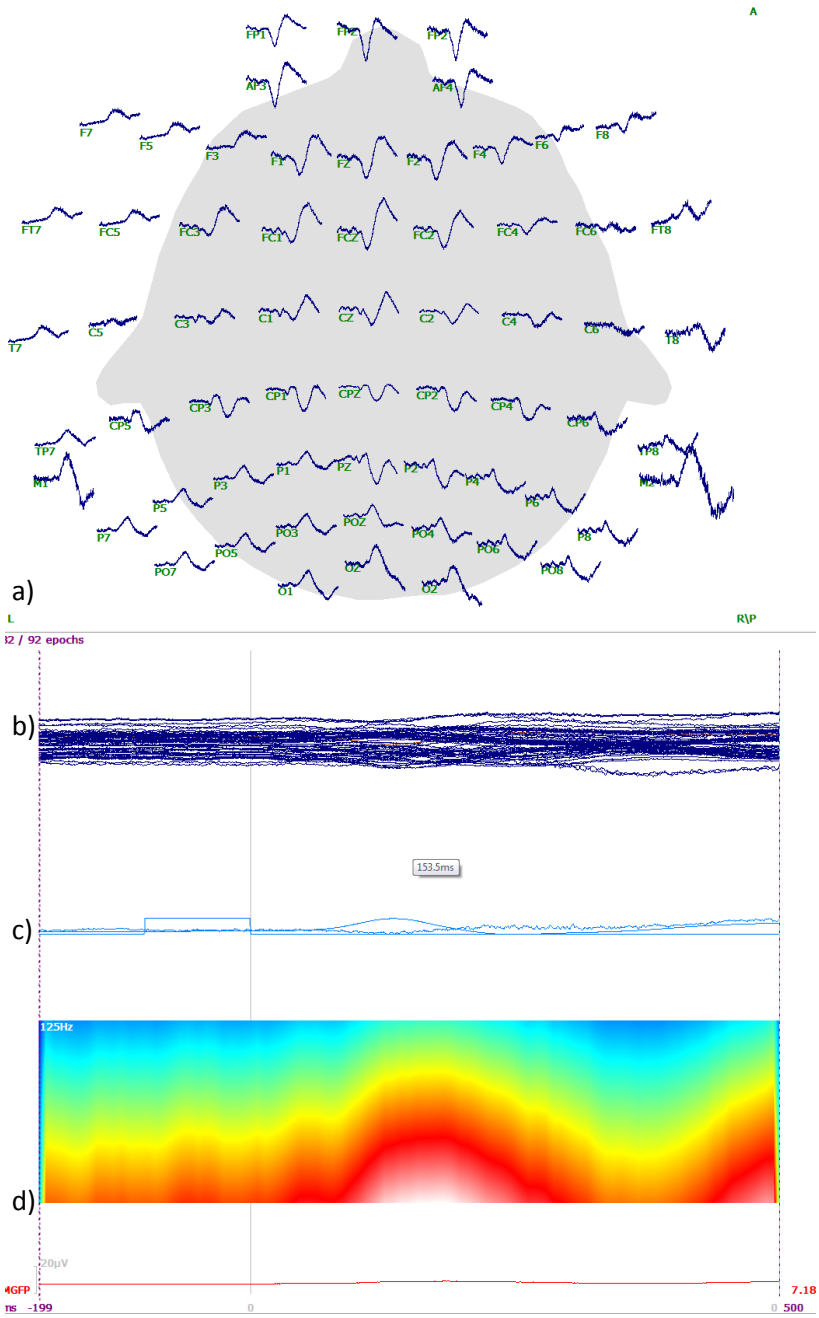

Figure 35 Averaged epoch for target 12 forearm supinated

a) Position plot of EEG values of each electrode from average of movements to target 12 by subject 1 with the forearm supinated (dark blue lines). EEG graphs are placed depending upon electrode position on scalp. Underlying head image is an indicator for direction with nose pointing anterior. b) Butterfly plot of average EEG results of movements to target 12 by subject 1 with the forearm supinated. c) Trigger and HEO channels of average EEG results of movements to target 12 by subject 1 with the forearm supinated. d) STFFT spectrum of average EEG results to of movements to target 12 by subject 1 with the forearm supinated. EEG shown in dark blue lines, HEO, VEO and the trigger shown in light blue. STFFT shown from 0 to 125 Hz. Averages taken from -0.2 s prior to target appearance to 0.5 s post target appearance.

On all plots similar shaped wave forms can be viewed over the M, T and TP electrodes and another waveform can be viewed across the CP electrodes indicating that synchronous activity is present within these areas.

STFFT plots show little connection between the directions. This is most likely due to the presence of artefacts within the averages, Figure 34b shows an especially large artefact at the end of this signal; this is most likely due to EMG based artefact within the data that was not rejected but may also be due to a later saccade in response to this direction.

As any activity in the central electrodes from C to Fp is masked by visual artefacts, artefact reduction must be performed before any waveform can be observed.

4.5.2 ICA of averages

Figure 36, Figure 37, Figure 38 and Figure 39 display the results of removing selected ICA components from the averaged data. The Curry 7 software allowed the selection or de-selection of individual ICA components, which removes the effects of the deselected component from the displayed waveform. The total number of components can be set with the software. The ICA algorithm will try to decompose the signal into the specified number of components, ensuring maximum statistical independence between each component. Components removed that were determined to originate from the peripheral electrodes or those with a percentage contribution to the resulting signal (WT%) above 15. These components were removed as they were determined to be caused by EOG and EMG. Prior to the ICA the data was filtered via a 70Hz high pass and 0.1 Hz low pass filter to remove non-EEG related signals.

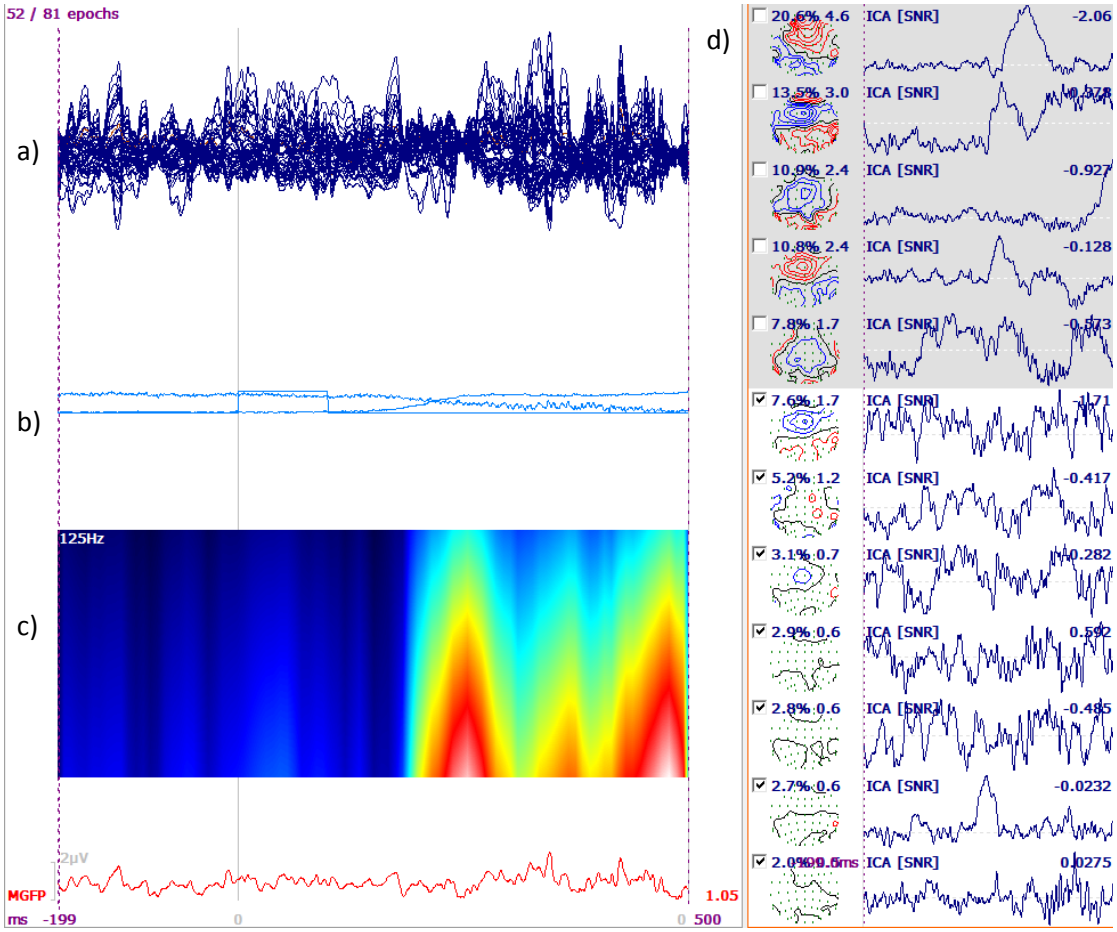

Figure 36 Example of an ICA analysis of averaged response to target 6 when the forearm is pronated

The 4 graphs on the left represent: a) butterfly plot of the ICA filtered average with selected components removed from subject 01 in response to target 06 with forearm pronated; b) non filtered trigger, HEO and VEO channels; c) spectrogram of pre-filtered average; d) detected ICA components present within EEG results are displayed on the right together with their corresponding scalp maps. Components determined from scalp maps to be related to artefacts were deselected and filtered from the butterfly plot. 12 components were assumed (number arbitrarily selected) which is the maximum number permissible by the software. Averages taken from -0.2 s prior to target appearance to 0.5 s post target appearance. Average filtered using 50Hz notch and 0.1-70Hz band pass filter prior to ICA analysis.

The ICA analysis of the averaged response to target 6 when the forearm is pronated detected 5 components originated from the peripheral electrodes one of which was over 15wt%. The components (20.6%, 7.8%) originated from eye sources and are most likely saccade related. The components (13.5%, 10.9%, 10.8%) originated from peripheral sources and are most likely muscle related. Removal of these components removed high potential difference peaks from the EEG data which were most likely caused by artefacts.

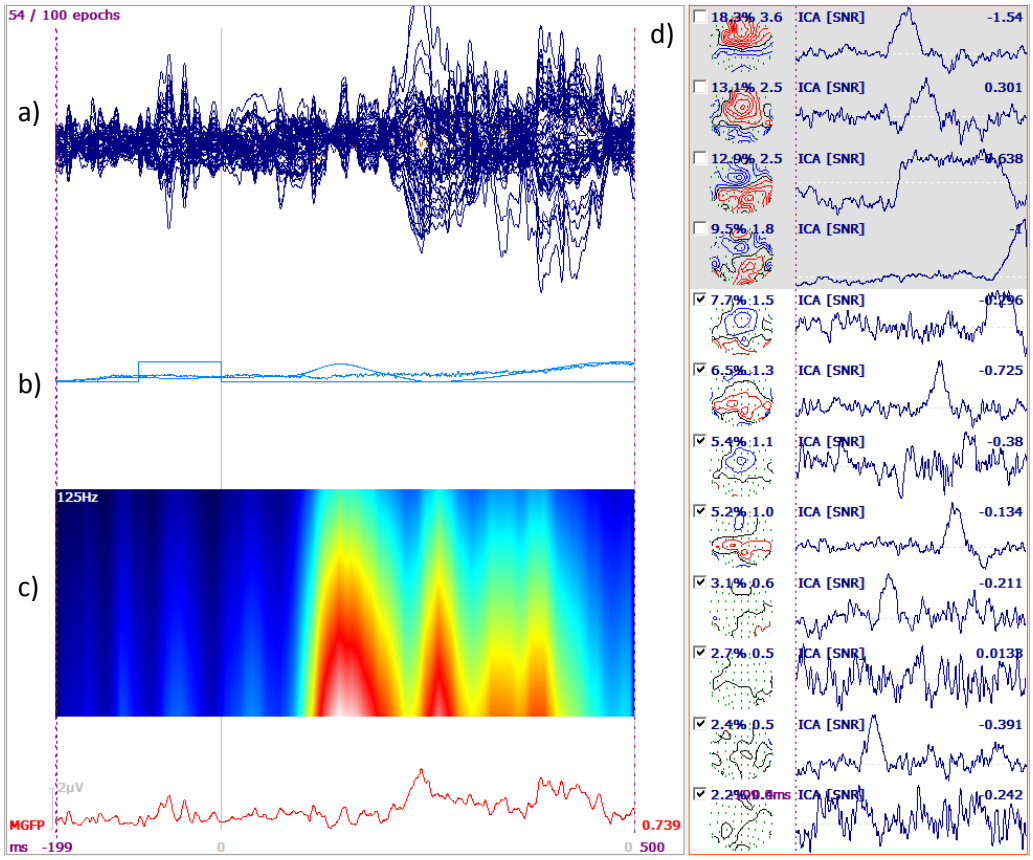

Figure 37 Example of an ICA analysis of averaged response to target 6 when the forearm is supinated

The 4 graphs on the right represent: a) butterfly plot of ICA filtered average with selected components removed from subject 01 in response to target 06 with forearm supinated; b) non filtered trigger, HEO and VEO channels of subject 01 in response to target 06 with forearm supinated; c) spectrogram of pre-filtered average of subject 01 in response to target 06 with forearm supinated; d) detected ICA components present within EEG results of subject 01 in response to target 06 with forearm supinated are displayed on the right together with their corresponding scalp maps. Components determined from scalp maps to be related to artefacts were deselected and filtered from the butterfly plot. 12 components were assumed (number arbitrarily selected) which is the maximum number permissible by the software. Averages taken from -0.2 s prior to target appearance to 0.5 s post target appearance. Average filtered using 50Hz notch and 0.1-70Hz band pass filter prior to ICA analysis.

The ICA analysis of the averaged response to target 6 when the forearm is supinated detected 4 components originated from the peripheral electrodes one of which was over 15wt%. The largest component 18.3% originated from eye sources and was most likely saccade related. The components: 13.1%, 12.9%, and 9.5% originated from peripheral sources and are most likely muscle related. Removal of these components removed high potential difference peaks from the EEG data which were most likely caused by artefacts.

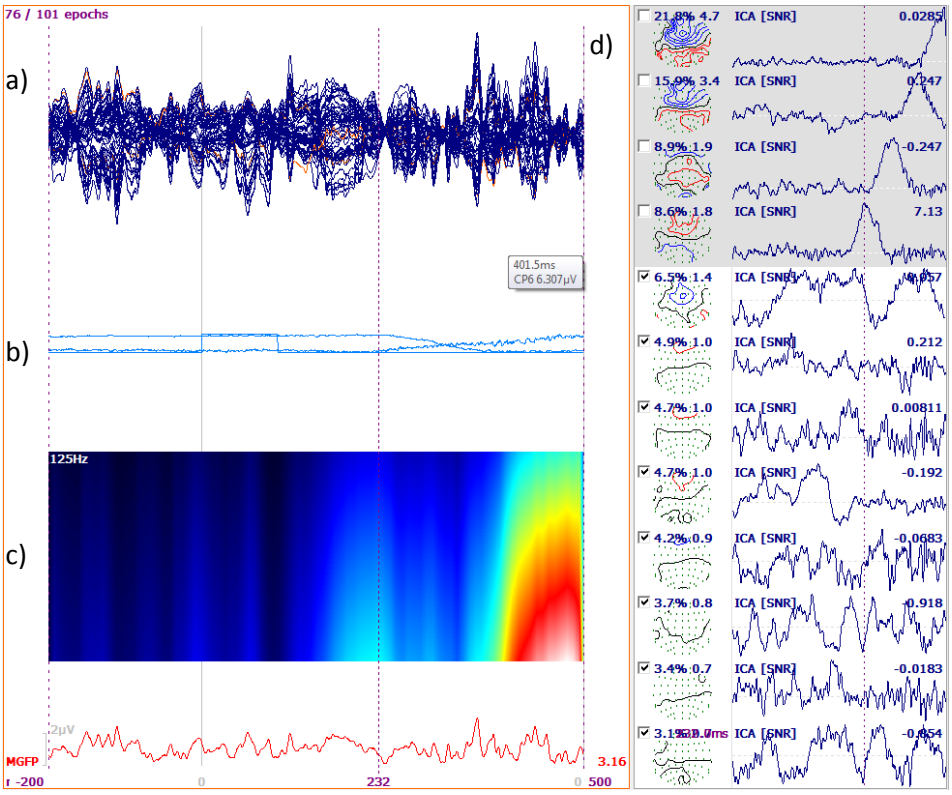

Figure 38 Example of an ICA analysis of averaged response to target 12 when the forearm is pronated

The 4 graphs on the right represent: a) butterfly plot of ICA filtered average with selected components removed from subject 01 in response to target 12 with forearm pronated; b) non filtered trigger, HEO and VEO channels of subject 01 in response to target 12 with forearm pronated; c) spectrogram of pre-filtered average of subject 01 in response to target 12 with forearm pronated; d) detected ICA components present within EEG results of subject 01 in response to target 12 with forearm pronated are displayed on the right together with their corresponding scalp maps. Components determined from scalp maps to be related to artefacts were deselected and filtered from the butterfly plot. 12 components were assumed (number arbitrarily selected) which is the maximum number permissible by the software. Averages taken from -0.2 s prior to target appearance to 0.5 s post target appearance. Average filtered using 50Hz notch and 0.1-70Hz band pass filter prior to ICA analysis.

The ICA analysis of the averaged response to target 12 when the forearm is pronated detected 4 components originated from the peripheral electrodes one of which was over 15wt%. The largest: 21.8%, 15.9%, 8.6% originated from eye sources and are most likely saccade related. The component 8.9% originated from peripheral sources and is most likely muscle related. Removal of these components removed high potential difference peaks from the EEG data which were most likely caused by artefacts.

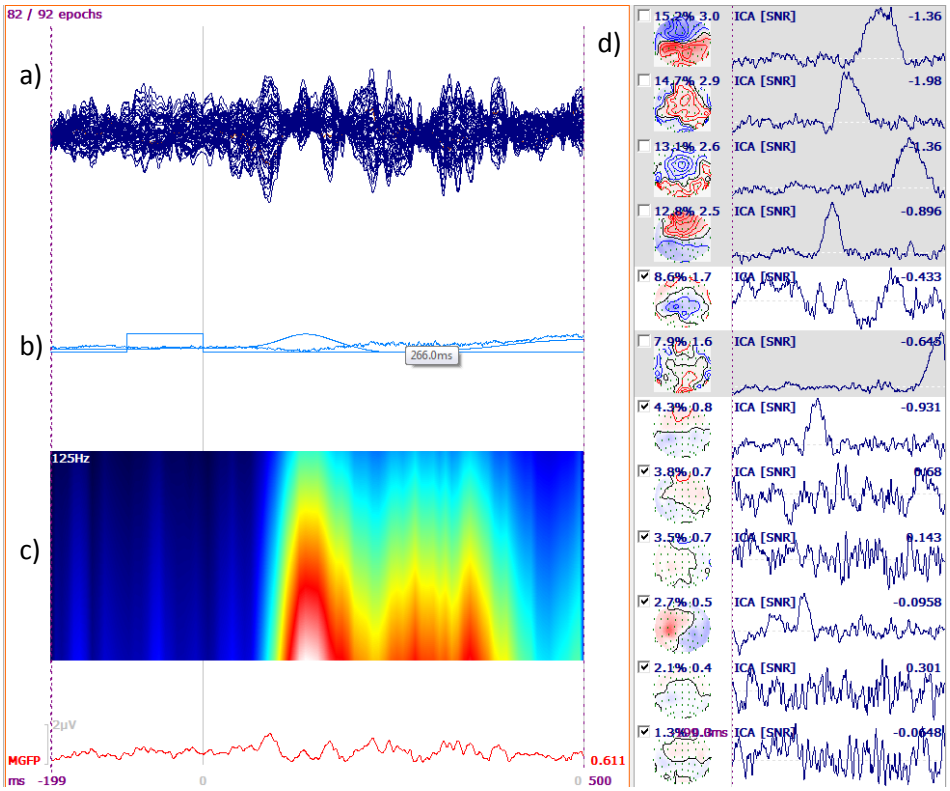

Figure 39 Example of an ICA analysis of averaged response to target 12 when the forearm is supinated

The 4 graphs on the right represent: a) butterfly plot of ICA filtered average with selected components removed from subject 01 in response to target 12 with forearm supinated; b) non filtered trigger, HEO and VEO channels of subject 01 in response to target 12with forearm supinated; c) spectrogram of pre-filtered average of subject 01 in response to target 12 with forearm supinated; d) detected ICA components present within EEG results of subject 01 in response to target 12 with forearm supinated are displayed on the right together with their corresponding scalp maps. Components determined from scalp maps to be related to artefacts were deselected and filtered from the butterfly plot. 12 components were assumed (number arbitrarily selected) which is the maximum number permissible by the software. Averages taken from -0.2 s prior to target appearance to 0.5 s post target appearance. Average filtered using 50Hz notch and 0.1-70Hz band pass filter prior to ICA analysis.

The ICA analysis of the averaged response to target 12 when the forearm is pronated detected 5 components originated from the peripheral electrodes one of which was over 15wt%. The components: 15.2%, 13.2%, and 12.8% originated from eye sources and are most likely saccade related. The components: 14.7% and 7.9% originated from peripheral sources and are most likely muscle related. Removal of these components

removed high potential difference peaks from the EEG data which were most likely caused by artefacts.

The largest contributing component to all averages is a visual originating component that occurs in a clear peak with above 15 WT% during (the component contributes to more than 15% of the epoch) the detected saccades. At least half of the components detected by the ICA could be attributed to a muscular source as they had peripheral distributions on their scalp maps. Such components always possessed a WT% greater than 7% indicating as much as half of the contributions to the EEG signal to be from artefact sources.

The STFFT plot shown applies to the data post filtering. There is an increase in all bands of EEG activity during saccades indicating that eye movements may be masking a large proportion of relevant EEG activity as described in section 4.3.

4.6 Source localisation dipole analysis

For the following analysis, dipole analysis methods were chosen. Due to a software error, linear source localisation methods were unavailable for analysis so dipole analyses of the EEG averages were conducted to observe the feasibility of results. As described in the review by Pizzagalli (Pizzagalli, 2007), the main limitation of dipole analysis was an unknown number of dipoles. This means dipole numbers are chosen based on the solution provided and even if the solution makes physiological sense it has no guarantee of being correct. Figure 40, Figure 41, Figure 42, Figure 43, Figure 44 and Figure 45 display the results of 3 dipole analyses for movements toward target 6 in each forearm orientation observed: moving dipole, rotating dipole and fixed ICA.

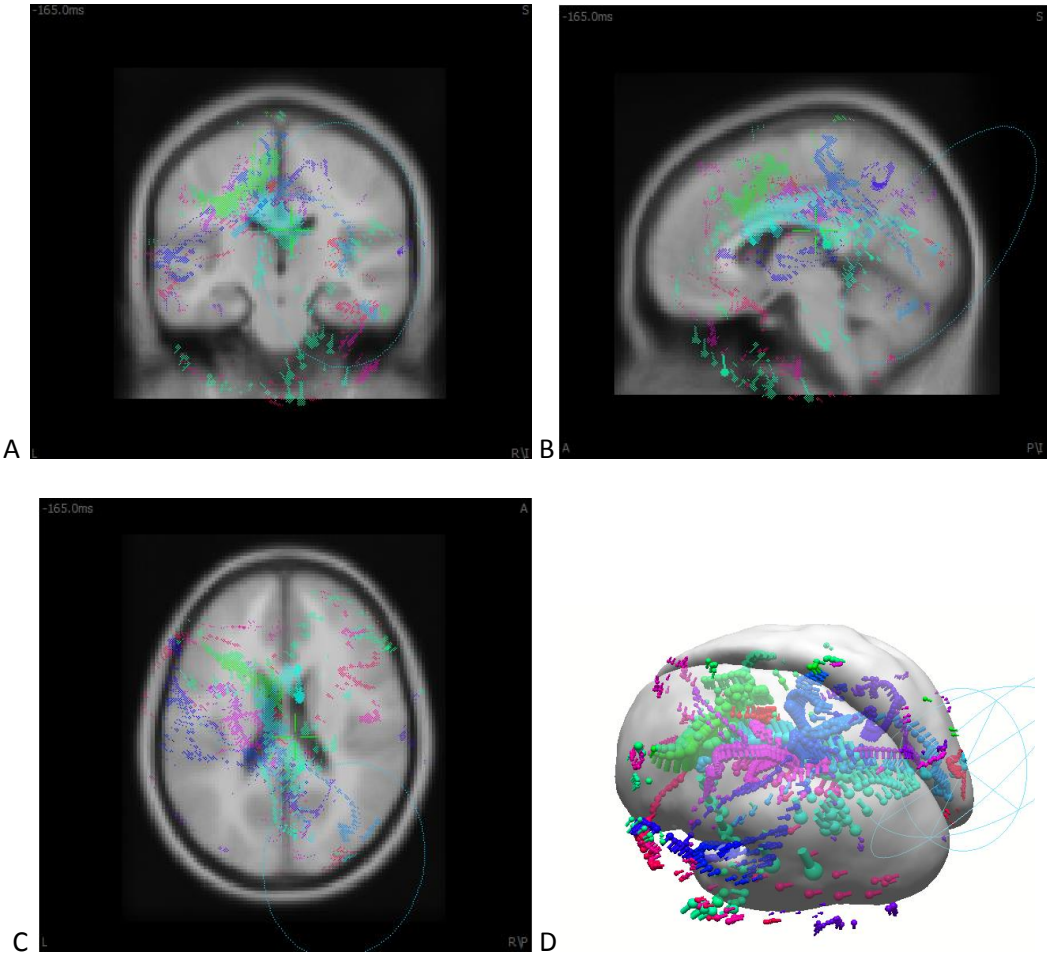

Figure 40 Example of a moving dipole source localisation of response to trigger 6 when forearm is pronated

A) Coronal section of the modelled brain and skull, displaying result of source localisation for Subject 01 response to target 6 with forearm pronated. B) Sagittal section, displaying result of source localisation for Subject 01 response to target 6 with forearm pronated. C) Transverse section, displaying result of source localisation for Subject 01 response to target 6 with forearm pronated. D) Whole brain image, displaying result of source localisation for Subject 01 response to target 6 with forearm pronated. The dipole is shown as a sphere with a cylinder attached. The size of the overall shape indicates the magnitude of the dipole and the direction of the cylinder indicates the alignment of the dipole. The colour of the dipole indicates the time point at which it occurred. The results were generated using an ICA filtered average and a single moving dipole. Visible ellipses are confidence limits indicating that the result of the dipole in the centre of the ellipse is not accurate.

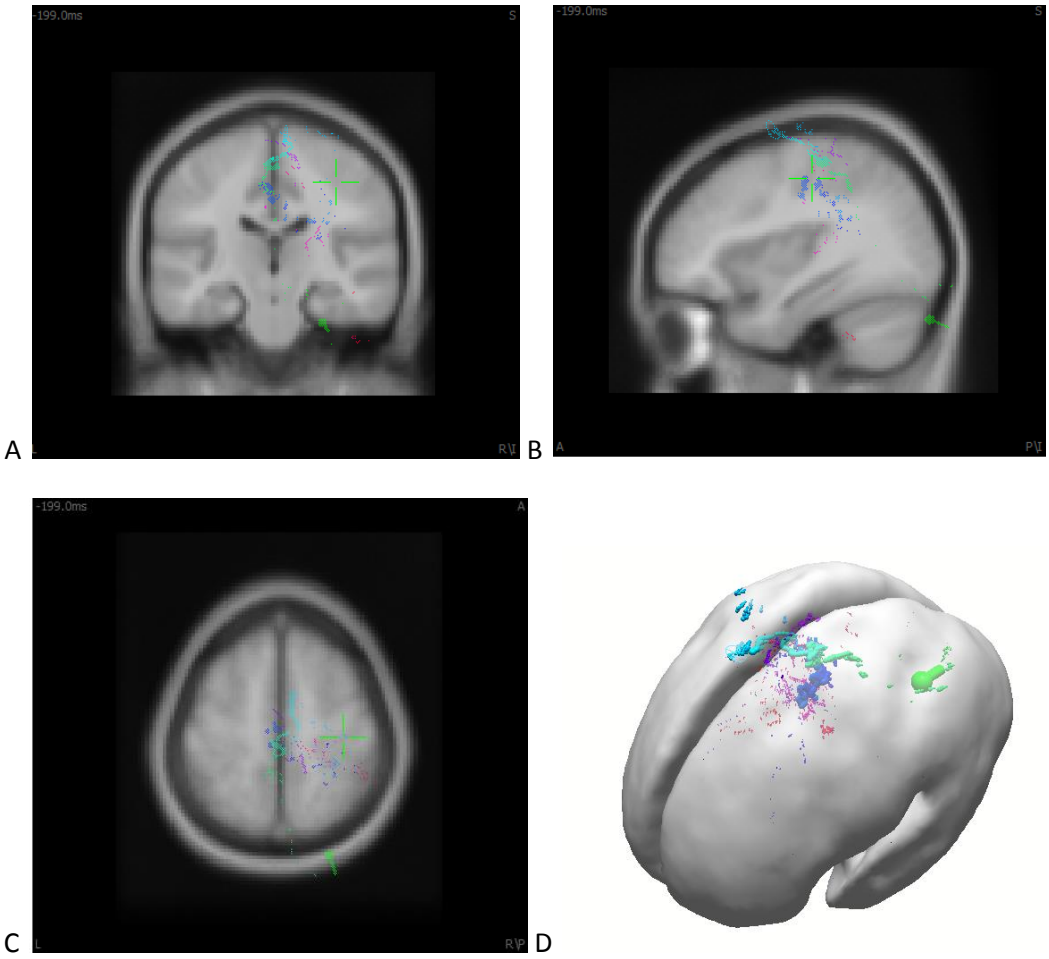

Figure 41 Example of a single moving dipole source localisation of response to trigger 6 when forearm is supinated

A) Coronal section of the modelled brain and skull, displaying result of source localisation for Subject 01 response to target 6 with forearm supinated. B) Sagittal section, displaying result of source localisation for Subject 01 response to target 6 with forearm supinated. C) Transverse section, displaying result of source localisation for Subject 01 response to target 6 with forearm supinated. D) Whole brain image, displaying result of source localisation for Subject 01 response to target 6 with forearm supinated. The dipole is shown as a sphere with a cylinder attached. The size of the overall shape indicates the magnitude of the dipole and the direction of the cylinder indicates the alignment of the dipole. The colour of the dipole indicates the time point at which it occurred. The results were generated using an ICA filtered average and a single moving dipole.

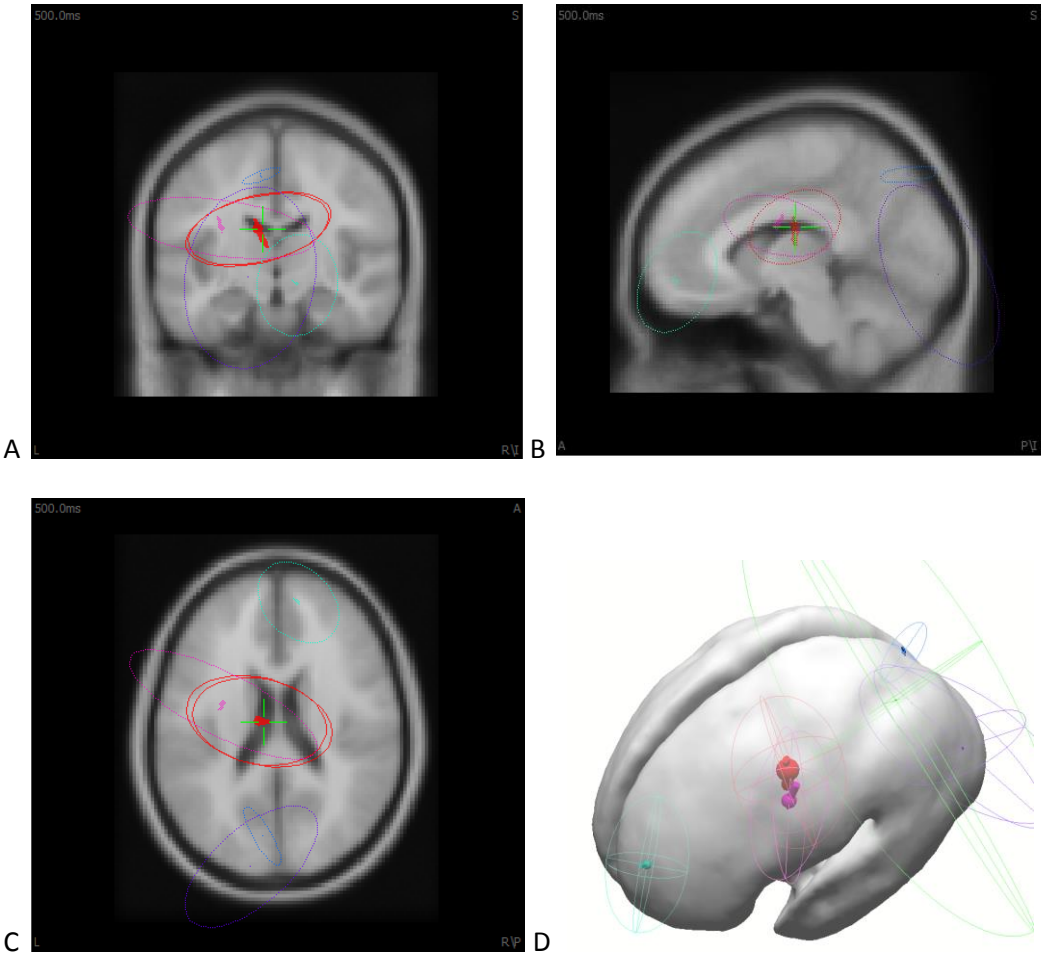

Figure 42 Example of a 6 rotating dipole source localisation of response to trigger 6 when forearm is pronated

A) Coronal section, displaying result of source localisation for Subject 01 response to target 6 with forearm pronated. B) Sagittal section, displaying result of source localisation for Subject 01 response to target 6 with forearm pronated. C) Transverse section, displaying result of source localisation for Subject 01 response to target 6 with forearm pronated. D) Whole brain Image, displaying result of source localisation for Subject 01 response to target 6 with forearm pronated. The dipole is shown as a sphere with a cylinder attached. The size of the overall shape indicates the magnitude of the dipole and the direction of the cylinder indicates the alignment of the dipole. Ellipsoids around each dipole indicate the confidence intervals. Visible ellipses are confidence limits indicating that the result of the dipole in the centre of the ellipse is not accurate.
Image was generated using an ICA Filtered average and single dipole was selected.

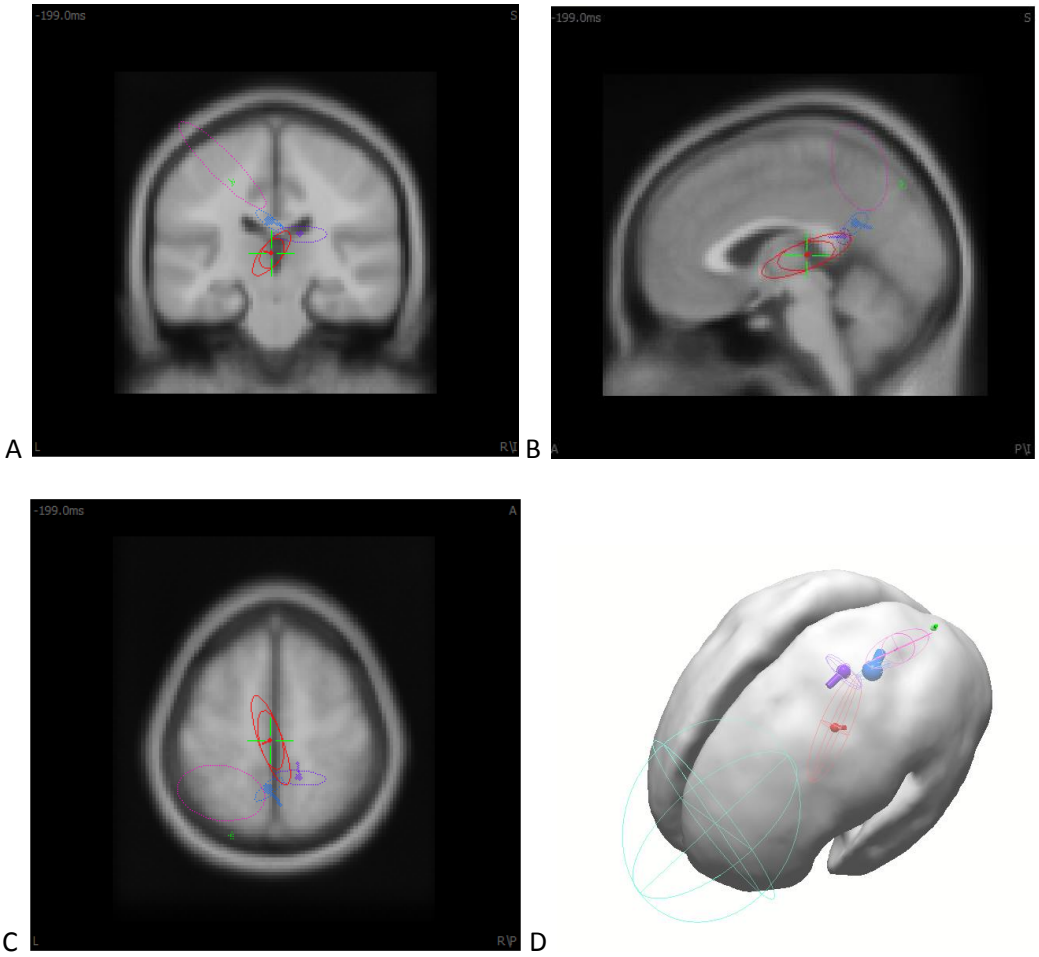

Figure 43 Example of a six rotating dipole source localisation of response to trigger 6 when forearm is supinated

A) Coronal section, displaying result of source localisation for Subject 01 response to target 6 with forearm supinated. B) Sagittal section, displaying result of source localisation for Subject 01 response to target 6 with forearm supinated. C) Transverse section, displaying result of source localisation for Subject 01 response to target 6 with forearm supinated. D) Whole brain image, displaying result of source localisation for Subject 01 response to target 6 with forearm supinated. The dipole is shown as a sphere with a cylinder attached. The size of the overall shape indicates the magnitude of the dipole and the direction of the cylinder indicates the alignment of the dipole. Ellipsoids around each dipole indicate the confidence intervals. Visible ellipses are confidence limits indicating that the result of the dipole in the centre of the ellipse is not accurate.

Image was generated using an ICA Filtered average and six dipoles were selected.

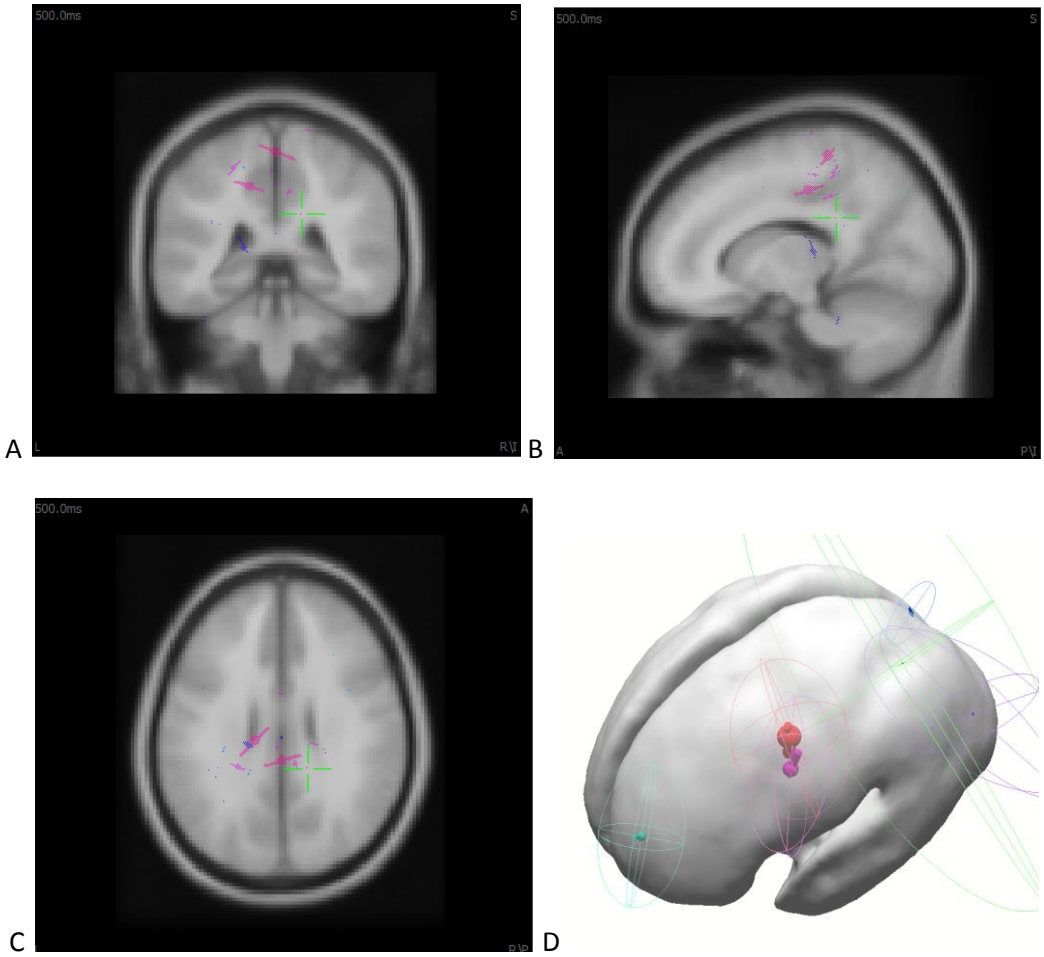

Figure 44 Example of a six fixed ICA dipole source localisation of response to trigger 6 when forearm is pronated

A) Coronal section, displaying result of source localisation for Subject 01 response to target 6 with forearm pronated. B) Sagittal section, displaying result of source localisation for Subject 01 response to target 6 with forearm pronated. C) Transverse section, displaying result of source localisation for Subject 01 response to target 6 with forearm pronated. D) Whole brain image, displaying result of source localisation for Subject 01 response to target 6 with forearm pronated. The dipole is shown as a sphere with a cylinder attached. The size of the overall shape indicates the magnitude of the dipole and the direction of the cylinder indicates the alignment of the dipole. Ellipsoids around each dipole indicate the confidence intervals. Visible ellipses are confidence limits indicating that the result of the dipole in the centre of the ellipse is not accurate. Visible ellipses are confidence limits indicating that the result of the dipole in the centre of the ellipse is not accurate. Image was generated using an ICA Filtered average and six dipoles were selected.

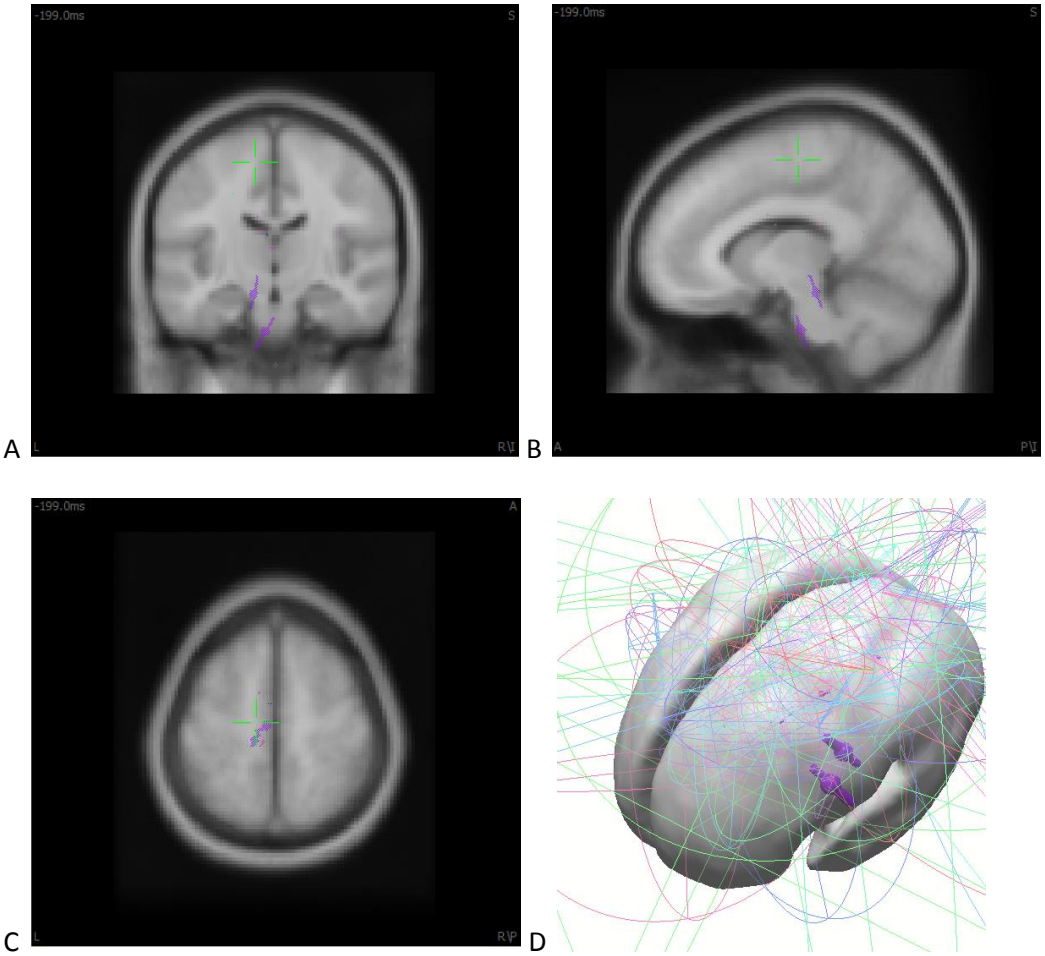

Figure 45 Example of a six fixed ICA dipole source localisation of response to trigger 6 when forearm is supinated

A) Coronal section, displaying result of source localisation for Subject 01 response to target 6 with forearm supinated. B) Sagittal section, displaying result of source localisation for Subject 01 response to target 6 with forearm supinated. C) Transverse section, displaying result of source localisation for Subject 01 response to target 6 with forearm supinated. D) Whole brain image, displaying result of source localisation for Subject 01 response to target 6 with forearm supinated. Image was generated using an ICA Filtered average and six dipoles were selected. Ellipsoids around each dipole indicate the confidence intervals.

The results of the above dipole analysis make little physiological sense for either forearm orientation with a large number of activation sources being predicted outside of the head or inside areas that contain no grey matter. None of the localisations attempted even detect activations from within the M1 which should be happening during the processing of a motor task. The only aspect of these localisations which makes physical sense is the grouping towards the left side of the brain, apart from Figure 40, consistent with processing of a movement on the right side of the body. As mentioned above the number of dipoles assumed is arbitrarily chosen: this could mean the inaccuracy is due to the difference between the assumed number of dipoles and reality. However it is this uncertainty which makes this method unsuited for studies that need high spatial accuracy.

This method is also unsuitable for the purpose of this study as it does not present an effective way of observing groupings of activations within M1 with sufficient spatial resolution to observe the distribution described in the study by Toxpeus et al (Toxopeus, et al., 2011c). As sources are assumed to be separate from each other and not in proximity there is little ability to observe differences from specifically within the M1 area.

5. Discussion

5.1 Implications due to EMG pilot

The results of the first EMG pilot (Appendix C) test showed a clear flaw in the experimental design resulting from the similar muscle groups used between the two original forearm orientations of pronation and mid-pronation. This resulted in a need to alter the experimental design to take account of the change in preferred pulling directions of the wrist muscles that can be observed during rotation of the wrist. The proposed change in experimental design to correct this flaw fortunately presented a method which displayed clear differences in muscle groups used between the two chosen forearm orientations of pronation and supination.

The results which can be seen in Figure A - 5, Figure A - 6, Figure A - 7 and Figure A - 8 Appendix C – EMG pilot test showed a clear difference between the muscles that were used during the two postures, with the most obvious difference between targets 6 and 12 due to the reversal of the muscles used for these movements. The results reported in section 4 were based upon experiments using movements in these two directions to increase the number of results available for event related averaging, increasing the chance of there being enough epochs to average after artefact rejection to provide an accurate representation of the neural processes underlying the event.

An interesting observation post-testing was that if the manipulandum was that during the test procedure, it was also found that rotating the handle by 5 degrees below horizontal during supination and rotating it by 5 degrees above horizontal during supination made it easier and more comfortable for the subject to grasp the handle. To reduce discomfort during experimentation it is recommended that this be done during further testing.

5.2 Implications of results of primate studies

Two of the results from the primate studies referenced within the literature review have great bearing upon the processing required during activations within the M1. These are the cosine-like response that individual cells make when processing movements and the presence of 80 µm vertical columns that process similar reaching directions. The cosine-like response means that cells in M1 will show signs of activity in directions separate from their preferred direction. The result is the requirement of a source localisation method that can distinguish between the maximal activations of cells responding to their PD and the reduced activity of cells responding to different directions than their PD. The size of the columns requires a spatial resolution capable of indicating areas of this size. As cells representing different reaching dimensions were determined to be 400 µm apart, this could present a lower resolution method of detecting these areas. Even so, an inverse method would most likely be required to present a localisation at 40 µm resolution to be able to distinguish between these areas.

5.3 Ideal experimental conditions

5.3.1 Experimental setup and design

The proposed change to the experimental setup as a result of the EMG pilot tests showed different muscle activation patterns between the 2 forearm orientations, supination and pronation, as evidenced by the results in Appendix C. This allowed the majority of the setup to remain the same as described in Appendix D with only a change to the handle orientation. During the test procedure it was also found that rotating the handle by 5 degrees below horizontal during supination and rotating it by 5 degrees above horizontal during supination made it easier and more comfortable for the subject to grasp the handle. However if the original handle orientation is maintained it should have little effect experimental results (movements will retain the same direction and forearm posture will remain mostly the same).

Reducing the number of targets from 4 to 2 is an effective way of increasing the number of averages available for event related averaging without increasing experiment runtime. While observation of the horizontal directions 3 and 9 will provide a representation of all 4 axes within a further study, these directions could be studied separately if the spatially distinct property viewed by Toxopeus et al (Toxopeus, et al., 2011a) is observable via linear source localisation techniques.

5.3.2 Removal of saccades

As mentioned in section 4.3, saccadic eye movement was observed to be time locked to the experimental task. The effects of the saccade were visible on the frontal electrodes and contaminated the central electrodes on all averages. This indicates that removal of the effects on EEG due to saccades is essential for EEG studies that rely upon a visually triggered response.

To remove the effects either a change must be made to the experimental task or artefact reduction methods must be performed on the saccadic eye movements.

As saccades are involuntary, a change in the task may still require training of participants to prevent eye movements. A notable task method that prevented eye movements while still allowing a similar response to the current task was used by Cowper-Smith et al (Cowper-Smith, et al., 2010) where targets were always present and an arrow in the centre target was used to indicate the direction of the final target, thus fixing the participants gaze on the centre target. This method can be modified to include a random indication of target or a random delay between starting of the task and appearance of the arrow. This would retain an element of uncertainty about which target to respond to and where to respond preventing preparation of a motor plan until a target is known. As this study is only concerning the directional processing within the M1 area, the processing involving mapping of the targets will not be observed meaning changes to the observed result should be minimal.

Alternatively to changing the experimental design, the effect of saccades can be removed via artefact reduction methods of which there are many documented (Nguyen, et al., 2012; Berg & Sherg, 1994; Keren, et al., 2010). It is important to note however that modifications to the data should be kept as minimal as possible to avoid any unnecessary changes to EEG data: changes in data can produce a large impact on the results of source localisation even if methods used had little effect upon other observed spatial results e.g. scalp maps (McMenamin, et al., 2010).

This current study tested methods of artefact reduction that were available in the Curry 7 software, the observations of which were described in section 5.2.4. As these methods were determined to be unreliable for artefact reduction, removal of saccadic artefact was done using ICA on the epoched EEG data.

5.3.3 Observation of artefact rejection and reduction methods

Prior to the selection of task-related epochs, the EEG channels were baseline corrected to remove any offset between the electrodes. Following this, large EOG artefacts such as those containing eye blinks were detected and zeroed using a $\pm 150\mu V$ threshold on the EOG channel HEO. This was done for two reasons: to allow detection of these 'bad blocks' of data to allow rejection of epochs containing them, an example of which is shown in Figure 46; and to prevent these artefacts from being detected by later reduction methods to detect saccades.

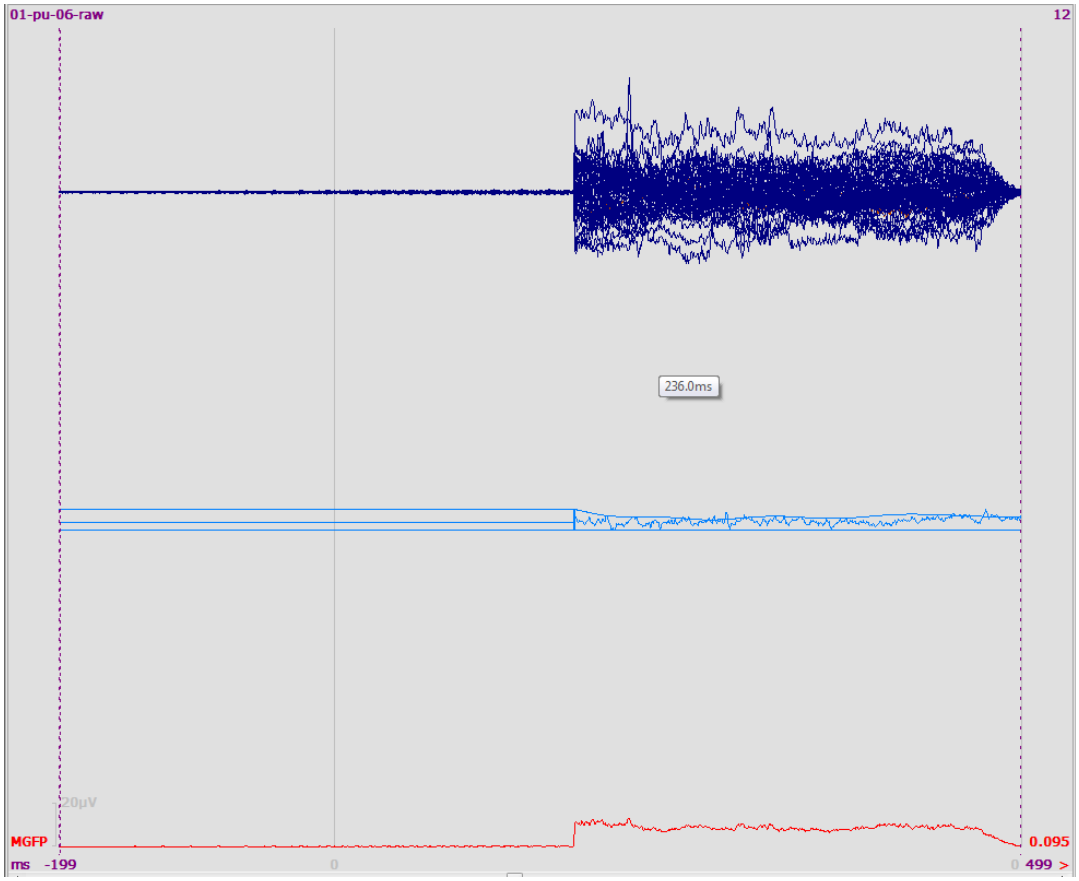

Figure 46 Example of an epoch rejected due to blink artefact

The epoch shown above was rejected due to the flat line observed. This is the result of all channels being zeroed over the duration of the blink artefact; this presented a simple method of detecting and rejecting the artefact.

As mentioned in section 4.3, saccades were observed and time locked to the experimental task. As these were time locked to the task, they occurred too frequently to be easily removed from averages by artefact rejection. Additionally, difficulty was experienced using methods such as thresholds to detect them due to their small sizes. Two channels were observed for the artefact, Fz and HEO, after larger eye blink artefacts were zeroed. Saccades could be detected using 50µV thresholds which were applied separately in positive and negative directions to take account of the change in polarity between upwards and downwards movements to targets.

Three methods present within the Curry software were used to remove artefact components from channels: a) subtraction, which removes the rolling average of the artefact detected; b) covariance, which removes a distance weighted component of the artefact from all present channels; and c) ICA, which automatically removed artefact components detected from all other selected channels. Removal based on HEO channels was found to be ineffective as an offset was always detected within the reduced channels as shown by Figure 47. Removal based on frontal channels such as FPz was hampered by difficulty detecting saccades as the effects were either masked by ongoing activity or too small to be detected by thresholds. The presence of higher frequency activity occurring during nominative EEG activity also hampered detection by using template matching as the superimposed higher frequency activity prevented detection of templates representing the saccade activity.

Example reduced artefact

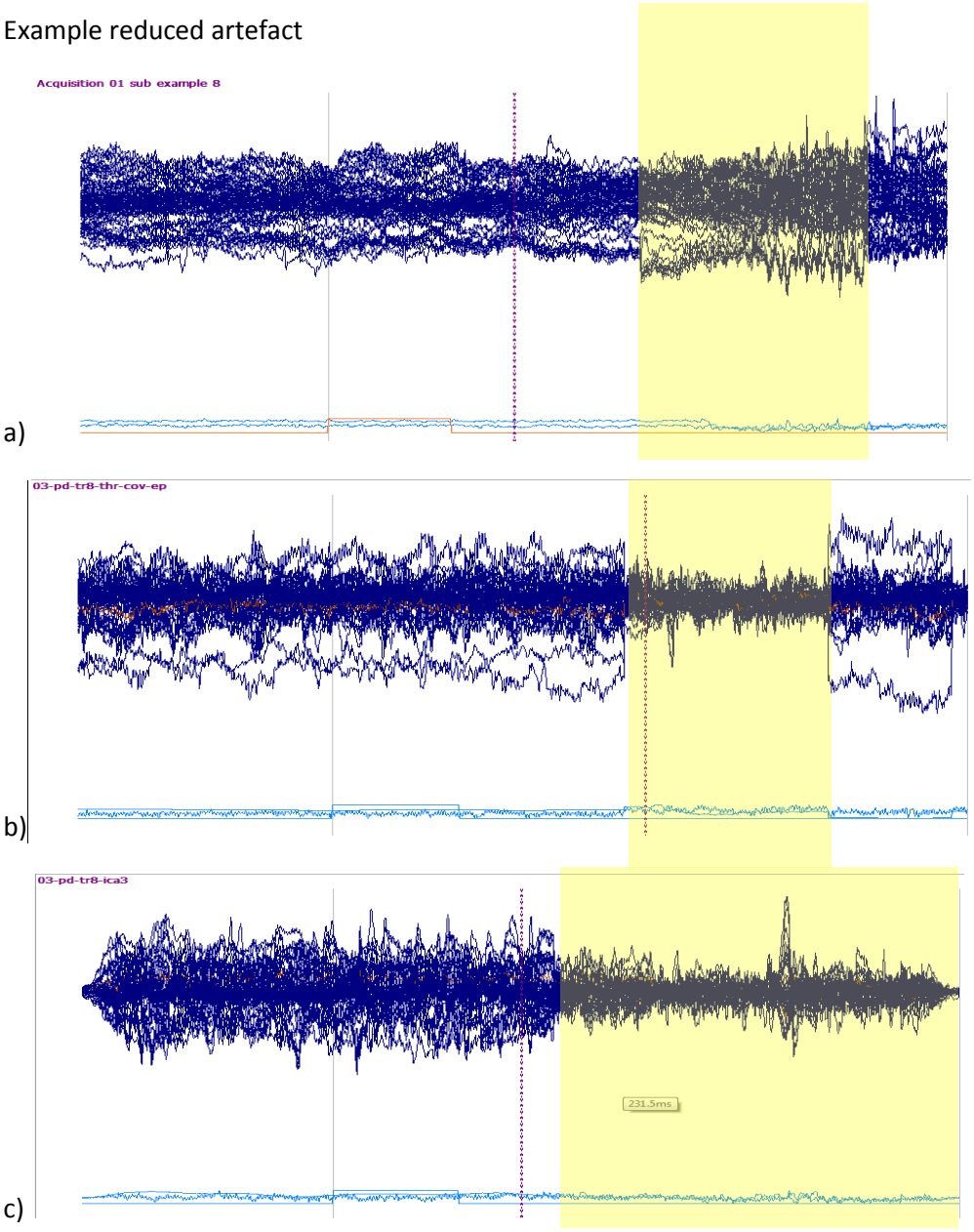

Figure 47 Effect of artefact reduction on HEO

a) Example effect of subtraction method on EEG results, visible offset is highlighted, b) Example effect of covariance method on EEG results, visible offset is highlighted, c) Example effect of ICA reduction method on EEG results, visible offset is highlighted. All samples are derived from different trigger points.

A commonly used method to remove artefacts is via ICA. While this study performed ICA on the averaged epochs, ICA is recommended to be performed individually on non-averaged epochs. Whilst time consuming, this presents a way of minimising the number of epochs that are altered during artefact rejection with minimal impact to EEG. Figure 48 displays example components detected and rejected using ICA while following experimental procedure.

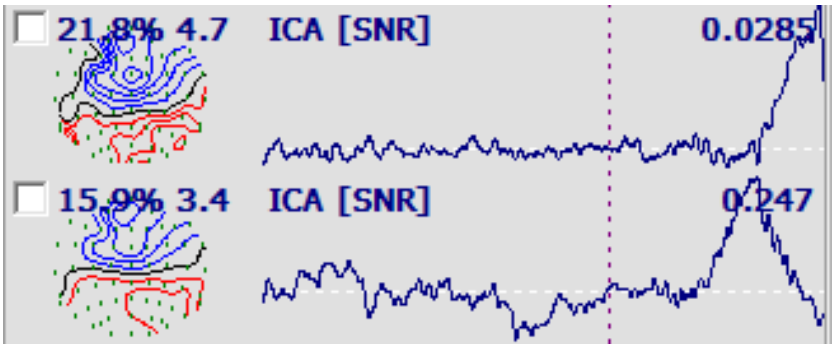

Figure 48 Example of components rejected using ICA

Example of components rejected using ICA. Components possess a wt% greater than 15%, show a noticeable spike of activity which contributes to the EEG epoch and yet are sourced from the peripheral electrodes.

Regardless of whether reduction methods were applied or not, event related epochs were examined visually for artefacts and epochs containing artefacts were rejected. The most obvious artefact was the zeroed blink artefact previously described. Other artefacts removed were those pertaining to electrode drift (Figure 49), evidenced by a large shift in baseline voltage across one or more channels, and those waveforms which could be viewed on scalp maps originating from localised areas on the peripheral and frontal electrodes, caused by EMG and EOG sources.

a)

b)

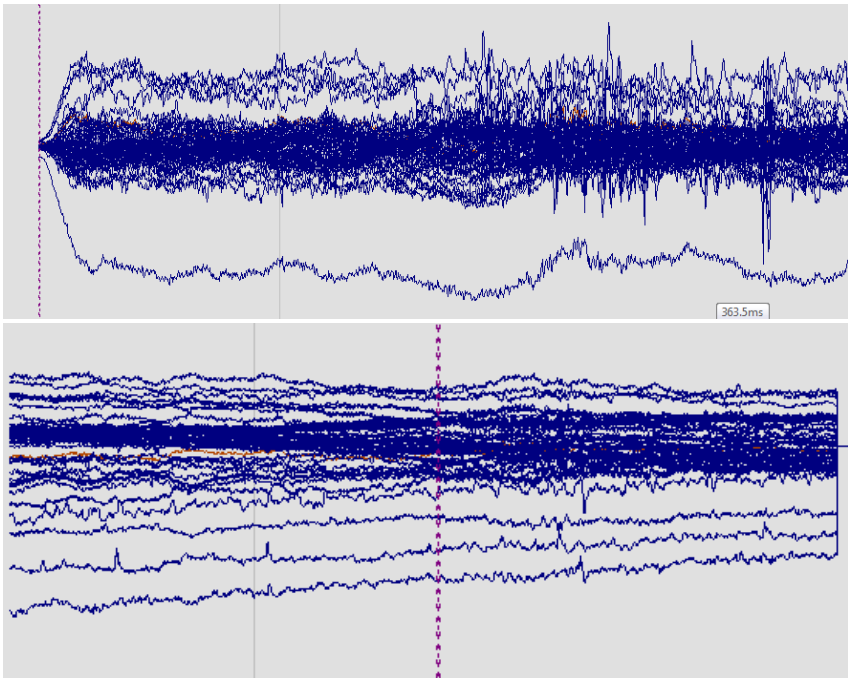

Figure 49 Example of rejected epochs

a) Epoch rejected due to large drift in one of the electrodes, spike of high frequency activity also present later in the signal. b) Artefact rejected due to electrode drift of several channels, beginning of zeroed eye blink artefact can also be viewed at the end of the signal.

Results of ICA analysis showed clear detection of components resulting from EOG with sources located on the frontal electrodes displayed by scalp maps. Other components were detected with activity originating from the peripheral of the map in a similar manner to EMG which could indicate EMG artefacts missed during artefact rejection.

5.3.4 Observation of source localisations

As previously indicated, dipole methods were determined to be unsuitable as a method of source localisation for this study (Pizzagalli, 2007). While activations were detected within the left cortex as is consistent with processing of movement on the right side of the body, activation locations made little physiological sense and detected areas have no guarantee of being correct due to being based on an arbitrarily chosen solution (the number of dipoles) rather than being fully based on prior knowledge.

For a full study, linear distribution source localisation techniques would be of more use. The main advantage of these methods is the assumption that all areas within the brain are active. In doing so, a calculated localisation will present as a distribution. The source localisation will have to be performed at a resolution high enough to observe the differences in activation for various movements within the representative area for the wrist within the M1 with minimal blurring.

The review of literature indicates that the standard LORETA method may experience difficulty detecting sources spaced close to each other, registering them as a single source. This may present a problem during the comparison of spatially distinct activations within M1, as they could be seen as a single source. The most effective method for linear interpolation would be Bayesian methods using a FEM model based on fMRI scans of the subject's head. However, as such methods require the input of additional information concerning the subject which may not be available, another method to consider would be Local Auto-Regressive Average (LAURA) using a FEM model based on averaged MRI scans created from previously recorded data at the MNI institute. As LAURA has been able to detect multiple synchronously activated sources in simulation it may be an applicable method for this study.

5.4 Further study

Before further investigation into the organisation of the M1 cortex using source localisation, three main issues have to be resolved. First is the identification of a method of preventing or removing the effect of saccadic artefacts upon recorded EEG. As saccades are made towards intended targets in conjunction with hand movements as a result of hand-eye coordination (Battaglia-Mayer, et al., 2003), their presence will be nigh on unavoidable during target-based tasks involving the hands. ICA presents a method of identifying saccade components and filtering them from the signal. However, this may result in consequences regarding the accuracy of source localisation (McMenamin, et al., 2010). As discussed in section 5.3.2 there are a number of

methods available for reducing EOG artefact, however the effect of these upon source localisation is largely un-investigated.

The second issue is achieving sufficient spatial resolution to distinguish between activation areas which respond to directions within the M1. EEG is less suited to observations within the spatial domain as opposed to other techniques such as FMRI and a source localisation method that can detect activations with a spatial resolution of 40 μm is required to observe activations within M1 according to the results of the primate studies (Naselaris, et al., 2006) Such a method would require high resolution MRI scans of the participant's head to produce the detailed head models necessary for localisation.

The third issue lies in the distinguishing of activations. As neurons within the M1 show activity in all directions, a source localisation method must be able to distinguish between areas of activation which will be 400 μm apart and possess as much as a 50% difference in output strength. The capabilities of models to do so would have to be determined prior to the study.

Once these issues have been resolved, the proposed paradigm can be used to confirm the role of direction within the motor cortex allowing a greater depth of understanding of the processes that take place within the brain.

6. Conclusion

In conclusion, the present study considered the feasibility of a paradigm that can be used to gather evidence of direction based processing within the M1 using scalp recorded EEG. The proposed paradigm made use of a wrist step tracking task with 2 forearm orientations to allow comparison between the activations within the M1 while disassociating extrinsic direction-based space from intrinsic muscle-based space. During pilot testing of the experimental setup, a flaw was determined with the original experimental design where a shift in forearm orientation between pronation and midway between pronation and supination had little effect on the specific muscle groups used during the step tracking task. This indicated that the original setup did not sufficiently disassociate extrinsic and muscle spaces, resulting in a need to change the experimental design. Proposed changes to the paradigm were tested and found sufficient, resulting in a reduction in the number directions involved in the step tracking task and a change in forearm posture from full pronation to full supination. The change in forearm posture was sufficient to dissociate the extrinsic and muscles spaces and the reduction in the number of targets increased the number of trials that could be recorded.

EEG trials were undertaken using the changes to the experimental paradigm. EEG data was recorded with a 64-channel montage, the resulting data was epoched and examined for common artefacts. An EOG artefact was found to be time locked to the experimental procedure that was caused by mapping the visual frame of reference with saccadic eye movements. Artefact reduction methods within the Curry 7 software were tested to detect and remove this artefact from the raw data, all of which were found to be unsuitable as they caused an offset between the corrected and original data.

The EEG epochs from one of the 3 subjects of the EEG trials were again visually inspected and epochs containing artefacts such as EMG, drift and eye blinks were removed. The epochs were averaged and an ICA filter was applied to remove

components determined to result from artefacts. The resulting averages were used for dipole based source localisation. As had previously been suspected, dipole analysis was confirmed to be unreliable for the experimental paradigm indicating that linear distributed source localisations were required to adequately observe the distributions intended.

In summary, while the final protocol was determined sufficient for the proposed paradigm, several issues were identified. Issues that were observed during testing were the presence of saccades time locked to the randomised step tracking task and the complex spatial requirements needed by inverse models used in source localisation. Both of these issues can be solved by choice of artefact reduction methods and correct localisation methods.

Bibliography

Baraduc, P., Guigon, E. & Burnod, Y., 2001. Recording Arm Position to Learn Visuomotor transformations. *Cerebral Cortex,* 11(10), pp. 906-917.

Battaglia-Mayer, A., Caminiti, R., Laquanti, F. & Zago, M., 2003. Multiple Levels of Representation of Reaching in the Parieto-frontal Network. *Cerebral Cortex,* 12(10), pp. 1009-1022.

Ben-Shaul, Y; Stark, E; Asher, I; Drori, R; Nadasdy, Z; Abeles, M, 2003. Dynamical Organization of Directional Tuning in the Primate Premotor and Primary Motor Cortex. *J Neurophysiol,* 89(2), pp. 1136-1142.

Berg, P. & Sherg, M., 1994. A multiple source approach to the correction of eye artifacts. *Neurophysiology,* 90(3), p.p. 229–241.

Caminiti, R., Johnson, P. B. & Urbano, A., 1990. Making Arm Movements Within Different Parts of Space - Dynamic Aspects in the Primate Motor Cortex. *Journal of Neuroscience,* 10(7), pp. 2039-2058.

Caminiti, R., S, F. & Mayer, A. B., 1998. Visuomotor transformations: Early cortical mechanisms of reaching. *Current Opinion Neurobiology,* 8(6), pp. 753-761.

Carl, C., Açık, A; König, P., Engel, A. K., Hipp, J. F., 2012. The saccadic spike artifact in MEG. *NeuroImage ,* 59(2), pp. 1657-1667.

Chiel, H. J., Ting, L. T., Ekeberg, O. & Hartmann, M. J. Z., 2009. The Brain in Its Body: Motor Control and Sensing in a Biomechanical Context. *The Journal of Neuroscience,* 29(41), pp. 12807-12814.

Cho, J., Kang, H. C., Jung, Y. J., Kim, H. D., Yoon, D. S., Lee, Y. H., Im, C. H., 2013. Localization of epileptogenic zones in Lennox–Gastaut syndrome using frequency domain source imaging of intracranial electroencephalography: a preliminary investigation. *Physiological Measurement 4,* 34(2), pp. 247-263.

Conway, B. A., Reid, C. & Halliday, D. M., 2004. Low Frequency Cortico-Muscular Coherence During Voluntary Rapid Movements of the Wrist Joint. *Brain Topography,* 16(4), pp. 221-224.

Cooper, R. P., 2010. *Forward and Inverse Models in Motor Control and Cognitive Control,* London: Proceedings of the International Symposium on AI Inspired Biology.

Cowper-Smith, C. D., Lau, E. Y. Y., Helmick, C. A., Eskes, G. A., Westwood, D. A, 2010. Neural Coding of Movement Direction in the Healthy Human Brain. *PLoS One,* 5(10).

de Rugy, A., Davoodi, R. & Carrol, T. J., 2012. Changes in wrist muscle activity with forearm posture:implications for the study of sensorimotor transformations. *J Neurophysiol,* 108(11), pp. 2884-2895.

Dyspraxia Foundation, 2013. What is dyspraxia? http://www.dyspraxiafoundation.org.uk/services/dys_dyspraxia.php.

Fuchs, M., Wagner, M. & Kastner, J., 2001. Boundary element method volume conductor models for EEG source reconstruction. *Clinical Neurophysiology,* 112(8), pp. 1400-1407.

Georgopoulos, A. P., Caminiti, R., Kalaska, J. F. & Massey, J. T., 1983. Spatial coding of movement: a hypothesis concerning the coding of movement direction by motor cortical populations. *Brain Research suppl.,* Volume 7, pp. 327 -336.

Georgopoulos, A. P., Taira, M. & Lukashin, A., 1993. Cognitive Neurophysiology of the Moror Cortex. *Science Volume,* 260(5104), pp. 47-52.

Gordon, J. & Ghez, C., 1984. EMG Patterns in Antagonist Muscles During Isometric Contraction in Man: relations to response dynamics. *Experimental Brain Research,* 55(1), pp. 167-171.

Hoffman, D. S., Strick, P. L. & Kakei, S., 1999. Muscle and movement representations in the primary motor cortex. *Science ,* 285(5436), pp. 2136-2139.

Humphrey, D. R. & Schmidt, E. M., 1991. Extracellular Single-Unit Recording Methods. *Neuromethods,* Volume 15, pp. 1-64.

J.C.Andrews, R., 1986. *Electrodiagnosis An Anatomical and Clinical Approach.* Philadelphia: J.B. Lippincot Company.

Kakei, S., Hoffman, D. S. & Strick, P. L., 2003. Sensorimotor transformations in cortical motor areas. *Neuroscience Research,* 46(1), pp. 1 - 10.

Kalaska, J. & Crammond, D., 1992. Cerebral Cortical Mechanisms of Reaching Movements. *Science,* 255(5051), pp. 1517-1523.

Kawato, M., 1999. Internal models for motor control and trajectory planning. *Current Opinion in Neurobiology,* 9(6), pp. 781-727.

Keren, A. S., Yuval-Greenberg, S. & Deouell, L. Y., 2010. Saccadic spike potentials in gamma-band EEG: Characterization. *NeuroImage,* 49(3), pp. 2248-2263.

Knyazev, G. G., 2013. Comparison of spatial and temporal independent component analyses of electroencephalographic data: A simulation study. *Clinical Neurophysiology,* 124(8), pp. 1557-1569.

Konrad, P., 2005. *The ABC of EMG.* s.l.:Noraxon INC. USA..

Lodish, B., Matsudaira, K., Krieger, S. & Zipursky, D., 2008. *Molecular cell Biology 5th ed,* s.l.: W.H. Freeman and Co.

Luck, S. J., 2012. Event-Related Potentials. In: *APA Handbook of Research Methods in Psychology.* s.l.:APA, pp. 1-18.

Martini, F. H., Nath, J. L. & Batholomew, E. F., 2012. *Fundamentals of Anatomy & Physiology Ninth Edition.* San Francisco: Pearson Education.

McMenamin, B W.; Shackman, A J.; Maxwell, J S.; Bachhuber, D R et al., 2010. Validation of ICA-basedmyogenic artifact correction for scalp and source-localized EEG. *NeuroImage,* 49(3), pp. 2416-2432.

Merletti, R. & Parker, P., 2004. *Electromyography:Physiology, Engineering, and Non-Invasive Applications.* s.l.:Wiley-IEEE Press.

Millslagle, D., 2013. *Introduction to motor Learning,* s.l.: University of Minnesota Duluth.

Naselaris, T., Merchant, H., B. A. & Georgopoulos, A. P., 2006. Large-Scale Organization of Preferred Directions in the Motor Cortex. *J Neurophysiol,* 96(6), pp. 3237-3247.

Nguyen, H. T., Musson, J., Li, F., Wang, W., Zhang, G et al., 2012. EOG artifact removal using a wavelet neural network. *Neurocomputing,* 97, pp. 374 -389.

Pizzagalli, D. A., 2007. Electroencephalography and High-Density Electrophysiological Source Localization. In: *Handbook of Psychophysiology Third Edition.* Cambridge: Cambridge University Press, pp. 56-84.

Plummer, C., Wagner, M., Fuchs, M., Vogrin, S. et al., 2010. Clinical utility of distributed source modelling of interictal scalp EEG in focal epilepsy. *Clinical Neurophysiology,* 121(10), pp. 1726-1739.

Purves, D., Augustine, G. J., Fitzpatrick, D. & al., e., 2001. Neural Control of Saccadic Eye Movements. In: 2, ed. *Neuroscience.* Sunderland: Sinauer Associates.

Saeid Sanei, J. C., 2008. *EEG signal processing.* s.l.:John Wiley & Sons Ltd.

Sanes, J. N., Suner, S., Lando, J. F. & Donoghue, J. P., 2007. Rapid reorganization of adult rat motor cortex somatic representation patterns after motor nerve injury. *PNAS,* 86(6), pp. 2003-2007.

Schmidt, R. A. & Lee, T. D., 2011. *Motor Control and Learning.* 5 ed. s.l.:Human Kinetics.

Scott, S. H., 2003. The role of primary motor cortex in goal-directed movements:insights from neurophysiological studies on non-human primates. *Current Opinion in Neurobiology,* 13(6), pp. 671-677.

Shadmehr, R., 1998. *The Equilibrium Point Hypothesis for Control of Movements,* Baltimore: Dept. of Biomedical Engineering Johns Hopkins University.

Shah, A., Fagg, A. H. & Barto, A. G., 2004. Cortical Involvement in the Recruitment of Wrist Muscles. *J Neurophysiol,* 91(6), pp. 2445-2456.

Shwartzman, D. J. & Kranczioch, C., 2011. In the blink of an eye: The contribution of microsaccadic activity to the induced. *International Journal of Psychophysiology,* 79(1), pp. 73-82.

Tortora, G. J. & Anagnostakos, N. P., 1984. *Principles of Anatomy and Physiology.* 4 ed. New York: Biological Sciences Textbooks, Inc.

Toxopeus, C. M., de Jong, B. M., Valsan, Gopal, Conway, B. A. et al., 2011a. Impairment of Gradual Muscle Adjustment during Wrist Circumduction in Parkinson's Disease. *PLoS One,* 6(9).

Toxopeus, C. M., Maurits, N. M., Valsan, G., Conway, B. A. et al., 2011b. Direction of Movement Is Encoded in the Human Primary. *PLoS ONE,* 6(11).

Toxopeus, C. M., de Jong, B. M., Conway, B. A., Leenders, K. L. et al., 2012. Cerebral Activations Related to Ballistic, Stepwise Interrupted and Gradually Modulated Movements in Parkinson Patients. *PLoS One,* 7(7).

WINE FOR SOUL, 2012. Vision, anatomy and physiology of wine tasting – Part 1, http://wine4soul.com/tag/visual-cortex/. 28 OCTOBER 28, 2012.

Wolpert, D. M. & Ghahramani, Z., n.d. *Motor Learning Models,* London: University College London, UK.

Woodworth, R. S., Jul 1899. Accuracy of voluntary movement. *The Psychological Review: Monograph Supplements,* 3(3), pp. i-114.

Appendix A – Participant information sheet

Participant information sheet

University of Strathclyde

Biomedical Engineering Department

Neurophysiology lab

Title of study

An EEG investigation to determine if primary motor cortex activations involved in step tracking wrist movements are movement-related or muscle-related

Introduction

This experiment is conducted by Ross Wilson, an MSc student at University of Strathclyde, Biomedical Engineering Department, as part of his research experiment. Dr Campbell Reid, a Research Fellow also at the Biomedical Engineering Department will supervise all experiments.

Ross Wilson, MSc Student

Neurophysiology lab, Biomedical Engineering Department, University of Strathclyde

Wolfson Centre, 106 Rottenrow, Glasgow G4 0NW, Scotland, UK

Mobile: +44(0)7775790719

Email: trb12177@uni.strath.ac.uk

What Is the Purpose of This Investigation?

The experiment is designed to study the brain activity of normal healthy adults with no previous history of neurological impairments, to confirm whether there is a link between the

direction of movement the brain is processing and the area of the brain involved in generating the movement.

You will be asked to sit in a chair and perform a motor step tracking task using a custom-built joystick. The task will involve rapidly moving the joystick in set directions in response to targets displayed on a screen. Afterwards the task will be repeated but with the joystick rotated through 90 degrees. During the experiment you will be wearing an Electroencephalography (EEG) cap. Electrodes on the cap will record your brain activity. These Electrodes contain foam inserts, saturated with saline solution (salt water), which fill the gap between the electrodes and your head. A secondary set of electrodes will be attached to your arm that is holding the joystick. These Electrodes will be used for Electromyography (EMG), the gap between your skin and these electrodes will be filled with a conductive gel. After the experiment a towel and shampoo will be provided for washing your head.

Do you have to take part?

Participation is completely voluntary. You are free to decide if you want to participate or not. There will be no consequences if you refuse to participate or if you withdraw from participation at any time before or during the experiment, for any reason.

What will you do in the project?

You will sit for the experiment, as previously described. We will attach the electrode cap, including electrodes to detect eye movement and EMG electrodes. Saline solution is injected through the top of the cap electrodes and gel is injected through the top of the other electrodes. Some of the saline solution may over flow for which you will be provided with a paper towel to wipe off the excess. An alcohol swab will be used to clean the skin under the electrodes regarding your eye movements and arm muscles. The gel used is water soluble and easy to wash out. It is highly unlikely you will have an allergic reaction to the gel, saline solution

or swabs, and we will test your skin before continuing. If you have a reaction at this point, or any point during the experiment we will remove the cap and electrodes and you can wash the gel and saline solution off quickly and easily. The setup of the cap and electrodes should take around 30 minutes, but can sometimes take up to 45 minutes.

Task

The task is a modified Step tracking task. You will sit facing a computer monitor with your arm strapped to a joystick. Each Trial consists of a number of randomly generated directions indicated by a square appearing on the screen.

At the start of each trial you will be required to keep the cursor in a central target. The cursor indicates the position of your wrist in the joystick. When a new square appears you are required to move the joystick in the direction of the new target as **fast as you can**. Since this test is designed to observe ballistic (rapid) responses, the initial accuracy of the movement is not important. This means that overshooting the target is not a problem. You will then keep the cursor in the new target until it disappears. Once the target disappears, you will move the cursor slowly back to the central target.

You will complete 60 movements to 4 targets, with 5 seconds between trials. This means that the 240 movements should take approximately 20 minutes. After the first task is completed you will be required to repeat it with the joystick rotated 90^{o}. Therefore the total experimental time will be around 45 minutes, and you will be able to take a break whenever you need to. The whole experiment, including setup, should take no more than 2 hours.

Site: University of Strathclyde, Biomedical Engineering Department , Neurophysiology lab.

Duration: Total time including the setup should be no more than 2 hours

Compensation/Payments: none

Why have you been invited to take part?

For this experiment normal, young, healthy participant are recruited. Participants with no neural, psychiatric, or musculoskeletal impairment or disease are included. No specific skill is required for the experiment. Participants need to have normal or corrected sight, normal hearing and normal upper limb function.

What are the potential risks to you in taking part?

The recording equipment devices are of medical grade, electrically isolated and periodically inspected. Consequently, no risk is predicted regarding the electrical or recording aspects. If you are allergic to (EEG) conductive gel, saline solution or (EMG) abrasive gels and pads, please inform the experimenter.

What happens to the information in the project?

Your personal information will not be disclosed to individuals out of our research group without your permission, unless required by law. Your anonymous recording results will be used in reports and scientific publications without any identifiable information included. Your experimental results will be stored on the computers and servers of the University of Strathclyde and researchers' personal computers.

The University of Strathclyde is registered with the Information Commissioner's Office who implements the Data Protection Act 1998. All personal data on participants will be processed in accordance with the provisions of the Data Protection Act 1998.

Thank you for Reading this Information – Please ask any questions if you are unsure about what is written here.

What happens next?

If you are happy to take part, please sign the accompanying consent form for confirmation. You can ask to be informed if the results are published.

This Investigation was Granted ethical approval by the Department of Biomedical Engineering ethics committee.

If you have any questions/concerns during or after the investigation, or wish to contact an independent person to whom any questions may be directed or further information may be sought from, please contact:

Campbell Reid, PhD, Research Fellow
Biomedical Engineering Department, University of Strathclyde
Wolfson Centre, 106 Rottenrow, Glasgow, G4 0NW, Scotland, UK
Tel: +44(0) 7757 904107,Fax: +44 141 552 6098,
E-mail: campbell.reid@strath.ac.uk

Chief investigator details

Bernard A. Conway, PhD, Research Fellow
Biomedical Engineering Department, University of Strathclyd
Wolfson Centre, 106 Rottenrow, Glasgow, G4 0NW, Scotland, UK
Tel: +44 141 548 3316, Fax: +44 141 552 6098,
E-mail: b.a.conway@strath.ac.uk

Appendix B – Participant consent form

University of Strathclyde

Biomedical Engineering

Department Neurophysiology lab

Title of the study: An EEG investigation to determine if primary motor cortex activations involved in step tracking wrist movements are movement-related or muscle-related.

- I confirm that I have read and understood the information sheet for the above project and the researcher has answered any queries to my satisfaction.
- I understand that my participation is voluntary and that I am free to withdraw from the project at any time, without having to give a reason and without any consequences.
- I understand that I can withdraw my data from the study at any time.
- I understand that any information recorded in the investigation will remain confidential and no information that identifies me will be made publicly available.
- I consent to being a participant in the project

Participant Signature:

_____ (PRINT NAME)	Hereby agree to take part in the above project
Signature of Participant: _____	Date: _____

Witness signature:

_____ (PRINT NAME)	
Signature of Participant: _____	Date: _____

Appendix C – EMG pilot test

Before gathering EEG data, two subjects undertook the test procedure, following the setup proposed in the initial setup design (section 3.3.1) with only EMG recorded. The results of this test were used to determine errors that could arise during testing and confirm that the experimental design used different specific muscle groups for each forearm orientation.

The data was processed using methods described in section 3.4.1, the results can be seen in Appendix C.2.1. The graphs of the resulting EMG averages for each muscle were produced for each movement direction and the EMG graphs were compared with those of movements in the same direction, identifying the agonist muscle by the largest recorded voltage.

The EMG results revealed that during the tasks many agonist and antagonist muscles were the same for both pronation and midway between pronation and supination, resulting in no disassociation between movement direction and muscle pulling direction. This then resulted in a need to change the experimental design.

After changes to experimental design were determined this test was repeated using the proposed changes to the task and setup again using the same subjects, the results of which can be observed in Appendix C.2.2.

Appendix C.1.1 – EMG pilot experimental design

Participants were asked to respond to the appearance of targets on a screen in front of them, a cursor controlled by the manipulandum in Figure A - 1 of similar design to the one used a study by Toxopeus et al (Toxopeus, et al., 2011c), was visible onscreen. After positioning the cursor in the centre target, a second target was displayed at one of the 4 positions: 0^{o}, 90^{o}, 180^{o}, 270^{o}, corresponding to the 12 o'clock, 3 o'clock, 6 o'clock, and 9 o'clock hours on a clock face. After the appearance of the target, the subject was instructed to execute a rapid wrist movement in the direction of the new

target. The target remained visible for 2 to 3 s before disappearing again. The participant was instructed to keep the cursor in the target while it was visible, and once it had disappeared to slowly move the cursor back to the central position, after which the next trial started. The participant completed 50 movements to each target, throughout which EMG was recorded. The order in which the targets appeared and the delay before the target appeared were randomised to prevent the participant from becoming habituated to the task.

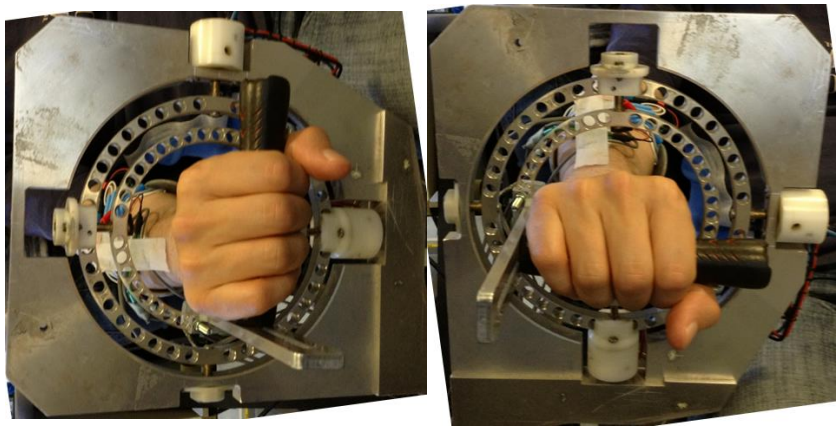

Figure A - 1 Example manipulandum design

The cursor was controlled by a manipulandum which transduced angular displacement of the wrist around 2 axes, displayed in Figure A - 1 B,C. Displacement of the manipulandum was registered by two potentiometers. The output of the potentiometers was calibrated such that the position show in Figure A - 1 A was defined as zero degrees and the cursor could be moved to the targets with clearly defined movements.

After completing the required number of trials in the first orientation, the manipulandum handle was rotated by 90^{o}, resulting in a change of orientation of the forearm from fully supinated to fully pronated, as shown in Figure A - 2, and the task repeated a second time.

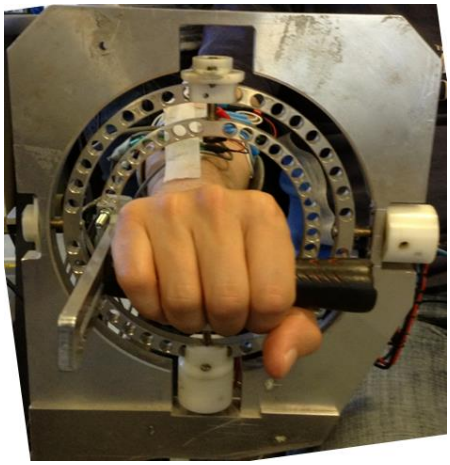

Figure A - 2 Manipulandum used in study with patients forearm supinated

Appendix C.1.2 – EMG pilot experimental setup

Before the start of each experiment, participants had 9 EMG electrodes attached to their right forearm: Extensor Carpi Radialis Brevis, Extensor Carpi Ulnaris, Flexor Carpi Radialis, Flexor Carpi Ulnaris, and an electrode to act as ground. The wires connecting the electrodes were taped to the arm to prevent artefacts generated by movement of the wires. Figure A - 3 displays these positions.

Participants were asked to sit in a comfortable chair and rest their arm on a support and grasp the manipulandum, with the thumb taped to the fingers to prevent movement of the fingers and improve the comfort of the participant. Participants performed the step tracking task in the first orientation, after which the manipulandum handle was rotated by 90^{o} to the second position and the task was repeated a second time. Two computers were used in this experiment; one computer ran the experimental control and EMG data acquisition while the other computer was used for the acquisition of the EEG data. The EMG analogue-to-digital (ADC) converter generating timing pulses related to the appearance of the targets that were also used to synchronise the EEG data and time locked it with the EMG data.

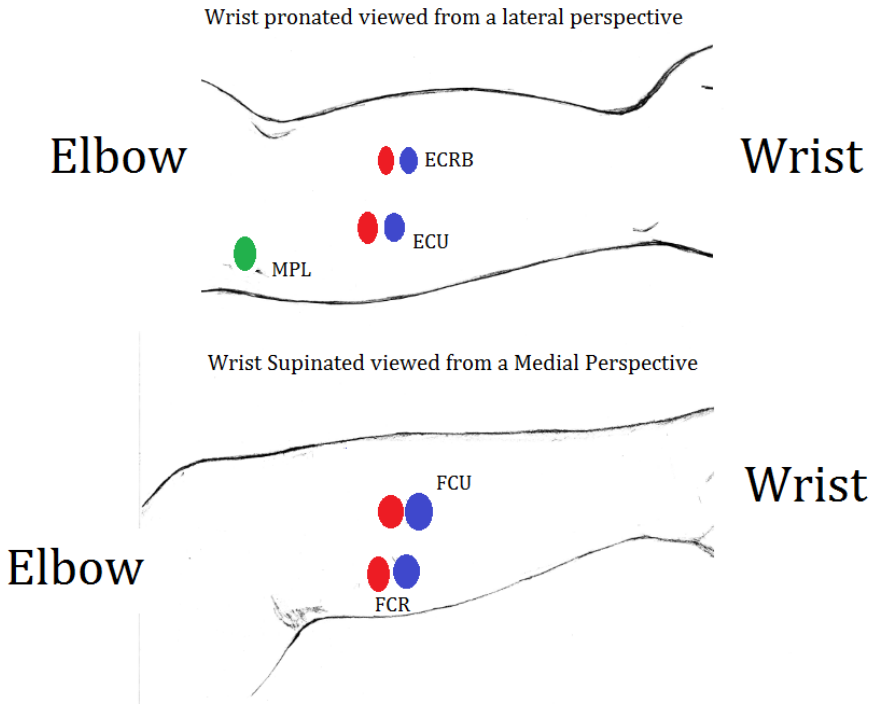

Figure A - 3 Initial position of EMG electrodes

Green electrodes represent reference electrodes that were attached to the processes of the humerus (MPL); Red electrodes represent positive lines while blue electrodes represent negative lines. Electrodes were used in pairs and placed over: Extensor Carpi Radialis Brevis (ECRB), Extensor Carpi Ulnaris (ECU), Flexor Carpi Ulnaris (FCU) and Flexor Carpi Radialis (FCR).

Appendix C.2 - EMG pilot results

The EMG results of the first pilot tests revealed that despite the change in orientation from pronation to semi-pronation, the same pattern of agonist and antagonist muscle activity was observed, with only the amplitude of the EMG bursts being altered. This resulted in a need to change the experimental design.

The second pilot test was undertaken to assess the changes made to the experimental setup by changing the forearm orientation from fully pronated to fully supine. The results showed that there were definite differences in agonist and antagonist muscles when moving to the same target under the two forearm orientations. As target 6 and

target 12 showed the clearest agonist/antagonist differences it was decided that they would be used in the final experimental design.

Appendix C.2.1 First pilot test results

The output graphs for the first EMG pilot test are shown in Figure A - 4 (target 03), Figure A - 5 (target 06), Figure A - 6 (target 09) and Figure A - 7 (target 12).

Table A - 1 Table of EMG electrodes for first pilot test

EMG channel	Muscle Abbreviation	Muscle name	Color on graph
Emg1	ECRB	Extensor Carpi Radialis Brevis	blue
Emg2	ECU	Extensor Carpi Ulnaris	green
Emg3	FCR	Flexor Carpi Radialis	red
Emg4	FCU	Flexor Carpi Ulnaris	black

It is clearly visible from the graphs in Figure A - 4 that the same muscles are used to achieve motion to target 3 (90°) for each orientation, with Extensor Carpi Ulnaris being the agonist for both the pronated (horizontal manipulandum position) and semi-prone (vertical manipulandum position) forearm orientation. The same occurs in Figure A - 6 with the agonist being Flexor Carpi Ulnaris, and Figure A - 7 with the agonist being Extensor Carpi Radialis Brevis. However due to the weak signal from the muscles this is harder to distinguish. This is possibly due to the muscle used being smaller or further away from the surface of the skin. Figure A - 5 is the only target that exhibits a different muscle response between the two orientations, with the agonist being: Extensor Carpi Ulnaris when the forearm is semi-prone, and Flexor Carpi Ulnaris when the forearm is fully pronated, but this could be due to one of the forearm orientations blocking muscles from activating.

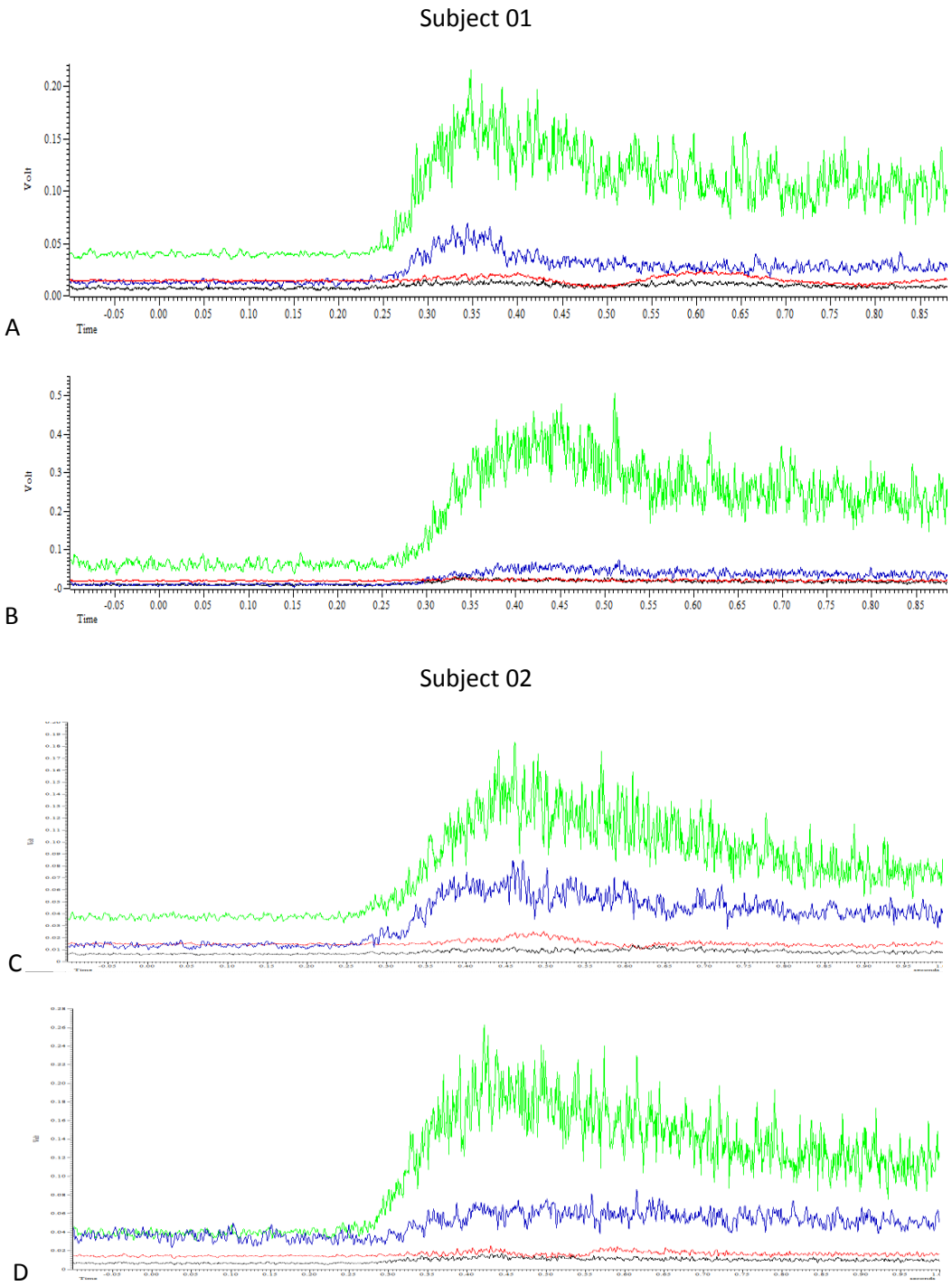

Figure A - 4 Average EMG results for movements in response to target 3

A) Average EMG activity (V) from movement to target 3 by subject 1 with the forearm semipronated. Displayed against time (s). B) Average EMG activity (V) from movement to target 3 by subject 1 with the forearm pronated. Displayed against time (s). C) Average EMG activity (V) from movement to target 3 by subject 2 with the forearm semipronated. Displayed against time (s). D) Average EMG activity (V) from movement to target 3 by subject 2 with the forearm pronated. Displayed against time (s). The four muscles presented are ECRB (blue line), ECU (green line), FCR (red line), FCU (black line). Averages taken from -0.2 s prior to target appearance to 0.5 s post target appearance. EMG voltage scale arbitrarily chosen.

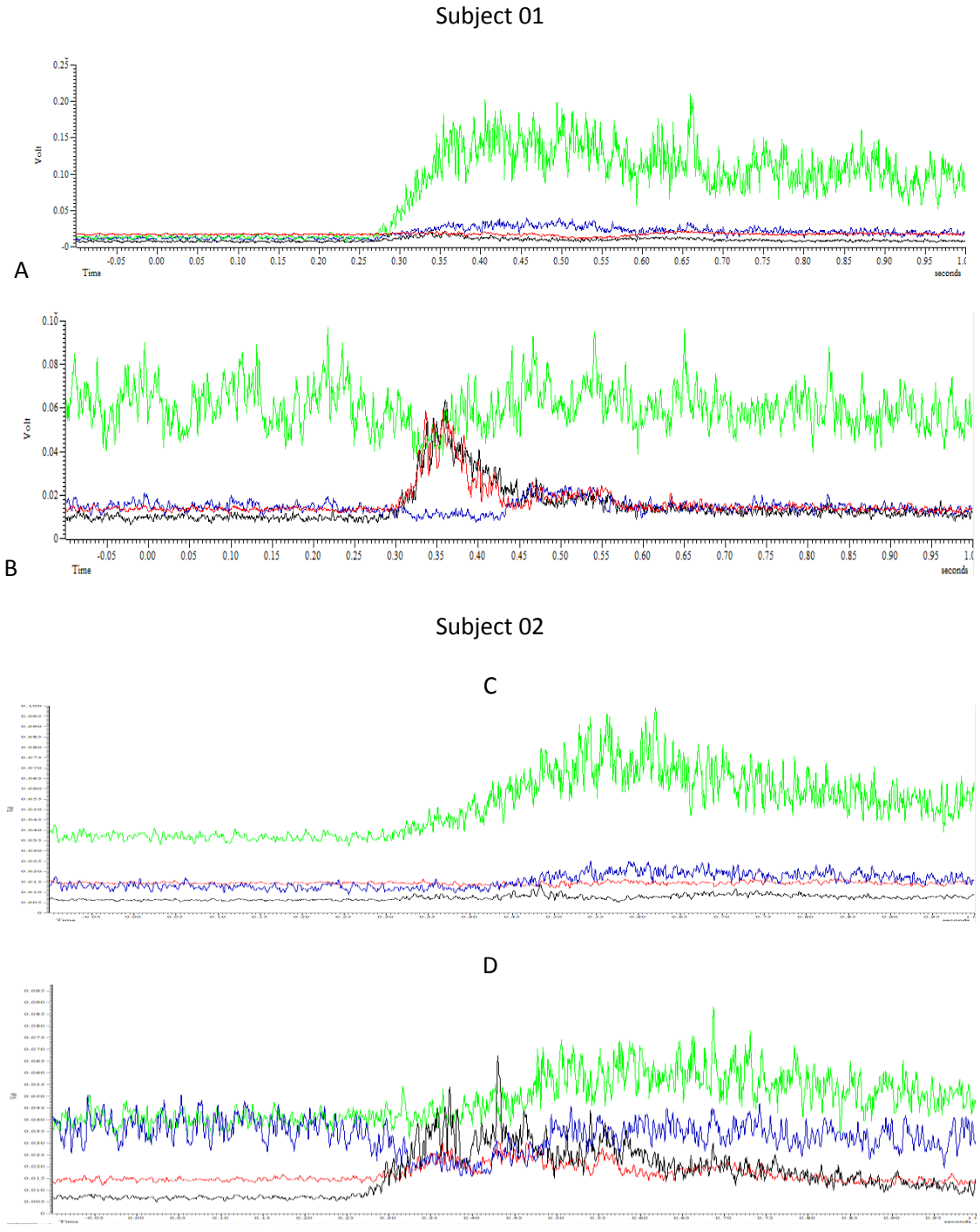

Figure A - 5 Average EMG results in response to target 6

A) Average EMG activity (V) from movement to target 6 by subject 1 with the forearm semipronated. Displayed against time (s). B) Average EMG activity (V) from movement to target 6 by subject 1 with the forearm pronated. Displayed against time (s). C) Average EMG activity (V) from movement to target 6 by subject 2 with the forearm semipronated. Displayed against time (s). D) Average EMG activity (V) from movement to target 6 by subject 2 with the forearm pronated Displayed against time (s). The four muscles presented are ECRB (blue line), ECU (green line), FCR (red line), FCU (black line). Averages taken from -0.2 s prior to target appearance to 0.5 s post target appearance. EMG voltage Scale arbitrarily chosen.

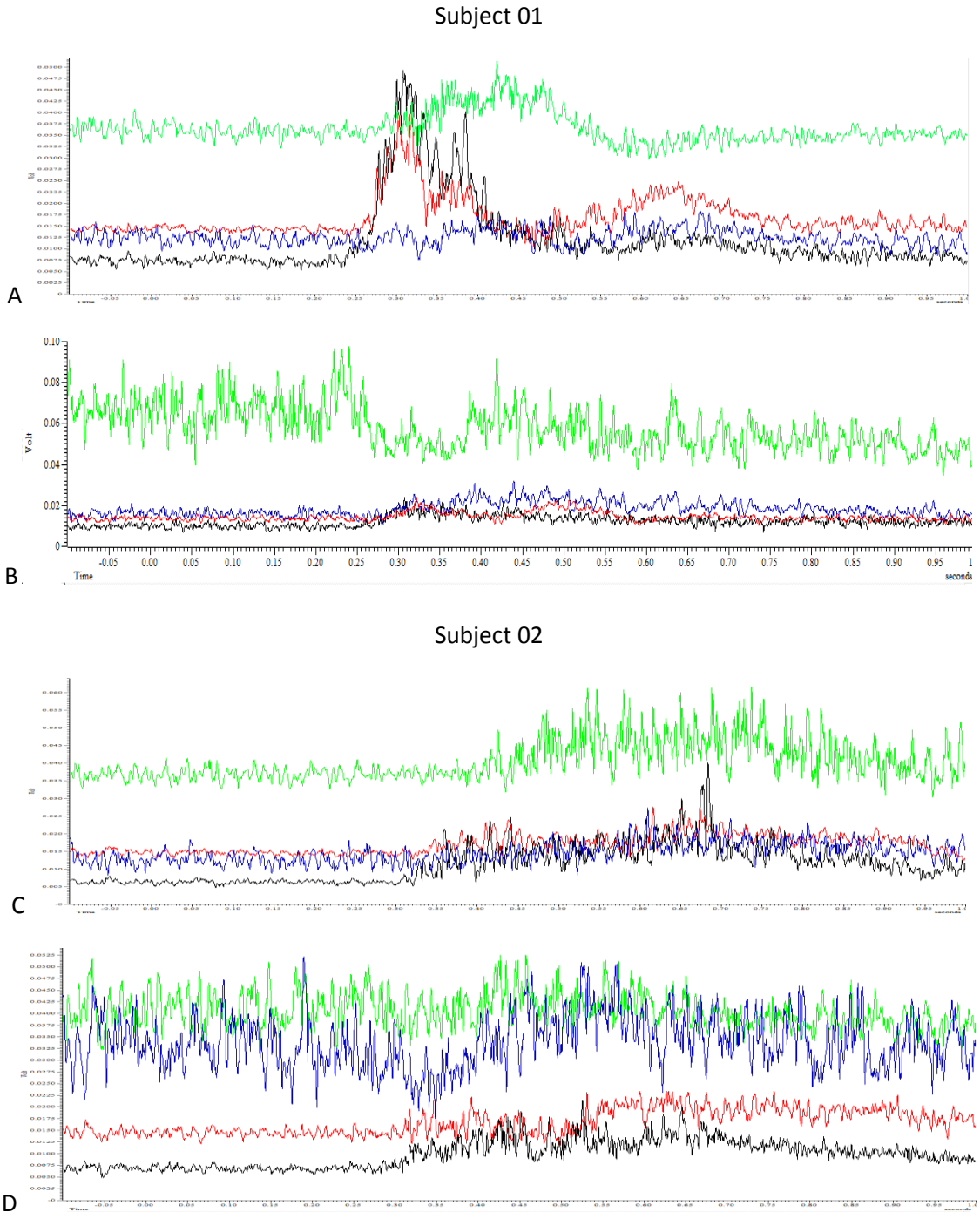

Figure A - 6 Average EMG results in response to target 9

A) Average EMG activity (V) from movement to target 9 by subject 1 with the forearm semipronated. Displayed against time (s). B) Average EMG activity from movement to target 9 by subject 1 with the forearm pronated. Displayed against time (s). C) Average EMG activity (V) from movement to target 9 by subject 2 with the forearm semipronated. Displayed against time (s). D) Average EMG activity (V) from movement to target 9 by subject 2 with the forearm pronated. Displayed against time (s). The four muscles presented are ECRB (blue line), ECU (green line), FCR (red line), FCU (black line). Averages taken from -0.2 s prior to target appearance to 0.5 s post target appearance. EMG voltage Scale arbitrarily chosen.

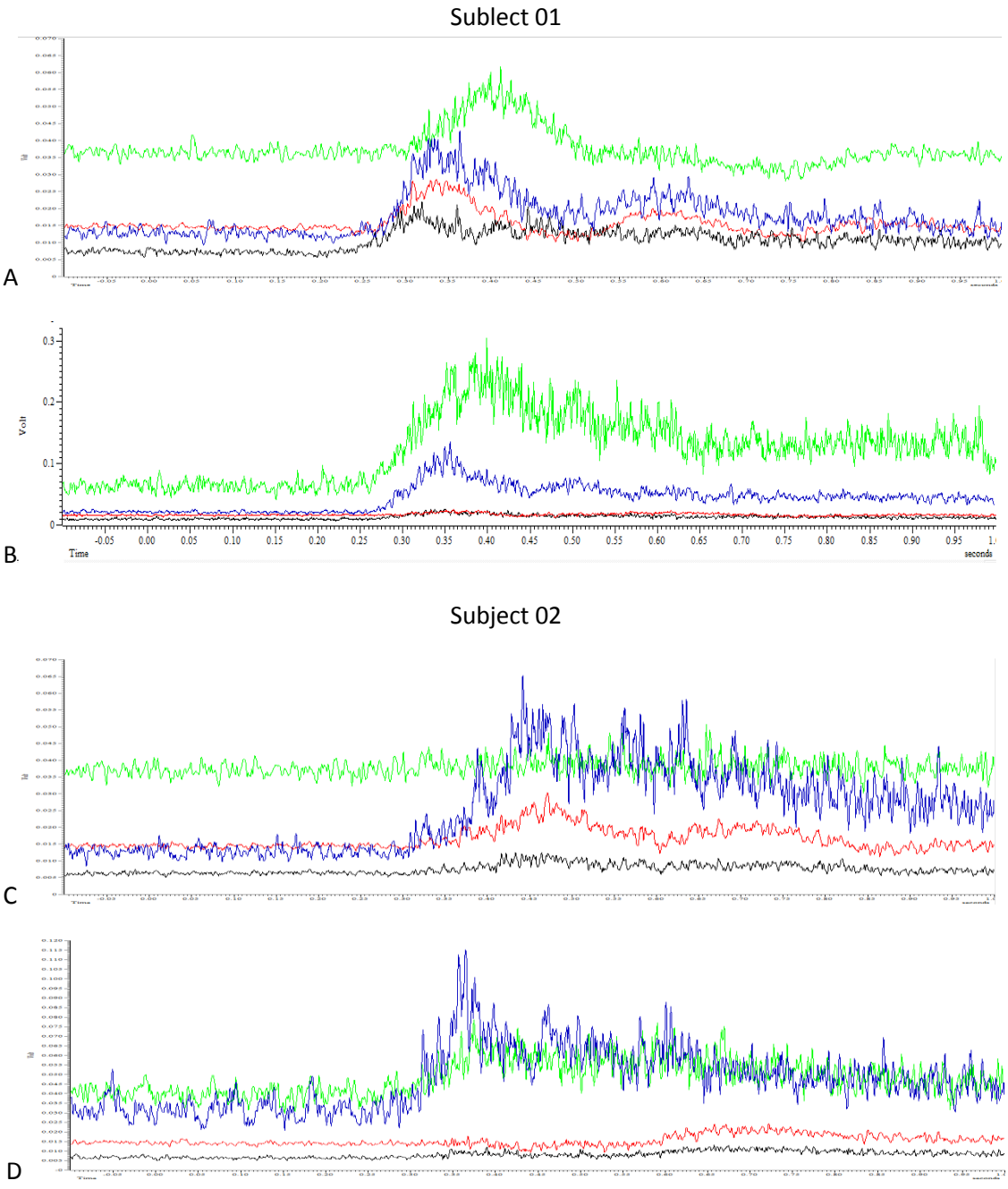

Figure A - 7 Average EMG results in response to target 12

A) Average EMG activity (V) from movement to target 12 by subject 1 with the forearm semipronated. Displayed against time (s). B) Average EMG activity (V) from movement to target 12 by subject 1 with the forearm pronated. Displayed against time (s). C) Average EMG activity (V) from movement to target 12 by subject 2 with the forearm semipronated. Displayed against time (s). D) Average EMG activity (V) from movement to target 12 by subject 2 with the forearm pronated Displayed against time (s). The four muscles presented are ECRB (blue line), ECU (green line), FCR (red line), FCU (black line). Averages taken from -0.2 s prior to target appearance to 0.5 s post target appearance. EMG voltage Scale arbitrarily chosen.

From the results it can be identified that aside from movements in the direction of target 6, the main contributing muscle to specific directional movement is the same for each forearm orientation observed. As the experiment intends to disassociate task direction from muscle direction, the initial forearm orientations were unsuitable for this study.

Appendix C.2.2 Second pilot test results

Output graphs for the second pilot test are shown in Figure A - 8, Figure A - 9, Figure A - 10 and Figure A - 11.

Table A - 2 EMG electrodes for second pilot test

EMG channel	Muscle Abbreviation	Muscle name	Color on graph
Emg1	ECRB	Extensor Carpi Radialis Brevis	blue
Emg2	ECU	Extensor Carpi Ulnaris	green
Emg3	FCR	Flexor Carpi Radialis	red
Emg4	FCU	Flexor Carpi Ulnaris	black

As shown in the graphs in Figure A - 9 and Figure A - 11 above, the flexion and extension of the wrists in directions 12 and 6 clearly use muscle groups that are distinct from one another, and as such are suitable for use in this study. Movements to direction 12 use Flexor Carpi Ulnaris as the agonist when supine and Extensor Carpi Ulnaris when pronated. Movements to direction 6 use Flexor Carpi Ulnaris when pronated and Extensor Carpi Ulnaris when supine. Directions 3 and 9 used the same muscles to achieve movement, however the primary agonist muscle alternated, which can be seen more clearly in Figure A - 8 A, B for target 3. The agonists were Extensor Carpi Radialis Brevis or Extensor Carpi Ulnaris for target 3 and Flexor Carpi Radialis or Flexor Carpi Ulnaris for target 9.

Due to Directions 12 and 6 showing clear differences in the contributing muscles, they were selected for the experiment, and targets 3 and 9 were removed from the step tracking task.

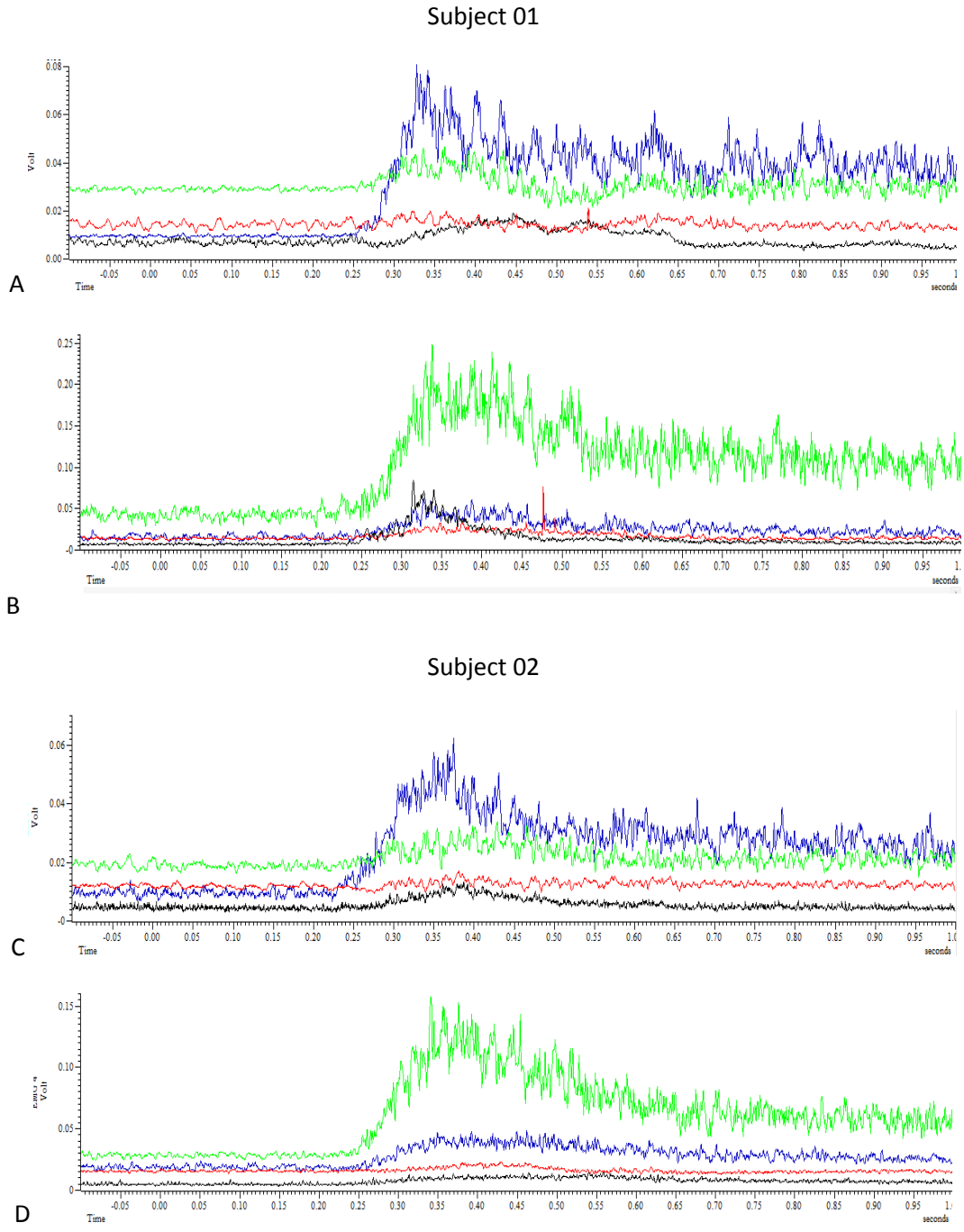

Figure A - 8 Average EMG results in response to target 3 second method

A) Average EMG activity (V) from movement to target 3 by subject 1 with the forearm supinated. Displayed against time (s). B) Average EMG activity (V) from movement to target 3 by subject 1 with the forearm pronated. Displayed against time (s). C) Average EMG activity (V) from movement to target 3 by subject 2 with the forearm supinated. Displayed against time (s). D) Average EMG activity (V) from movement to target 3 by subject 2 with the forearm pronated. Displayed against time (s). The four muscles presented are ECRB (blue line), ECU (green line), FCR (red line), FCU (black line). Averages taken from -0.2 s prior to target appearance to 0.5 s post target appearance. EMG voltage Scale arbitrarily chosen.

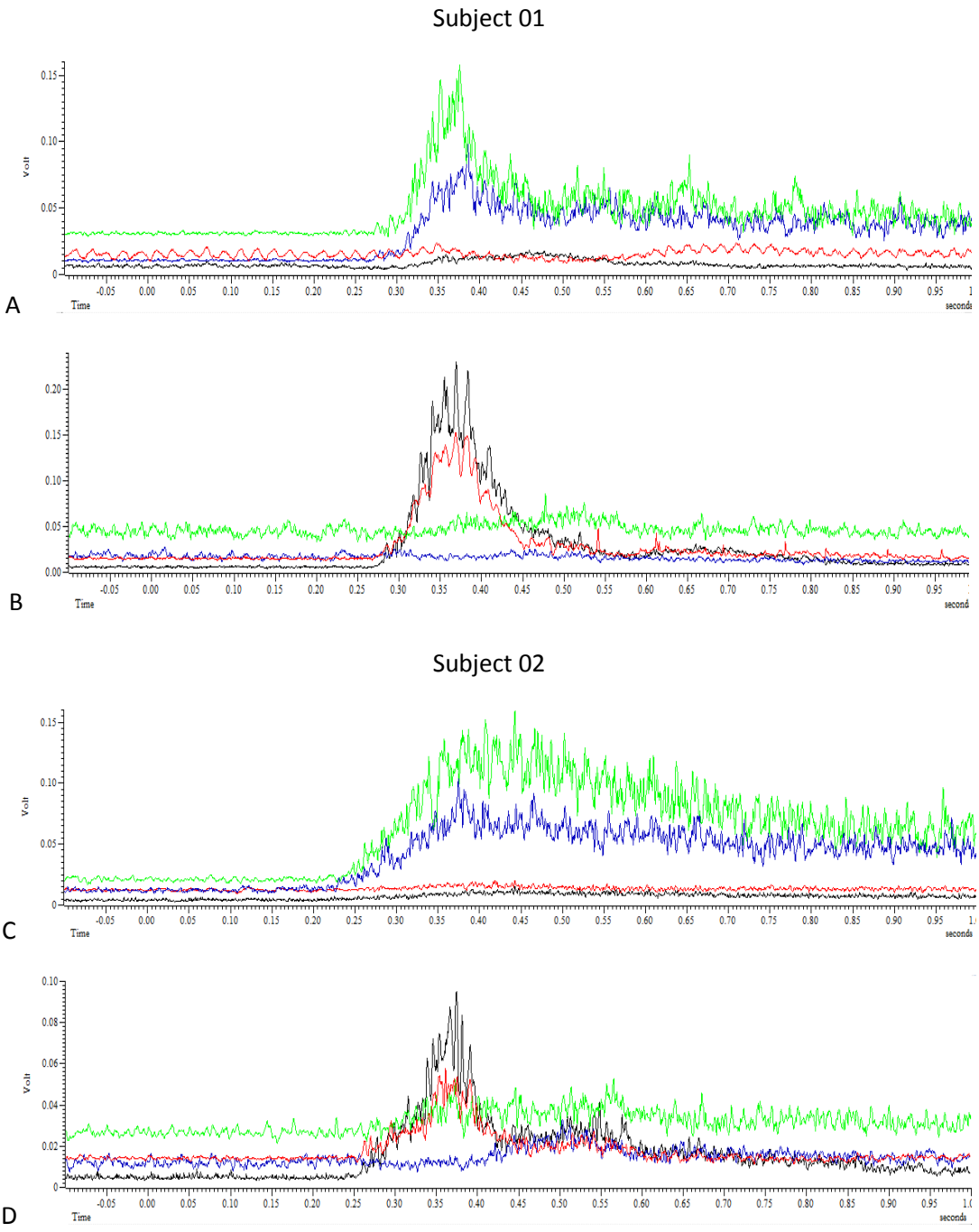

Figure A - 9 Average EMG results in response to target 6 second method

A) Average EMG activity (V) from movement to target 6 by subject 1 with the forearm supinated. Displayed against time (s). B) Average EMG activity (V) from movement to target 6 by subject 1 with the forearm pronated. Displayed against time (s). C) Average EMG activity (V) from movement to target 6 by subject 2 with the forearm supinated. Displayed against time (s). D) Average EMG activity (V) from movement to target 6 by subject 2 with the forearm pronated. Displayed against time (s). The four muscles presented are ECRB (blue line), ECU (green line), FCR (red line), FCU (black line). Averages taken from -0.2 s prior to target appearance to 0.5 s post target appearance. EMG voltage Scale arbitrarily chosen.

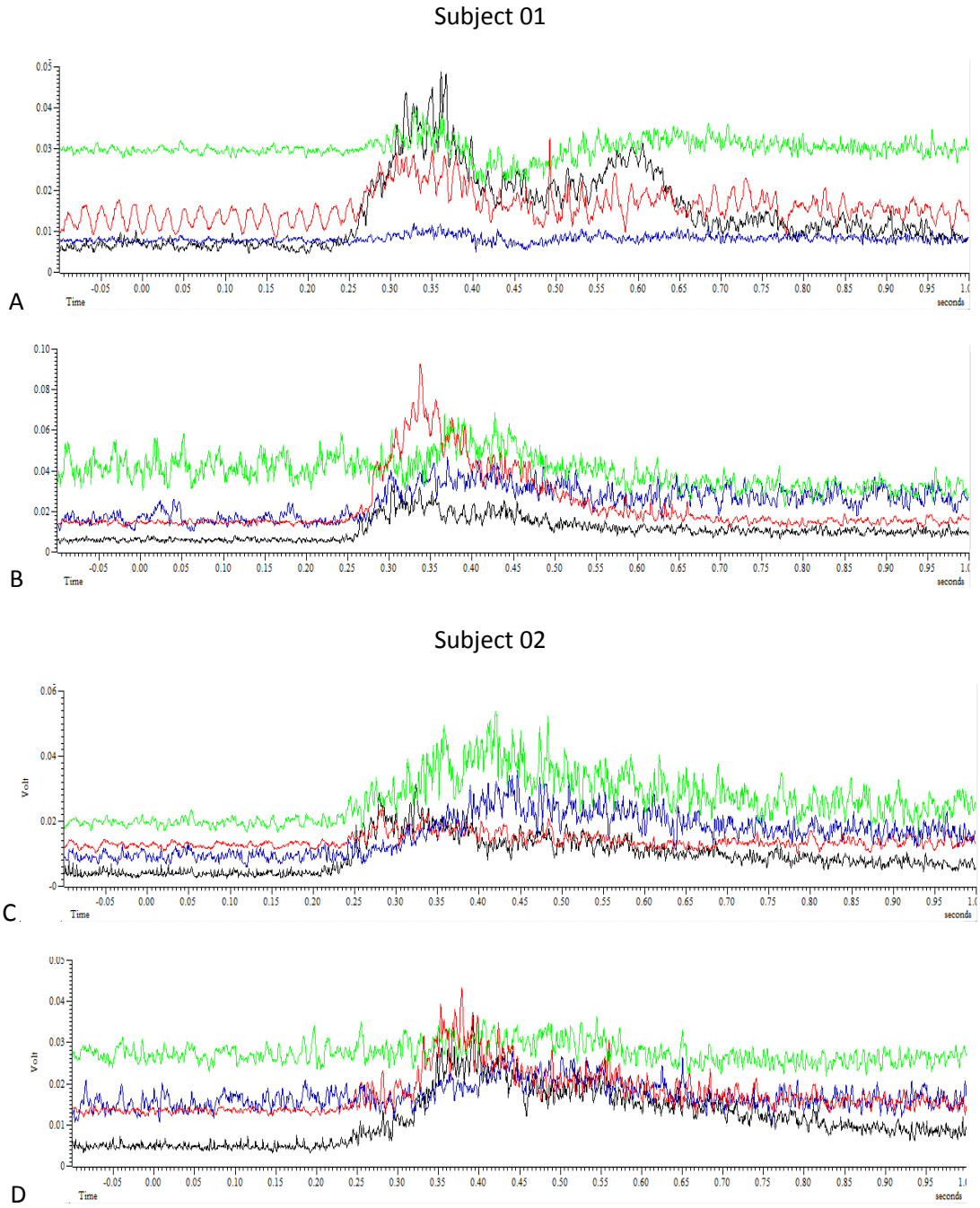

Figure A - 10 Average EMG results in response to target 9 second method

A) Average EMG activity (V) from movement to target 9 by subject 1 with the forearm supinated. Displayed against time (s). B) Average EMG activity (V) from movement to target 9 by subject 1 with the forearm pronated. Displayed against time (s). C) Average EMG activity (V) from movement to target 9 by subject 2 with the forearm supinated. Displayed against time (s). D) Average EMG activity (V) from movement to target 9 by subject 2 with the forearm pronated. Displayed against time (s). The four muscles presented are ECRB (blue line), ECU (green line), FCR (red line), FCU (black line). Averages taken from -0.2 s prior to target appearance to 0.5 s post target appearance. EMG voltage Scale arbitrarily chosen.

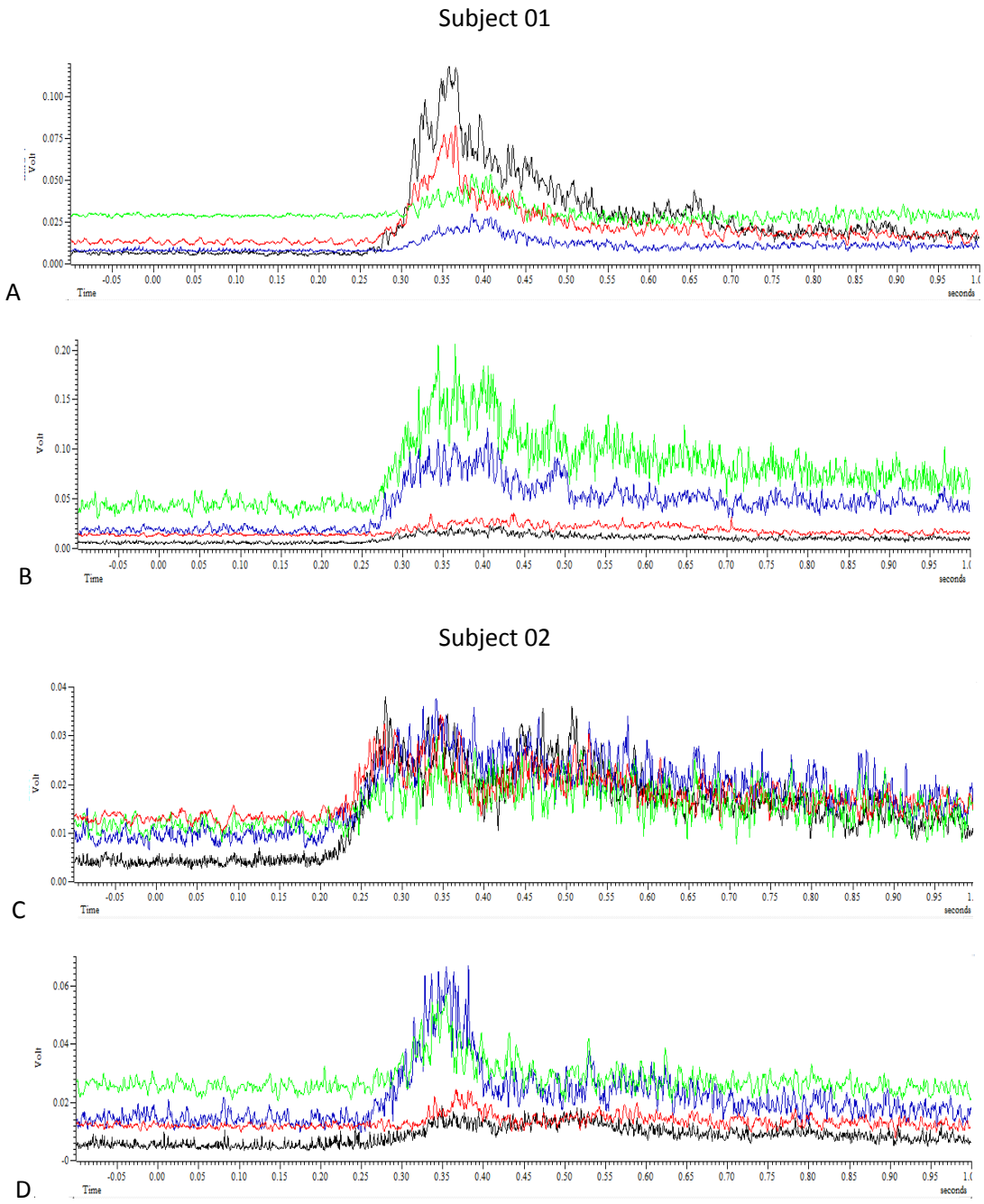

Figure A - 11 Average EMG results in response to target 12 second method

A) Average EMG activity (V) from movement to target 12 by subject 1 with the forearm supinated. Displayed against time (s). B) Average EMG activity (V) from movement to target 12 by subject 1 with the forearm pronated. Displayed against time (s). C) Average EMG activity (V) from movement to target 12 by subject 2 with the forearm supinated. Displayed against time (s). D) Average EMG activity (V) from movement to target 12 by subject 2 with the forearm pronated. Displayed against time (s). The four muscles presented are ECRB (blue line), ECU (green line), FCR (red line), FCU (black line). Averages taken from -0.2 s prior to target appearance to 0.5 s post target appearance. EMG voltage Scale arbitrarily chosen.

Appendix D – Changes made to experimental setup and design

Appendix D.1 - Changes to experimental setup

Two proposed alternate methods of changing the specific muscle groups used in each direction for the current experimental design were considered:

1) Ensuring a full 180^{o} forearm rotation between each position.
2) Maintaining forearm orientation but shifting the upper arm 90 degrees by raising the shoulder.

Due to time constraints the first method was chosen.

This was achieved by altering the initial setup so that during the second of the two tasks, the participant grasped the manipulandum such that their forearm was in a supine position when undertaking the task.

The change from pronation to supination allowed disassociation of the muscle pulling direction from movement direction between the two tasks.

Additionally, the number of muscles EMG was recorded from increased from 4 to 6 to record the activity of the Flexor Digitorum Profundus and the Extensor Carpi Radialis Brevis which were determined to play a role in extension and flexion.

Appendix D.2 - Changes to experimental Design

Results from the second EMG pilot revealed that movements to directions 12 and 6 created the clearest differences in the contributing muscles.

To increase the amount of data available from EEG recordings for each direction the task was altered, removing targets 3 and 9 from the step tracking task. In doing so, while the duration of the experiment remained the same, a greater number of trials could be recorded for each of the 2 remaining targets during the experiment, reducing

the likeness of experimental error due to noise and improving the accuracy of the averaged event related potentials (ERPs).

Therefore, the final experimental protocol involved the participant making two wrist moments, wrist flexion and wrist extension, controlling a cursor in response to targets presented on screen in 2 forearm orientations: fully supine and fully pronated. The participants completed 100 movements to each target in each orientation, throughout which EMG and EEG data were recorded. The target position and delay before the target appears were still randomised to prevent the participants from learning the task.